

**SEISMIC RETROFIT OF CRUCIFORM-SHAPED COLUMNS
IN THE AURORA AVENUE BRIDGE USING FRP WRAPPING**

By

BRIAN JOHN WALKENHAUER

A thesis submitted in partial fulfillment of
the requirements for the degree of

MASTER OF SCIENCE IN CIVIL ENGINEERING

WASHINGTON STATE UNIVERSITY
Department of Civil and Environmental Engineering

MAY 2010

To the Faculty of Washington State University

The members of the Committee appointed to examine the thesis of BRIAN JOHN WALKENHAUER find it satisfactory and recommend that it be accepted.

David I. McLean, Chair

David G. Pollock

Mohammed A. ElGawady

ACKNOWLEDGEMENT

Funding for this research was provided by the Washington State Department of Transportation.

I would like to thank the chair of my committee, Dr. David McLean, and my other committee members, Dr. David Pollock and Dr. Mohammed ElGawady, for giving me the opportunity to further my education and for their support and guidance throughout this research.

I would like to express my gratitude to Robert Duncan and Scott Lewis for all of the technical help they provided in the lab. I would also like to thank Tim Vaughan for his assistance throughout the construction and testing phases of the project.

SEISMIC RETROFIT OF CRUCIFORM-SHAPED COLUMNS IN THE AURORA AVENUE BRIDGE USING FRP WRAPPING

Abstract

**By Brian John Walkenhauer, M.S.
Washington State University
May 2010**

Chair: David McLean

One of the major problems associated with the seismic response of older reinforced concrete bridges has been brittle shear failure of inadequately reinforced bridge columns. The study reported in this thesis consisted of an experimental investigation of cruciform-shaped column specimens representative of columns in the SR-99 Aurora Avenue Bridge located in Seattle, Washington. The primary goal was to evaluate the effectiveness of fiber reinforced polymer (FRP) composite wrapping for enhancing the seismic shear strength of the columns.

Five large-scale cruciform-shaped columns were subjected to increasing levels of cyclic displacements representative of seismic loading. Parameters varied in the tests included the presence or absence of FRP wrapping, presence or absence of reentrant corner anchorage, type of reentrant corner anchorage used, and the presence or absence of plastic hinge zone confinement. Two unretrofitted specimens were tested to examine the performance of the as-built columns with deficient transverse reinforcement, and three specimens were tested after retrofitting with carbon fiber FRP composite wrapping. The performance of the tested specimens was evaluated based on failure mode, peak displacement levels attained before failure, and hysteretic behavior.

The as-built column specimens experienced a brittle shear failure at limited displacement levels. Retrofitting using FRP wrapping but without reentrant corner anchorage slightly improved the seismic performance of the column, but the specimen still experienced a brittle shear failure at only slightly larger displacement levels than those attained in the as-built specimens. Column specimens retrofitted with FRP wrapping and reentrant corner anchorage showed significant improvement in the seismic performance with enhanced strength, energy and ductility capacities. Evaluation of the FRP jacket stresses indicated that the FRP jacket remained elastic under large cyclic shear forces and provided the required shear strength enhancement. To prevent bulging in the plastic hinge region, one specimen was retrofitted with a grout filled steel collar throughout the plastic hinge length.

Design and detailing guidelines for retrofitting cruciform-shaped columns are proposed. The guidelines include jacket thicknesses and reentrant corner anchorage required to prevent shear failure in the column.

TABLE OF CONTENTS

CHAPTER 1: INTRODUCTION

1.1 INTRODUCTION AND BACKGROUND	1
1.2 RESEARCH OBJECTIVES	2

CHAPTER 2: HISTORY OF THE AURORA AVENUE BRIDGE

2.1 INTRODUCTION	3
2.2 HISTORY	3
2.3 LAYOUT OF THE BRIDGE	4
2.3.1 South Approach	5
2.3.2 Main Span	5
2.3.3 North Approach	5
2.4 SEISMIC RETROFIT	8
2.4.1 Shear Strengthening of Concrete Columns	8

CHAPTER 3: LITERATURE REVIEW

3.1 BACKGROUND	10
3.2 COLUMN DEFICIENCIES	10
3.3 COLUMN RETROFITTING	11
3.3.1 Steel Jacketing	13
3.3.2 Fiber Reinforced Polymer Wrapping	13

CHAPTER 4: DESIGN, CONSTRUCTION AND TESTING PROCEDURES

4.1 INTRODUCTION	17
4.2 BRIDGE COLUMN DETAILS	17
4.3 SCALING PROCEDURE	19

4.4 SPECIMEN DESCRIPTION.....	20
4.4.1 Footing Description	20
4.4.2 Column Description.....	21
4.4.3 Load Stub Description	24
4.4.4 Retrofit Description	25
4.5 MATERIAL PROPERTIES	30
4.6 ESTIMATION OF TEST COLUMN STRENGTH	31
4.7 SPECIMEN CONSTRUCTION.....	32
4.8 TEST SETUP.....	32
4.8.1 Design Considerations for the Test Setup.....	34
4.9 INSTRUMENTATION	34
4.10 TEST PROCEDURES	35
CHAPTER 5: TEST RESULTS	
5.1 INTRODUCTION	37
5.2 BEHAVIOR OF AS-BUILT COLUMN 1	37
5.2.1 Overall Response	38
5.2.2 Reinforcement Strain Plots	40
5.3 BEHAVIOR OF AS-BUILT COLUMN 5	45
5.3.1 Overall Response	45
5.3.2 Reinforcement Strain Plots	47
5.3.3 Summary of As-Built Performance	48
5.4 BEHAVIOR OF RETROFITTED COLUMN 2.....	52
5.4.1 Overall Response	52

5.4.2 Reinforcement Strain Plots	55
5.5 BEHAVIOR OF RETROFITTED COLUMN 3.....	62
5.5.1 Overall Response	62
5.5.2 Reinforcement Strain Plots	65
5.6 BEHAVIOR OF RETROFITTED COLUMN 4.....	72
5.6.1 Overall Response	72
5.6.2 Reinforcement Strain Plots	75
5.7 COMPARISON OF AS-BUILT AND RETROFITTED COLUMNS.....	82
CHAPTER 6: CONCLUSIONS AND RECOMMENDATIONS	
6.1 CONCLUSIONS.....	87
6.2 RECOMMENDATIONS.....	88
REFERENCES	90
APPENDIX.....	92

LIST OF TABLES

Table 4.3.1	Dimensions for Bridge and Test Columns	19
Table 4.4.1	Retrofit Test Parameters	26
Table 4.5.1	Material Strengths of Components for Test Columns	31
Table 4.6.1	Estimated Shear Strength of Test Columns	31
Table 5.7.1	Column Test Results	83
Table A-1	Loading Frame Bill of Materials.....	105

LIST OF FIGURES

Figure 2.1.1	Location of the Bridge	3
Figure 2.3.1	Overall Layout of the Aurora Avenue Bridge	5
Figure 2.3.2	Layout of the North Approach.....	6
Figure 2.3.3	Typical Solid and Split Columns in the North Approach	7
Figure 2.3.4	Troll under the North Approach	7
Figure 4.2.1	Column As-Built Details.....	18
Figure 4.4.1	Footing and Load Stub Reinforcement Details.....	22
Figure 4.4.2	Column Details	23
Figure 4.4.3	Torsion Design in the Top Load Stub.....	25
Figure 4.4.4	Steel Bent Plate with Anchor Bolts Retrofit Details.....	28
Figure 4.4.5	FRP Anchor Retrofit Details.....	29
Figure 4.4.6	FRP Anchor Installation	30
Figure 4.8.1	Test Setup.....	33
Figure 4.10.1	Loading Protocol: Sequential Displacements	36
Figure 5.2.1	Column 1 Lateral Load vs. Displacement Hysteresis Curves.....	39
Figure 5.2.2	Column 1 Test Setup.....	39
Figure 5.2.3	Column 1 Shear Cracking Near the End of Testing	40
Figure 5.2.4	Column 1 Transverse Strain Gage Data.....	42
Figure 5.2.5	Column 1 Longitudinal Strain Gage Data at the Top of the Column	43
Figure 5.2.6	Column 1 Longitudinal Strain Gage Data at the Bottom of the Column.....	44
Figure 5.3.1	Column 5 Lateral Load vs. Displacement Hysteresis Curves.....	46
Figure 5.3.2	Column 5 Test Setup.....	46

Figure 5.3.3	Column 5 Shear Cracking Near the End of Testing	47
Figure 5.3.4	Column 5 Transverse Strain Gage Data.....	49
Figure 5.3.5	Column 5 Longitudinal Strain Gage Data at the Top of the Column	50
Figure 5.3.6	Column 5 Longitudinal Strain Gage Data at the Bottom of the Column.....	51
Figure 5.4.1	Column 2 Lateral Load vs. Displacement Hysteresis Curves.....	53
Figure 5.4.2	Column 2 Test Setup.....	54
Figure 5.4.3	Column 2 Pullout of FRP Jacket from Reentrant Corners.....	54
Figure 5.4.4	Column 2 Large Shear Cracks Under FRP Jacket at the End of Testing	55
Figure 5.4.5	Column 2 Transverse Strain Gage Data.....	57
Figure 5.4.6	Column 2 Longitudinal Strain Gage Data at the Top of the Column	58
Figure 5.4.7	Column 2 Longitudinal Strain Gage Data at the Bottom of the Column.....	59
Figure 5.4.8	Column 2 Parallel FRP Jacket Strain Gage Data.....	60
Figure 5.4.9	Column 2 Perpendicular FRP Jacket Strain Gage Data.....	61
Figure 5.5.1	Column 3 Lateral Load vs. Displacement Hysteresis Curves.....	63
Figure 5.5.2	Column 3 Test Setup.....	64
Figure 5.5.3	Column 3 Bulging of FRP Jacket at the Top of the Column	64
Figure 5.5.4	Column 3 Reentrant Corner Anchorage Failure	65
Figure 5.5.5	Column 3 Transverse Strain Gage Data.....	67
Figure 5.5.6	Column 3 Longitudinal Strain Gage Data at the Top of the Column	68
Figure 5.5.7	Column 3 Longitudinal Strain Gage Data at the Bottom of the Column.....	69
Figure 5.5.8	Column 3 Parallel FRP Jacket Strain Gage Data.....	70
Figure 5.5.9	Column 3 Perpendicular FRP Jacket Strain Gage Data.....	71
Figure 5.6.1	Column 4 Lateral Load vs. Displacement Hysteresis Curves.....	73

Figure 5.6.2	Column 4 Test Setup.....	74
Figure 5.6.3	Column 4 Longitudinal Rebar Fracture	74
Figure 5.6.4	Column 4 Near the End of Testing	75
Figure 5.6.5	Column 4 Transverse Strain Gage Data.....	77
Figure 5.6.6	Column 4 Longitudinal Strain Gage Data at the Top of the Column	78
Figure 5.6.7	Column 4 Longitudinal Strain Gage Data at the Bottom of the Column.....	79
Figure 5.6.8	Column 4 Parallel FRP Jacket Strain Gage Data.....	80
Figure 5.6.9	Column 4 Perpendicular FRP Jacket Strain Gage Data.....	81
Figure 5.7.1	Envelope Lateral Load vs. Displacement Hysteresis Curves	84
Figure A-1	Strain Gage Locations Inside All Specimens.....	92
Figure A-2	Strain Gage Locations on Retrofitted Specimens	93
Figure A-3	Loading Frame Assembly Diagram	94
Figure A-4	Loading Frame Front View.....	95
Figure A-5	Loading Frame Front View (2).....	96
Figure A-6	Loading Frame Side View	97
Figure A-7	Loading Frame Side View (2).....	98
Figure A-8	Loading Frame Top View	99
Figure A-9	Loading Frame Top View (2)	100
Figure A-10	Loading Frame Section A-A.....	101
Figure A-11	Loading Frame Isometric View	102
Figure A-12	Loading Frame c1001	103
Figure A-13	Loading Frame p1001	104

CHAPTER ONE

INTRODUCTION

1.1 – INTRODUCTION AND BACKGROUND

The 1971 San Fernando earthquake and other more recent earthquakes have demonstrated that bridges built using older design codes may be vulnerable to damage under seismic loading. Many of the interstate bridges in the United States were constructed in the 1950s and 1960s and incorporate deficiencies that must be addressed in order to avoid major damage or even collapse under strong ground motion.

Common deficiencies found in bridges built prior to 1971 are insufficient transverse reinforcement and inadequate lap splice length. In addition, poor detailing including lack of proper anchorage of the transverse reinforcement, rare use of crossties, and lap splices located in potential plastic hinge regions make older columns susceptible to failure. Possible failure modes of deficient columns are shear failure, premature flexural failure and lap splice failure.

It is not financially feasible to replace all deficient bridges, and hence retrofitting of existing deficient bridges is a necessary option. Several retrofitting techniques such as reinforced concrete jacketing and steel jacketing have been developed to rehabilitate structurally-deficient bridge columns. In the last decade, fiber reinforced polymer (FRP) composite wrapping has attracted the attention of researchers and bridge owners as an alternative method for retrofitting reinforced concrete bridge elements.

This thesis presents the findings of an experimental study conducted on cruciform-shaped columns retrofitted using FRP composite materials. Five 1/3-scale column specimens representative of columns in the Aurora Avenue Bridge in Seattle, Washington were tested. Two unretrofitted specimens were tested to examine the performance of the as-built columns with

deficient transverse reinforcement, and three specimens were tested after retrofitting with carbon fiber FRP composite wrapping. Two of the retrofitted specimens also incorporated reentrant corner anchorage for the FRP, while the remaining retrofitted specimen did not have reentrant corner anchorage. All specimens were subjected to pseudo-static, reverse-cyclic loading. The performance of the tested specimens was evaluated based on failure mode, peak displacement levels attained before failure, and hysteretic behavior.

1.2 – RESEARCH OBJECTIVES

The overall goals of this study were to assess the seismic performance of existing cruciform-shaped bridge columns with known structural deficiencies and to evaluate the effectiveness of FRP composite retrofit measures for improving the performance of deficient columns. To achieve these goals, four objectives were established:

- 1) Identify the vulnerabilities of the cruciform-shaped columns in the Aurora Avenue Bridge under seismic loading;
- 2) Evaluate FRP composite wrapping as a retrofit measure for improving the seismic performance of cruciform-shaped bridge columns;
- 3) Determine whether reentrant corner anchorage is required to engage the full capacity of the FRP composite wrapping; and
- 4) Draw conclusions on the feasibility and effectiveness of FRP composite wrapping for retrofitting deficient cruciform-shaped bridge columns.

CHAPTER TWO

HISTORY OF THE AURORA AVENUE BRIDGE

2.1 – INTRODUCTION

The George Washington Memorial Bridge (commonly called the Aurora Avenue Bridge) is a cantilever truss bridge that carries Aurora Avenue North (State Route 99) over the west end of Seattle's Lake Union between Queen Anne and Fremont, just east of the Fremont Cut as shown in Figure 2.1.1. The bridge is 2,945 ft (898 m) long, 70 ft (21 m) wide, and 167 ft (51 m) above the water. It is owned and operated by the Washington State Department of Transportation (WSDOT).

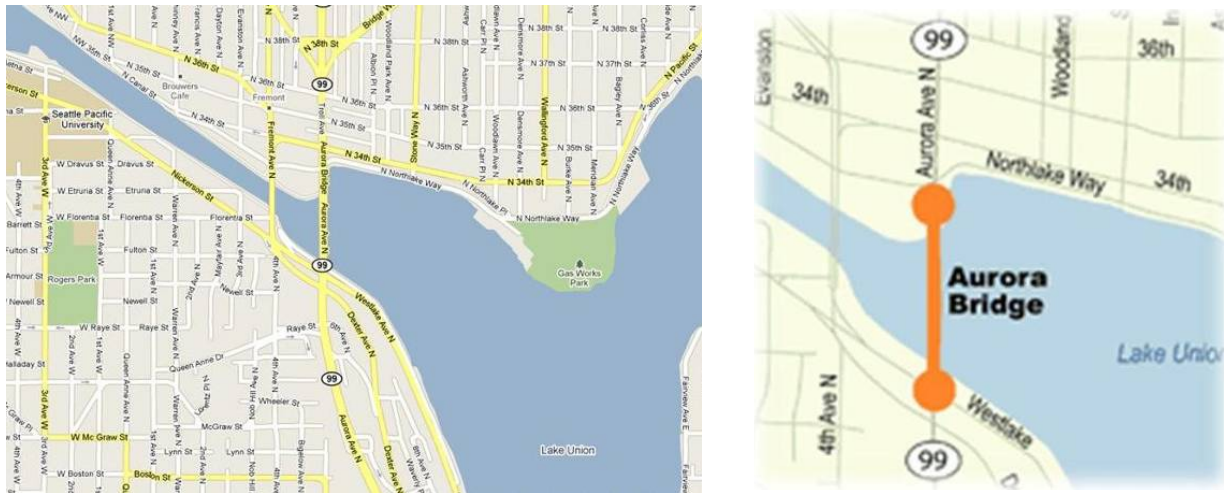


Figure 2.1.1 – Location of the Bridge

2.2 – HISTORY

At the time of its construction, the Aurora Avenue Bridge was a highly controversial project. The state Highway Department wanted a new bridge to carry through traffic on U.S. Highway 99, the state's primary north-south route at the time, more efficiently through Seattle. Several routes for a high bridge over Lake Union were proposed, with possible crossings at

Stone Way, Albion Place, Whitman Avenue, and Linden Avenue considered in addition to Aurora Avenue. On June 30, 1930, following the advice of city and state highway engineers, the Seattle City Council approved an ordinance extending Aurora Avenue through Woodland Park. The council's decision to bisect Woodland Park's 200-acre (81-hectare) urban wilderness triggered outrage among park supporters and other bridge opponents. With the steadfast backing of the *Seattle Times*, speedway opponents gathered enough signatures to force a referendum on the council decision. However, despite these efforts, voters approved the speedway ordinance that November by a substantial margin, with more than 37,000 in favor and around 29,000 opposed. Despite the referendum's passage, the bridge remained a heated topic and the city and state agreed to split responsibility for the project. The state oversaw design and construction of the bridge itself, while the city took charge of constructing the bridge approaches, placing the controversy over the park route squarely in the city's hands. Construction of the bridge was finished in February of 1932, completing the final link of U.S. Highway 99 from Canada to Mexico. Currently the bridge has an estimated Annual Daily Traffic (ADT) of over 100,000 vehicles, and it was added to the national register of historic places in 1982.

2.3 – LAYOUT OF THE BRIDGE

The layout of the Aurora Avenue Bridge can be broken down into three distinct sections: the south approach, the main span, and the north approach. Figure 2.3.1 shows the overall layout of the bridge.

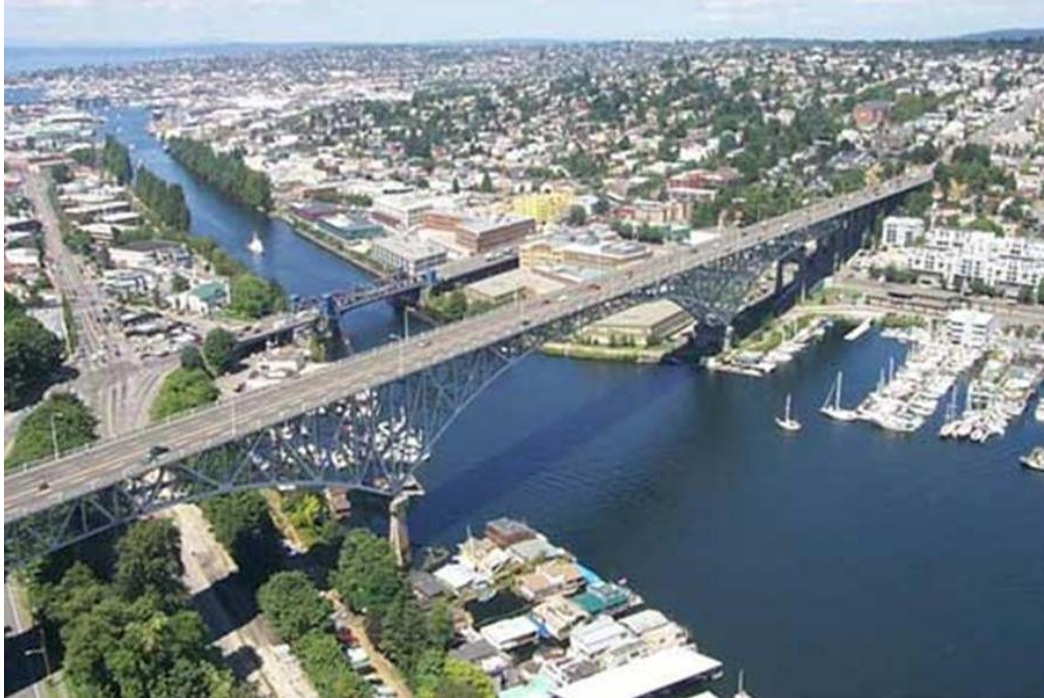


Figure 2.3.1 – Overall Layout of the Aurora Avenue Bridge

2.3.1 – South Approach

The south approach features three spans of reinforced concrete construction as well as three spans of steel deck truss. This section of the bridge is mostly hidden by the abundance of vegetation surrounding it and thus is not well known for its architectural features.

2.3.2 – Main Span

The main span of the bridge, however, is much more visible. It features three spans of steel deck truss cantilevered off of two large piers on opposite sides of the channel. At 1,450 ft (442 m) in length, the main span accounts for almost half of the total length of the bridge.

2.3.3 – North Approach

The north approach features twelve spans of reinforced concrete construction. These twelve spans are separated into five independent frames by split columns which allow for expansion and contraction of the bridge due to temperature and shrinkage effects. Figure 2.3.2 shows the layout of the north approach. The piers themselves are unusual in that they are in the



(a)



(b)

Figure 2.3.3 – Typical Solid and Split Columns in the North Approach



Figure 2.3.4 – Troll under North Approach

2.4 – SEISMIC RETROFIT

Following the 2001 Nisqually earthquake in Washington State, the WSDOT determined that the Aurora Avenue Bridge would be unable to resist another large earthquake. TY Lin International, a consulting engineering firm specializing in retrofit of existing structures, was then hired to perform a seismic evaluation of the structure and determine any deficiencies. TY Lin performed both time-history and pushover analyses of the bridge and found several deficiencies, including axial capacity of the main span truss members, footing overturning capacity, flexural capacity of girders, rotational capacity of crossbeams, and shear capacity of the columns. A seismic retrofit plan was then created which split the retrofit into three stages. The first stage focused on base isolation of the main truss span as well as adding restrainers on simple span trusses. The second stage included retrofitting the foundations to prevent overturning and strengthening of the main span truss members. Both of these stages have already been completed, with the third stage yet to begin. The third stage of the retrofit will involve adding confinement to crossbeams, flexural strengthening of longitudinal girders, and shear strengthening of the concrete columns. This study focuses on the shear strengthening of the concrete columns.

2.4.1 – Shear Strengthening of Concrete Columns

Several retrofit options were considered to add shear strength to the concrete columns, including: external frame strengthening, which would not be effective without cross-bracing; concrete jacketing, which would be expensive and would alter the shape of the column cross-sections; friction pendulums at the base of the columns, which would have to be implemented in many locations; and finally fiber reinforced polymer (FRP) wrapping, which would require testing to verify its effectiveness on cruciform-shaped columns. For the south approach of the

bridge, which is mainly secluded, concrete jacketing was chosen because it is an established retrofit method and the aesthetics of the columns were not important. However, on the north approach, there was a large public demand to keep the cruciform shape of the columns and the overall aesthetic appeal of the bridge intact. Because of this, FRP composite wrapping was chosen to retrofit the columns on the north approach of the bridge.

CHAPTER THREE

LITERATURE REVIEW

3.1 – BACKGROUND

Many older bridges were designed primarily for gravity loads with little or no consideration of lateral forces from seismic events. As a result, recent earthquakes have caused substantial damage in older bridges. Several inadequacies in previous design codes and construction practices have been highlighted in these past earthquakes, resulting in a need for seismic retrofit in order to prevent future loss to human life and property.

3.2 – COLUMN DEFICIENCIES

The majority of bridge column failures resulting from structural response during recent earthquakes can largely be attributed to:

- 1) Flexural failure of piers at locations of maximum moment due to inadequate ductility capacity. This is a result of low lateral design force coefficients typically used in the 1950's and 1960's which may cause high ductility demands. Another cause of inadequate flexural ductility is insufficient transverse reinforcement which does not provide sufficient confinement of longitudinal bars to develop the full flexural capacity of the cross section and thus limits the ultimate curvature in the plastic hinge region when the concrete cover spalls off.
- 2) Failure associated with undependable flexural strength due to insufficient lap length required for longitudinal reinforcement spliced with starter bars from the footing. Starter bars often extend 20 to 35 times the column longitudinal bar diameter (d_b) from the footing. A lap splice of $20d_b$ has been shown to be inadequate to transfer the full tensile force of the

longitudinal reinforcement to the starter bars in the foundation (Haroun et al., 2005; Iacobucci et al., 2003; Memon et al., 2005; Seible et al., 1995). Columns with longer lap splices have been shown to perform better. Tests on circular columns with a $35d_b$ lap splice have demonstrated relatively ductile performance, with displacement ductility levels of up to 4 being reported (Coffman et al., 1993; Stapleton et al., 2005). Many existing bridge columns in Washington State include lap splices of the column longitudinal reinforcement with a lap length of $35d_b$ (Endeshaw, 2008).

- 3) Shear failure resulting from the underestimation of lateral seismic forces due to the use of code-specified empirical equations as well as inadequate transverse reinforcement for shear. Typically, No. 3 or No. 4 hoops at 12 in. (0.3 m) on center were used as transverse reinforcement regardless of the column size or lateral design force. These hoops were anchored by 90-degree hooks with short extensions which become ineffective once the cover concrete spalls off. Also, underestimation of the flexural strength caused by very conservative elastic design methods, coupled with much less conservative shear strength provisions during the 1950's and 1960's, typically results in column shear strength being much less than actual flexural capacity, thereby creating a tendency for a brittle shear response of the column.

3.3 – COLUMN RETROFITTING

The ability of structures to achieve adequate deformation capacity plays a significant role in the prevention of structural failures in seismic events. Ductile structures dissipate more energy and thereby may be designed for lower lateral loads than brittle structures. The deformation capacity of existing bridges can be enhanced by modifying certain substructure elements and connections. Usually it is the bridge piers which are chosen as an effective system for dissipation

of seismic induced energy, as the design of the bridge superstructure is governed by dead load and live loads and hence it is undesirable to allow any inelastic action to occur in this region. Also, the footings are inaccessible beneath the ground and are generally deemed unfit for any ductile response either. Hence the selection of suitable and properly detailed plastic hinges is made to occur at the ends of the columns, where moments from lateral response are at a maximum.

To ensure against shear failure in a bridge, the shear strength of the bridge pier should be set higher than the shear corresponding to the maximum feasible flexural strength, taking into account overstrength factors for concrete and steel strengths as well steel strain hardening effects at large deformations. Thus, the design shear forces are not necessarily related to the design horizontal inertia forces specified by design codes and may exceed the latter by substantial margins, depending on the degree of conservatism in the flexural design. This process, known as Capacity Design, also ensures that significant variations in ductility demands from expected values can be accommodated without any loss of resistance to lateral loads.

Several methods for increasing the strength and/or ductility of bridge columns have been used in the past. These methods are aimed at upgrading the seismic performance of bridge columns, which have various typical structural deficiencies, so as to prevent collapse of all or part of the bridge. Some of the methods for enhancing the performance of bridge columns involve the use of reinforced concrete jackets containing longitudinal and transverse reinforcement, site-welded thin steel jackets filled with high-strength grout, fiber reinforced polymer wrapping, external hoops tensioned by turnbuckles, active confinement by wrapping with prestressed wire, and containment by a fiberglass/epoxy semi-active confinement jacket. Another alternate means of effective seismic retrofitting can be achieved by seismic isolation

techniques, especially if the superstructure is supported on columns by bearings which can be replaced by isolation devices to significantly reduce the seismic forces. Of these techniques, steel jacketing is the most widely used method to retrofit bridge columns (FHWA, 2006).

3.3.1 – Steel Jacketing

Previous research studies (Chai et al. 1991; Priestley and Seible, 1991) have shown that steel jacketing is an effective retrofit technique for seismically-deficient concrete columns. Based on satisfactory laboratory results, steel jackets have been employed to retrofit both circular and rectangular columns around the world. For circular columns, two half-circle steel shells, which have been rolled to a radius equal to the column radius plus $\frac{1}{2}$ in. to 1 in. (13 mm to 25 mm) for clearance, are positioned over the portion of the column to be retrofitted, and the vertical seams are then welded (FHWA, 2006). The space between the jacket and the column is flushed with water and then filled with a pure cement grout. To avoid any significant increase in the column flexural strength, a gap of approximately 2 in. (50 mm) is typically provided between the end of the jacket and any supporting member (e.g., footing, cap beam, or girders) since at large drift angles the jacket can act as a compression member as it bears against the supporting members (Chai et al., 1991; FHWA, 2006; Priestley et al., 1996; Endeshaw, 2008).

3.3.2 – Fiber Reinforced Polymer Wrapping

Recent developments in the manufacturing of fiber reinforced polymer (FRP) composite materials have made these materials available for a wide range of applications, including seismic retrofit of reinforced concrete columns. Compared to steel and concrete jacketing, FRP wrapping has several advantages, including very high strength-to-weight ratios, a high modulus of elasticity, resistance to corrosion, and ease of application. In addition, unidirectional FRP

wrapping can improve column ductility without considerable stiffness amplification, thereby maintaining the original dynamic properties of the bridge (Haroun et al., 2005).

Commonly employed FRP composite materials are carbon fiber reinforced polymer (CFRP), glass fiber reinforced polymer (GFRP) and aramid fiber reinforced polymer (AFRP). Most FRP materials exhibit nearly linear elastic behavior up to failure. In general, CFRP has a higher modulus of elasticity than AFRP or GFRP. In terms of tensile strength, CFRP has the highest strength, followed by AFRP and GFRP. Despite GFRP's lower mechanical properties, it is preferable for many civil engineering applications due to its lower cost (ACI 440, 2006; Xiao et al., 2003). However, the durability of GFRP is a concern for applications in wet environments, such as that of Western Washington. The *WSDOT Bridge Design Manual M 23-60* (2006) recommends using CFRP to retrofit bridge columns in Washington since it is less affected by moisture.

The California Department of Transportation (Caltrans) funded several research studies carried out at the University of California at San Diego to develop design guidelines for FRP retrofit systems. The findings and recommendations of these studies are given in *Suggested Revisions to Caltrans Memo to Designers 20-4 to Cover Fiberglass/Epoxy Retrofit of Columns* (SEQAD 1993), ACTT-95/08 (Seible et al., 1995) and Priestley et al., 1996. These documents present similar design equations with only minor differences. The FHWA's *Seismic Retrofitting Manual for Highway Structures* (2006) has adopted these design guidelines for application to circular columns.

Caltrans primarily uses steel jacketing to retrofit deficient columns, with composite fiber wrapping listed as an alternative. Composite material retrofitting is approved only for cases that have been verified through experimental testing. The Caltrans *Memo to Designers 20-4* (1996)

limits composite material retrofitting of rectangular columns with cross-sectional aspect ratios or 1.5 or less and a maximum dimension of 3 ft (1 m). Other restrictions include axial dead load not more than 15% of the column capacity, longitudinal reinforcement ratios of 2.5% or less, and a maximum displacement ductility of 3. The guideline also stipulates that rectangular columns with lap splices in a potential plastic hinge region must not be retrofitted with composite fiber unless slippage of reinforcing bars is allowed.

ACTT-95/08 provides design equations to determine the required jacket thickness for each mode of failure (i.e., shear failure, confinement failure and lap splice failure) (Seible et al., 1995). The shear strength of FRP wrapped columns can be calculated using the following equation:

$$V = V_C + V_S + V_{FRP} \quad (\text{Equation 3-1})$$

Where V_C is the shear strength of the concrete, V_S is the contribution of the transverse reinforcement, and V_{FRP} is the contribution of the FRP to the shear strength of the column. The shear contribution of the FRP can be calculated using Equation 3-2:

$$V_{FRP} = 2 * f_{jd} * t_j * D * \cot(\theta) \quad (\text{Equation 3-2})$$

In equation 3-2, t_j is the thickness of the FRP, D is the column dimension in the loading direction, and θ is the inclination of the shear crack of principal compression strut. The design stress level for the jacket, f_{jd} , is calculated to be less than the ultimate stress capacity of the composite material, f_{ju} , due to limitations by the concrete. When the dilation strain in the concrete exceeds 0.004, the contribution of the concrete to the shear capacity, V_C , decreases due to aggregate interlock degradation (Preistley et al., 1996). As shown in equation 3-3, the design stress of the FRP, f_{jd} , is therefore determined using an allowable strain of 0.004.

$$f_{jd} = 0.004E_j \quad (\text{Equation 3-3})$$

In equation 3-3, E_j , is the elastic jacket modulus in the hoop direction. After simplifying the previous equations, the required jacket thickness can be calculated as follows:

$$t_j = \frac{\frac{V_o}{\Phi} - (V_c + V_s)}{2f_{jd}D \cot \theta} \quad (\text{Equation 3-4})$$

V_o can be estimated as 1.5 times the shear capacity of the original column at a displacement ductility level, μ_Δ , of 1.0, and Φ is taken as 0.85 (Seible et al., 1995).

ACI 440 (2006) uses similar equations but with additional safety factors. The design stress of the FRP, f_{jd} , should not exceed $0.75\epsilon_{ju}E_j$, where ϵ_{ju} is the ultimate strain of the FRP and E_j is the modulus of elasticity of the FRP jacket. Besides the shear strength reduction factor, Φ , ACI 440 (2006) imposes an additional safety factor of 0.95 on the contribution of the FRP to the shear strength, V_{FRP} , to account for loss of strength over time.

CHAPTER FOUR

DESIGN, CONSTRUCTION AND TESTING PROCEDURES

4.1 – INTRODUCTION

This chapter provides details of the design and construction of five large-scale cruciform-shaped column specimens, comprising two as-built columns and three columns retrofitted with fiber-reinforced polymer (FRP) jackets. The specimens were constructed to be representative of the cruciform-shaped columns present in the Aurora Avenue Bridge located in Seattle, Washington and were expected to be vulnerable to shear failure.

4.2 – BRIDGE COLUMN DETAILS

As-built column details for the test specimens were based on “Bridge 99-560 Approach Span As-Built Plans” provided by the WSDOT. Material properties for the bridge construction were not available, so material properties were obtained from the 1931 *Standard Specification for Highway Bridges* (AASHTO, 1931). This standard required all concrete to have a minimum compressive strength at 28 days of 3500 psi (24 MPa) and steel reinforcement conforming to ASTM A15-30. Due to the strength gain of concrete with time, it was estimated that the concrete strength of the in-place concrete in the bridge would now be about 5000 psi (34 MPa). Information on ASTM A15-30 steel was found in “FEMA 356 – Prestandard for the Seismic Rehabilitation of Buildings”, which lists the yield strength of A15, Intermediate Grade steel as 40 ksi (276 MPa).

Details for the column specimens were modeled after columns in Bent N13 in the as-built plans. Figure 4.2.1 shows the column dimensions and reinforcement details for Bent N13.

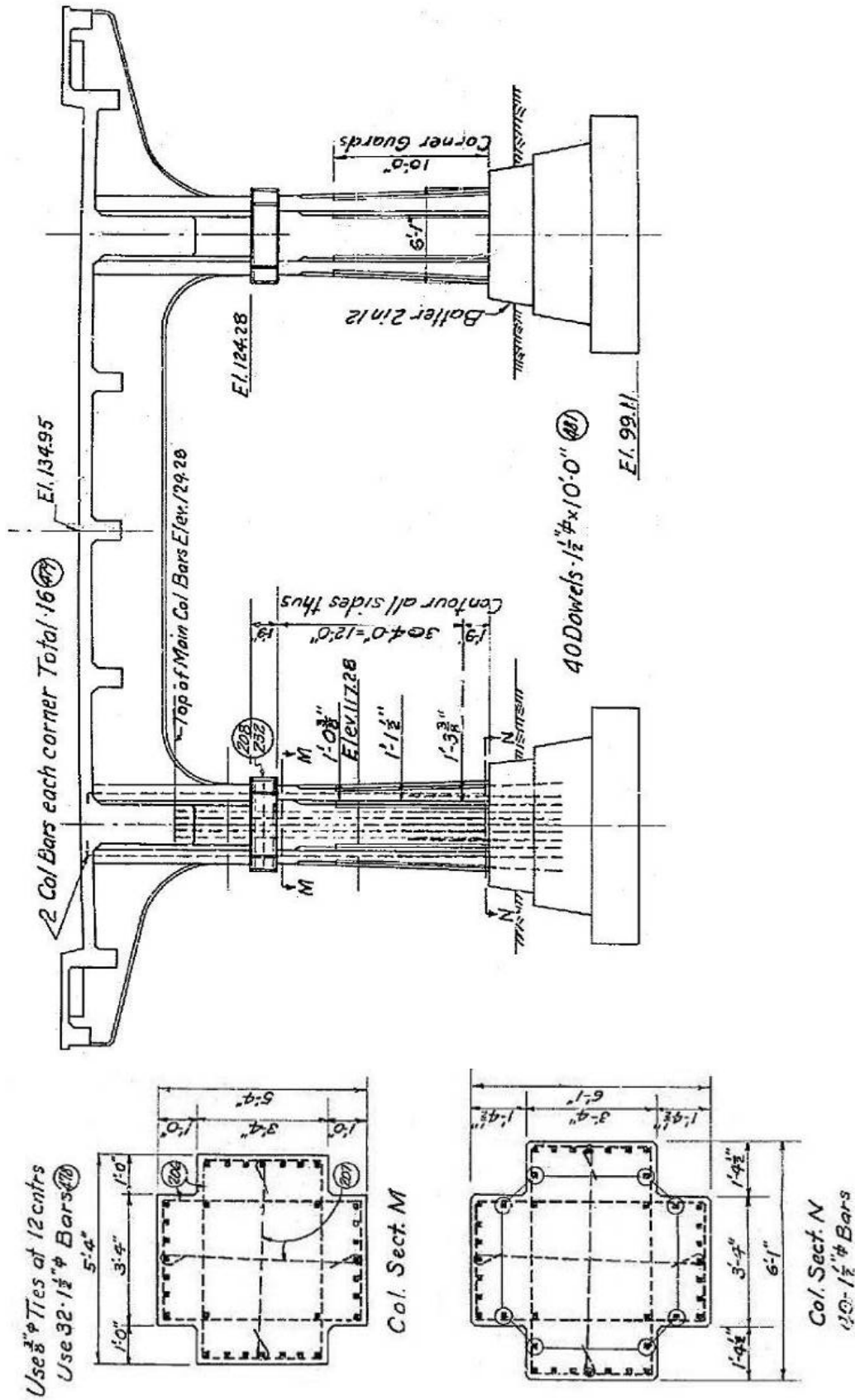


Figure 4.2.1 - Column As-Built Details (1 in. = 25.4 mm)

4.3 – SCALING PROCEDURE

Within the limits of available equipment and funding, the test columns were designed to be as large as possible. A geometric scale of $\frac{1}{3}$ (1:3) was adopted to model the prototype dimensions, reinforcement, detailing, and material properties. Table 4.3.1 illustrates the scaling process and includes relevant dimensions and reinforcement details for the test specimens.

Table 4.3.1: Dimensions for Bridge and Test Columns

Parameter	Bridge	Test Specimen
Width at base	6 ft 1 in. (1.85 m)	2 ft $\frac{3}{8}$ in. (0.62 m)
Width at top	5 ft 4 in. (1.63 m)	1 ft 9 $\frac{3}{8}$ in. (0.54 m)
Height	15 ft (4.6 m)	5 ft 6 in. (1.7 m)
Concrete Cover	2 in (51 mm)	$\frac{3}{4}$ in (19 mm)
Concrete Strength f'_c	5000 psi (35 MPa)	5000 psi (35 MPa)
Longitudinal Steel	A15-30 (40) 1½ in.x1½ in.	Grade 40 (40) No. 4
Transverse Steel	A15-30 No. 3 hoops @ 12 in. (0.3 m) o.c.	A36 $\frac{1}{4}$ -in. (6.5-mm) diameter hoops @ 4 in. (0.1 m) o.c.

The column height in the bridge is 15 ft (5 m) neglecting the height of the load stub at the top of the column. This load stub was not modeled to simplify testing. However, in reality the center of fixity of the column will occur somewhere within the load stub instead of at the top of the column. To account for this, the height of the column test specimens was set at 5.5 ft (1.7 m), 6 in. (0.2 m) higher than the equivalent height of the column in the bridge.

The longitudinal steel in the bridge consists of (40) 1½ in. x 1½ in. (38 mm x 38 mm) square bars. No equivalent bar diameter is available for the scaled test specimens, so (40) No. 4 rebars were used, which resulted in a 21.5% decrease in the amount of flexural reinforcement in

the test columns. The tested yield strength of the test column longitudinal bars was approximately 48 ksi (331 MPa), 20% higher than the required yield strength of Grade 40 steel. Taking into account the higher yield strength resulted in longitudinal steel in the test columns that was effectively only 5.8% less than the equivalent steel in the columns of the bridge. Because it was determined shear failure would govern the column capacity, this distortion in the model column was deemed acceptable.

The transverse steel in the bridge columns consisted of No. 3 hoops spaced at 12 in. (0.3 m) on center. An equivalent area of steel in the test columns would be $\frac{1}{8}$ -in. (3-mm) diameter hoops spaced at 4 in. (0.1 m) on center. Placing strain gages on $\frac{1}{8}$ -in. (3-mm) diameter bar would be very difficult, so the size of the transverse steel in the test columns was increased to $\frac{1}{4}$ -in. (6-mm) diameter bar in order to obtain accurate strain gage measurements. To account for the increased area of steel, A36 bar was used in place of Grade 40 steel. This resulted in a transverse steel capacity that was significantly higher than in the bridge; however, the contribution to shear strength of the No. 3 hoops at 12 in. (0.3 m) on center in the bridge is small in comparison to the overall shear strength of the column so the distortion in scaling of the hoops should not significantly alter the shear strength of the test columns.

4.4 – SPECIMEN DESCRIPTION

4.4.1 – Footing Description

All specimens were constructed on heavily-reinforced footings. Footings of the same size and having the same reinforcement were used for all column specimens. The footings were 66 in. (1.7 m) long, 32 in. (0.81 m) wide, and 20 in. (0.51 m) tall. The footings were designed to provide a rigid support at the base of the columns and were anchored to a laboratory strong floor through eight high-strength bolts running through PVC tubes that were cast into the footings.

Footings reinforcement consisted of a top and bottom mat of (7) No. 6 straight bars with 90° hooks, (2) No. 6 straight bars with 90° hooks on each face, (11) No. 5 hoops, (44) No. 5 cross-ties, and (2) pairs of No. 6 diagonal bars placed adjacent to the critical column/footing region as shown in Figure 4.4.1. All footing reinforcement was Grade 60 steel. Four lifting hooks were installed near the ends of the footings so that specimens could be moved with an overhead crane.

4.4.2 - Column Description

Figure 4.4.2 shows the details of the column specimens. Longitudinal reinforcement consisted of (40) No. 4 Grade 40 rebars distributed around the perimeter of the column with (7) bars on each face and (3) bars in each reentrant corner. (2) bars in each reentrant corner were terminated at 3 ft (1 m) above the top of the footing. All other longitudinal reinforcement extended into both the top load stub and the footing. Unlike the columns in the bridge, there was no lap splice between the footing and column reinforcement in the test columns. Transverse reinforcement consisted of ¼-in. (6-mm) diameter, A36 hoops and crossties at 4 in. (0.1 m) on center. A cover of ¾ in. (19 mm) was provided for the column reinforcement as compared to 2 in. (51 mm) in the bridge.



4.4.3 - Load Stub Description

A heavily-reinforced load stub was constructed at the top of the column specimen in order to attach the loading frame to the specimen. Figure 4.4.1 shows the layout of reinforcement in the loading stub. The top load stub contained (30) No. 5 Grade 60 straight bars with 90° hooks running in the horizontal direction and evenly distributed around the top load stub. (8) No. 5 Grade 60 hoops and (16) No. 5 Grade 60 crossties were provided in the vertical direction. (4) 3-in. (76 mm) diameter standard steel pipes were cast into the load stub to connect the load stub to the load frame. (3) No. 6 Grade 60 hairpins were provided between each of the four steel pipes to resist the design shear and the torsion force developed at the four steel pipe locations due to the column top moment and applied shear forces, as shown in Figure 4.4.3. These hairpins were provided in both the horizontal and vertical directions for a total of (12) hairpins, which provided a lateral tension capacity of 158 kips (703 kN) at each bend. This was considered to be adequate to resist the worst possible case shown in Figure 4.4.3, where a maximum likely shear force, V , equal to 120 kips (534 kN), and an equivalent moment, M , equal to 427 k-ft (579 kN-m) at the center of the load stub, resulted in a maximum possible value of T_x equal to 98 kips (436 kN) at each bend.

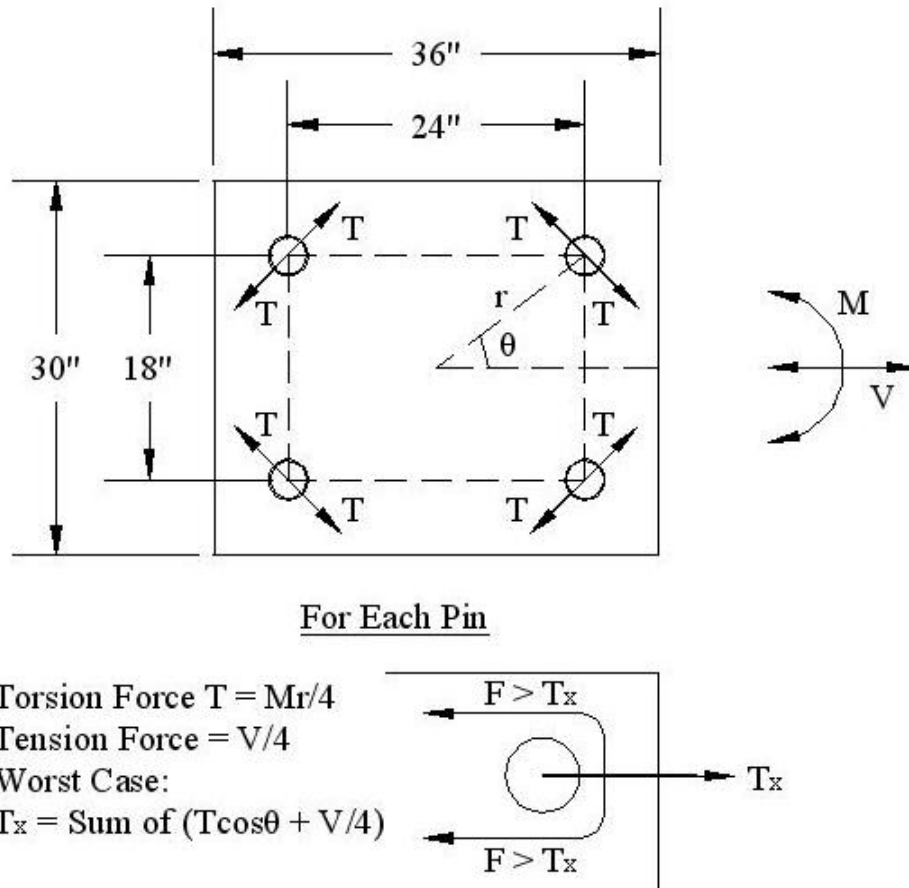


Figure 4.4.3 – Torsion Design in Top Load Stub (1 in. = 25.4 mm)

4.4.4 – Retrofit Details

Two column specimens were tested without any retrofitting to reveal vulnerabilities present in the existing columns and to establish benchmarks for evaluating the effectiveness of the applied retrofit measures. All other columns were wrapped with two layers of 0.014-in. (0.36-mm) thick commercially-available FRP fabric with primary fibers oriented in the horizontal direction. One retrofitted column was tested without reentrant corner anchorage to evaluate whether such anchorage was necessary to fully engage the FRP jacket. Reentrant corner anchorage was provided for the other two retrofitted columns. Table 4.4.1 summarizes the retrofit test parameters being analyzed in each test column.

Table 4.4.1 – Retrofit Test Parameters

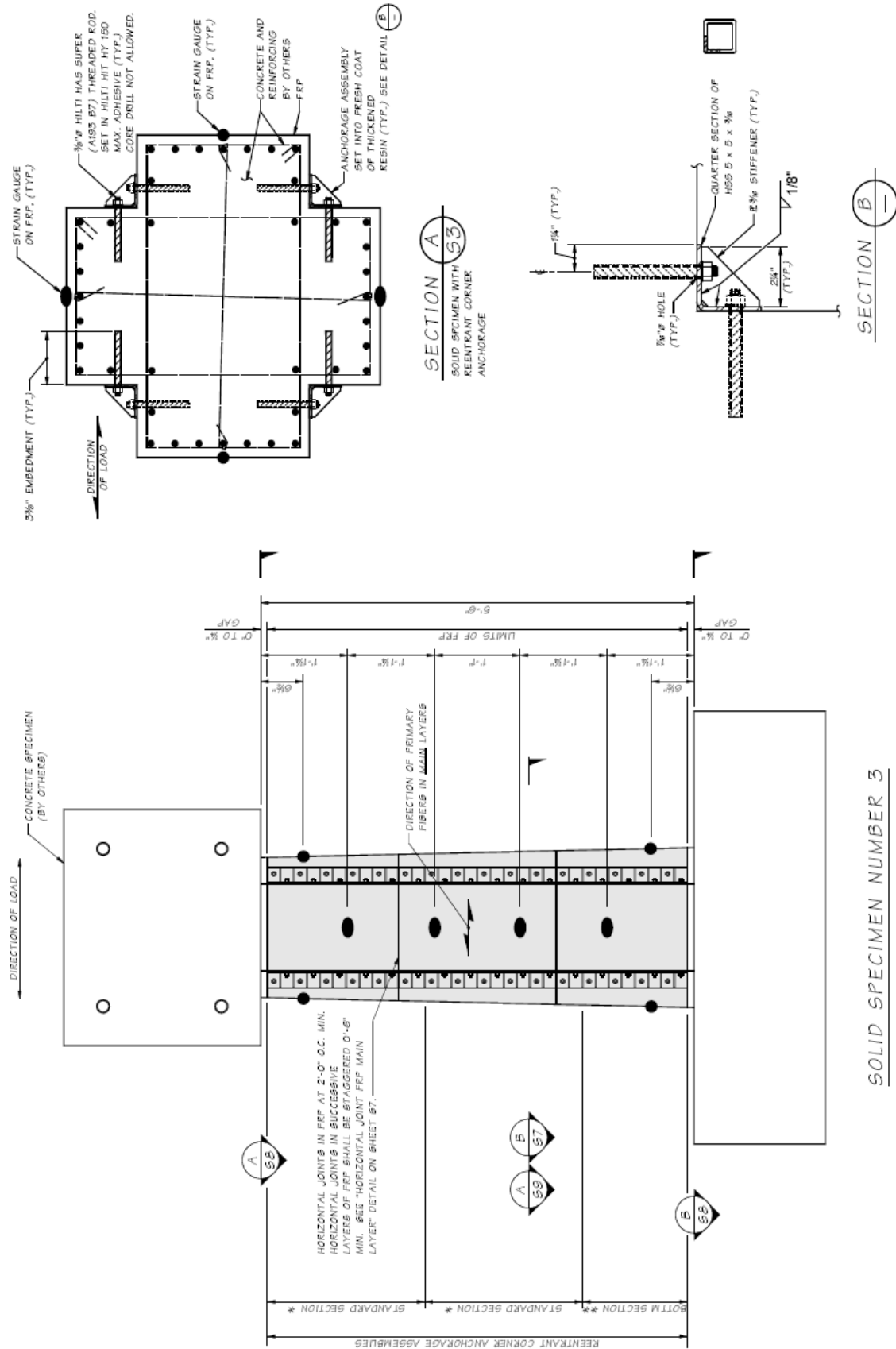
Specimen #	FRP Wrap	Reentrant Corner Anchorage
1		
2	X	
3	X	X
4	X	X
5		

A dry lay-up method in accordance with the manufacturer's recommendations was used to install the FRP wrap on Columns 2 and 3. To avoid stress concentrations in the FRP jacket, the corners of the columns were rounded to a minimum $\frac{3}{4}$ -in (19 mm) radius before the FRP wrap was applied. The FRP application procedure consisted of first coating the column with a layer of epoxy followed by applying the dry FRP fabric in the arrangement shown in Figure 4.4.4. After the fabric was in place, a second layer of epoxy was applied to the column. This process was repeated for the second layer of FRP wrap. A wet lay-up method was used to install the FRP wrap on Column 4 in accordance with recommendations from the anchorage manufacturer. This procedure was similar to the dry lay-up except that no epoxy was applied to the column prior to installing the FRP fabric. Instead, the dry FRP fabric was saturated with epoxy on the ground and then applied to the column. Also, no additional epoxy was applied to the column in between FRP layers except to smooth out irregularities around the corner anchorages.

The reentrant corner anchorage for Column 3 consisted of a $\frac{3}{8}$ -in. (10-mm) thick steel bent plate with $\frac{3}{16}$ -in. (5-mm) stiffener plates at 2 in. (51 mm) on center. Figure 4.4.4 shows the corner anchorage as a quarter-section of HSS tube; however, this was later changed to a bent plate due to residual stresses present in the HSS section which caused it to warp when cut. $\frac{7}{16}$ -in. (11-mm) diameter anchor bolts holes were drilled through the FRP wrap extending $3\frac{3}{8}$ in. (86

mm) into the concrete column. These anchor bolt holes were staggered at 4 in. (0.1 m) on center up each face of the reentrant corners. The steel plate was predrilled with ½-in. (13-mm) diameter holes at 4 in. (0.1 m) on center and anchored to the column using A 193 B7 threaded rod anchors with 3¾-in. (86-mm) embedment and epoxy adhesive as shown in Figure 4.4.4. The reentrant corners for this specimen were also reinforced with two additional layers of FRP oriented at 45° from the horizontal and filled with thickened epoxy resin to a minimum 1-in. (25-mm) radius.

The reentrant corner anchorage for Column 4 consisted of ½-in. (13-mm) diameter FRP anchors as shown in Figure 4.4.5. These anchors were installed at 4 in. (0.1 m) on center up each face of the reentrant corners. The anchors were designed assuming they were effective only in tension (Ozbakkaloglu et al. 1996). Shear strength of the FRP anchors was neglected, and thus anchors were proportioned to carry the full anchorage demand in tension on one face of the reentrant corner. Prior to installation of the first layer of FRP, 7/16-in. (11-mm) diameter anchor holes extending 5 in. (0.13 m) into the concrete column were drilled and filled with epoxy and the reentrant corner of the column was filled with epoxy to a minimum ¾-in. (19-mm) radius. After installation of the first FRP jacket layer, the dry FRP anchors were soaked in epoxy and then pushed through a small cut in the FRP jacket. The end fibers of the FRP anchors were then splayed out and laid flat onto the surface of the FRP jacket as shown in Figure 4.4.6. After the FRP anchors were installed, a coating of epoxy was applied over the top of the anchors to fill any voids between anchor locations. The second FRP jacket layer was then applied. Following installation of the FRP jacket, a ¼-in. (6-mm) thick by 6-in. (0.15-m) tall A36 steel collar was installed at the top and bottom of the column and filled with high-strength non-shrink grout. A 1-in. (25-mm) gap was provided between the collars and the footing and top loading blocks.



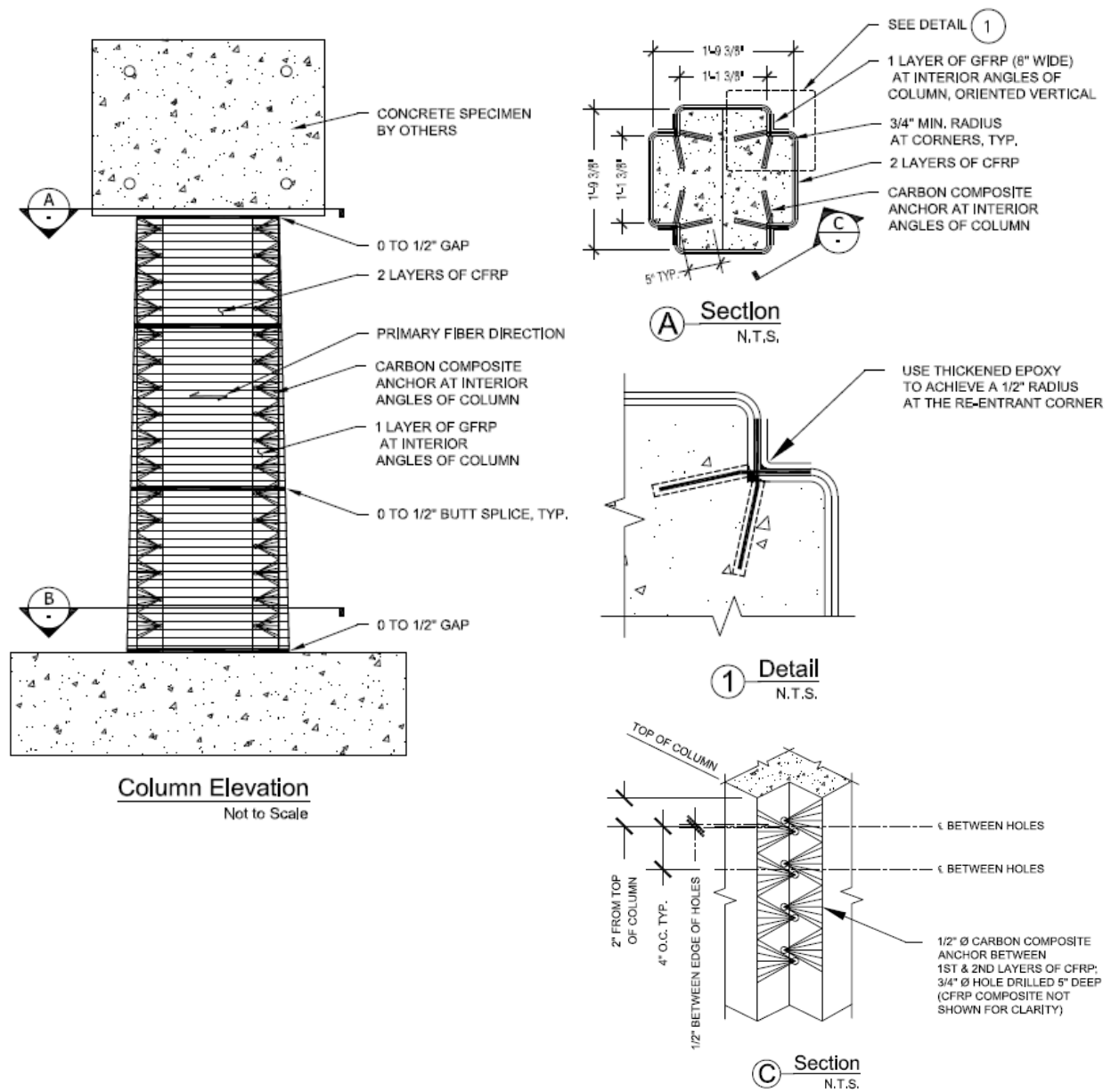


Figure 4.4.5 – FRP Anchor Retrofit Details (1 in. = 25.4 mm)



Figure 4.4.6 – FRP Anchor Installation

4.5 – MATERIAL PROPERTIES

A summary of the material strengths for each column specimen is provided in Table 4.5.1. The target concrete strength for the test columns was 5000 psi (35 MPa). Test specimens 1, 2 and 5 were built with concrete with strengths significantly below that value. The concrete compressive strength was determined by averaging the results for three 6-in (0.15-m) diameter cylinders tested at 100 days.

The Grade 40 No. 4 longitudinal rebar had an average measured yield strength of 48 ksi (331 MPa). The A36 $\frac{1}{4}$ -in. (6-mm) diameter transverse hoops had an average measured yield strength of 62 ksi (427 MPa). The cured FRP composite had a specified ultimate strength of 150 ksi (1035 MPa) and a specified elastic modulus of 10,100 ksi (69,600 MPa). The specified ultimate strength of the FRP anchors was 108 ksi (745 MPa).

Table 4.5.1 – Material Strengths of Components for Test Columns

Column #	f'_c (at 100 days) psi (MPa)	f_{yl} (rebars) ksi (MPa)	f_{yh} (hoops) ksi (MPa)	f_{uf} (FRP) ksi (MPa)	f_{ua} (FRP) ksi (MPa)
1	3215 (22.2)	48 (331)	62 (427)	-	-
2	3156 (21.8)	48 (331)	62 (427)	150 (1035)	-
3	5465 (37.7)	48 (331)	62 (427)	150 (1035)	-
4	4881 (33.6)	48 (331)	62 (427)	150 (1035)	108 (745)
5	3892 (26.8)	48 (331)	62 (427)	-	-

4.6 – ESTIMATION OF TEST COLUMN STRENGTHS

The estimated shear strength of the as-built column specimens were approximated using the shear strength provisions found in ACI 318-08. The additional shear strength provided by the FRP jacket was calculated using FHWA provisions. The applicable equations for the various components of shear strength are as follows:

$$V_c = 2 * \sqrt{f'_c} * b_w * d$$

$$V_s = A_v * f_y * (d/s)$$

$$V_{FRP} = 2 * f_{jd} * t_j * D * \cot(\theta)$$

A summary of the estimated shear strength for each column specimen is provided in Table 4.6.1.

Table 4.6.1 – Estimated Shear Strength of Test Columns

Column #	V_c kips (kN)	V_s kips (kN)	V_{FRP} kips (kN)	V_n kips (kN)	ΦV_n kips (kN)
1	35.8 (159)	53.9 (240)	-	89.8 (399)	67.3 (299)
2	35.5 (158)	53.9 (240)	90.6 (403)	180.0 (801)	135.0 (601)
3	46.7 (208)	53.9 (240)	90.6 (403)	191.2 (851)	143.4 (638)
4	44.2 (196)	53.9 (240)	90.6 (403)	188.7 (839)	141.5 (629)
5	39.4 (175)	53.9 (240)	-	93.3 (415)	70.0 (311)

4.7 – SPECIMEN CONSTRUCTION

Test specimens were constructed by Central Pre-Mix Prestress Co. in Spokane, Washington. Column rebar and top load stub cages were tied horizontally on the ground and then lifted into the concrete formwork. The column and top load stub were cast monolithically, horizontally on the ground. After one day, the forms were stripped and the footing rebar cage was tied onto the finished column. The entire column was then lifted into the footing formwork and the footing concrete placed with the column standing vertically.

Air pockets up to $\frac{1}{4}$ - in. (6-mm) deep formed on the uppermost face of the column during concrete pouring due to the unique nature of the formwork and the inability of air to escape. These blemishes were then patched and did not significantly affect the strength of the finished column.

4.8 – TEST SETUP

The test setup for the column specimens was adapted from testing performed at the University of California at San Diego. Figure 4.8.1 shows the overall shear test setup, which was designed to load the test columns in double bending.

A moment-curvature analysis of the top and bottom cross sections of the column was used to locate the point of zero moment in the test column. A stiff loading frame connected the column top block to a horizontal double-acting actuator aligned at the point of zero moment, inducing double bending in the column specimen. An articulating clevis provided the connection between the loading frame and the actuator through a 220 kip (980 kN) load cell. The actuator was then fixed to a strong reaction frame at the other end, which was bolted to the strong floor. The force capacity of the actuator was 330 kips (1470 kN) in compression, and 220 kips (980 kN) in tension, with an available stroke of 20 in (0.5 m). The columns framed into a 32 in. (0.8

m) x 20 in. (0.5 m) x 66 in. (1.7 m) strong footing at the base and into a 30 in. (0.8 m) x 36 in. (0.9 m) x 30 in. (0.8 m) heavily reinforced load stub at the top. Moment was transferred through the loading frame into the top load stub by means of the 3-in. (76-mm) diameter steel pipes located in the load stub. The footing was bolted to the strong floor using (8) 1¼-in. (32-mm) diameter bolts to prevent any overturning from occurring. Sliding of the footing base was prevented by two stiff brackets which were bolted to the floor, each using (4) 1¼-in. (32-mm) diameter bolts. Load stub eccentricity was compensated for by a load balancing system which included a load-follower jack with a 6-in. (0.15-m) travel in each direction, which balanced the extra bending moment transmitted to the load stub and column due to the self-weight of the large loading arm and half of the weight of the actuator.

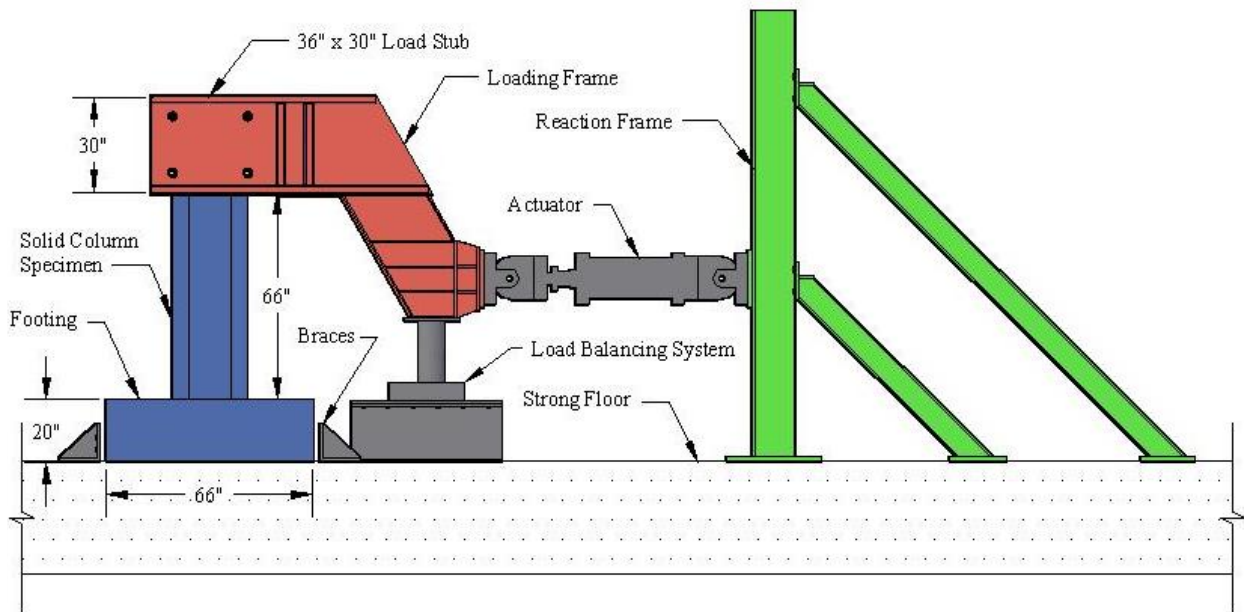


Figure 4.8.1 – Test Setup (1 in. = 25.4 mm)

4.8.1 – Design Considerations for the Test Setup

The design of the top load stub was governed by a no damage criteria. (4) 3-in. (76-mm) diameter standard steel pipes, together with 1½-in. (38-mm) thick steel side plates, formed the initial skeleton of the top load stub. The diameter of the pipes was chosen so as to provide minimum clearance between the steel pins connecting the load stub and the loading arm. A ⅛ in. (3 mm) clearance between the pipes and the steel pins was deemed as practically feasible and together with shim plates would prevent any loss of moment transfer under cyclic loading.

The loading frame (see Figure 4.8.1) was made up of two steel plates extending horizontally from the top load stub and connected by a double I-beam extending downwards. The double I-beam was inclined to the vertical at an angle of thirty degrees and reinforced with web stiffeners. The inclined beams framed into the load cell and the actuator aligned with the neutral axis of the column. No buckling was allowed in any part of the loading frame, this being achieved by the use of several stiffener plates. Details of the design of the loading frame are provided in Appendix A.

The load balance system was designed to balance the moment imparted onto the column by the 5.03 kips (22 kN) of loading arm weight. A constant pressure of 200 psi (1.4 MPa) was maintained in the load-balancing system to provide the uplift pressure necessary to achieve this balance. A 6-in. (0.15-m) travel on the load follower in either direction allowed the jack to match the column top displacement.

4.9 – INSTRUMENTATION

All test columns were instrumented with 28 strain gages mounted on the longitudinal and transverse reinforcement in the column. Retrofitted columns were instrumented with an additional 14 strain gages mounted on the FRP jacket. 120 Ohm strain gages, having a nominal

length of $\frac{1}{4}$ in. (6 mm), were used for longitudinal steel strain measurements. Similar gages having a nominal length of $\frac{1}{8}$ in. (3 mm) were used for transverse reinforcement steel strain measurements. Manufacture-prescribed procedures were followed for mounting these strain gages, starting from grinding the rebar surface, using sand paper to make the surface smooth, cleaning the surface with acid, applying a neutralizer, and finally wiping the surface dry. A super glue was used as a bonding agent, and gages were tested for electrical connectivity following application of several water-proofing agents and a nitrile rubber coating for mechanical protection.

For the FRP jacket, 120 Ohm strain gages, having a nominal length of $\frac{1}{4}$ in. (6 mm), were used. The surface of the FRP jacket was cleaned and wiped dry before a super glue was used to bond the strain gages to the FRP jacket.

4.10 – TEST PROCEDURES

All test columns were tested under displacement control and were subjected to the cyclic pattern of loading shown in Figure 4.10.1. Displacements were applied at a constant rate of 0.005 in./s (0.13 mm/s) for three complete cycles at displacement levels of ± 0.33 , ± 0.67 and ± 1 times Δ_y , then increased to a constant rate of 0.01 in./s (0.26 mm/s) for three complete cycles at displacement levels of ± 1.5 , ± 2 , ± 3 , ± 4 , ± 5 , ± 6 , ± 8 , ± 10 , ± 12 , ± 14 , ± 16 , ± 18 and ± 20 times Δ_y , unless failure occurred first. Failure was defined as a 20% drop in peak lateral load for each specimen. Δ_y was theoretically determined from moment-curvature analyses of each test column.

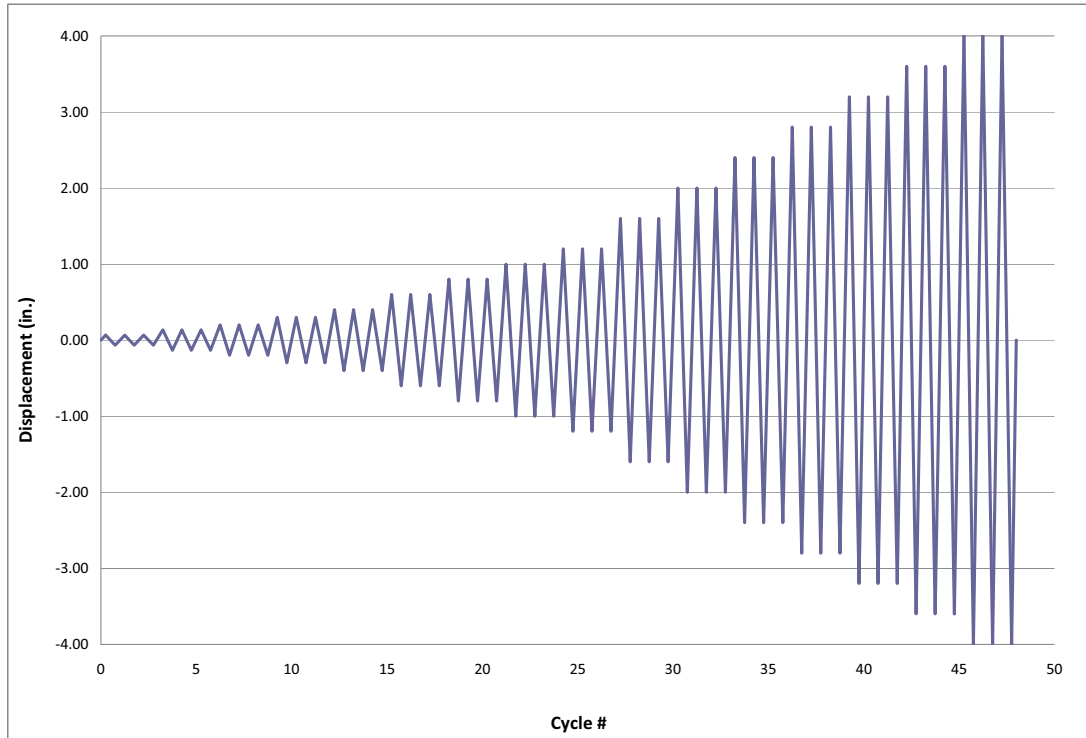


Figure 4.10.1 – Loading Protocol: Sequential Displacements (1 in. = 25.4 mm)

CHAPTER FIVE

TEST RESULTS

5.1 – INTRODUCTION

This chapter presents the experimental results from cyclic tests of five large-scale cruciform-shaped columns. Discussion of the test results for the as-built columns is provided first, followed by discussion of the test results for the retrofitted columns and a comparison of the as-built and retrofitted column results. Column performance is assessed with respect to the overall hysteretic behavior, shear strength, failure mode and any observable characteristics such as crack patterns. Other aspects considered for the case of the as-built columns are the lateral hoop strain variation along the column height and longitudinal bar strains at the top and bottom of the column. For the retrofitted columns, in addition to the above aspects, FRP jacket strains corresponding to the shear and confinement effects are also considered.

5.2 – BEHAVIOR OF AS-BUILT COLUMN 1

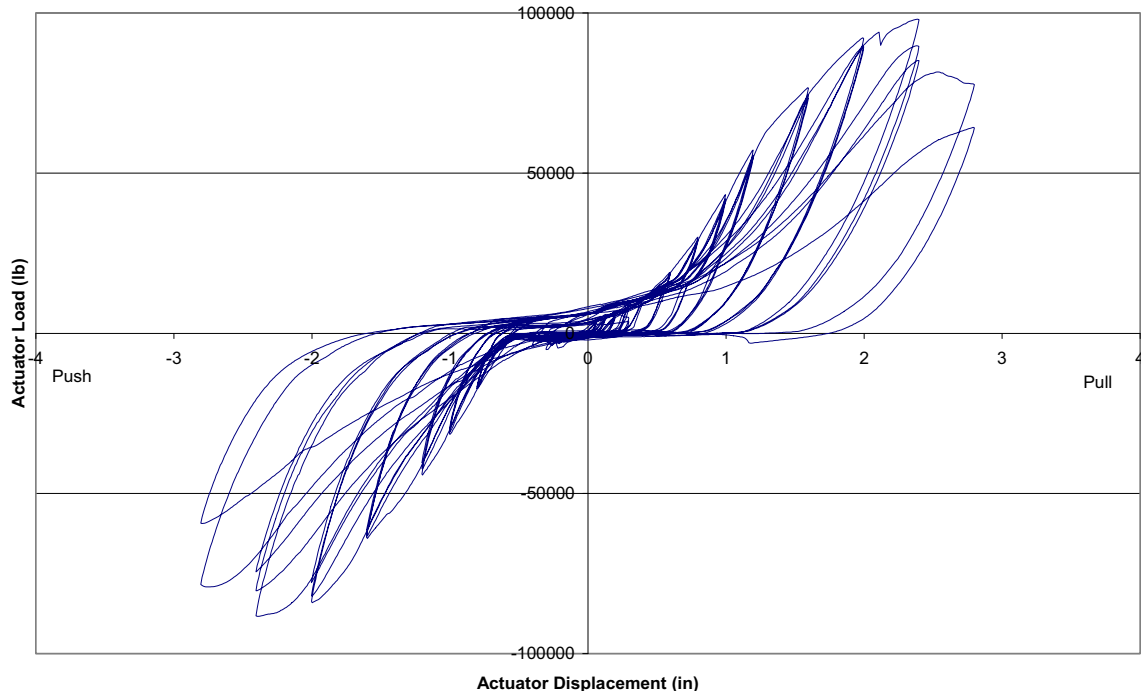
Column 1 was the first column to be tested in this project and was designed to be representative of typical as-built column conditions with deficient transverse reinforcement. The shear reinforcement was comprised of $\frac{1}{4}$ -in. (6-mm) diameter hoops at 4 in. (0.1 m) spacing, and the theoretical relative strength index (defined as the ratio of the theoretical column shear strength to the shear force corresponding to the theoretical ideal flexural capacity of the column) for this specimen was equal to 1.06. Thus, initially stable flexural response followed by shear failure with limited ductility was expected. The performance of this column was intended to reveal the vulnerabilities in the existing columns and establish benchmarks for evaluating the effectiveness of the applied retrofit measures.

5.2.1 – Overall Response

Figure 5.2.1 shows the overall hysteretic performance of Column 1 in terms of the lateral force vs. actuator displacement. The displacements shown in Figure 5.2.1 include unintentional displacements due to gaps between the steel pipes cast into the load stub and the steel loading rods used to connect the loading frame. These gaps were intended to provide construction tolerances for placing the loading rods, but also resulted in flat spots in the hysteresis curves. i.e., displacements under zero lateral force. These unintended displacements were later removed from the data for the purpose of comparing results with other tests. Shims between the steel pipes in the load stub and the loading pins were also installed in later tests to minimize these unintended displacements.

Column 1 exhibited moderate energy dissipation capacity but little ductility. The stiffness of the column showed minor degradation up to a displacement level of 1.2 in. (30 mm), with a loss in stiffness at later displacement levels up to the peak load. The peak lateral load achieved was 98 kips and occurred at a lateral displacement of 2.4 in. (61 mm). The column exhibited a significant decrease in lateral stiffness and strength at a displacement level of 2.8 in. (71 mm), and the applied load dropped below 80% of the peak load during the first cycle at this displacement. The test was stopped after the second cycle at a displacement level of 2.8 in. (71 mm).

Figure 5.2.2 shows Column 1 at the beginning of the test. Yielding of the longitudinal bars first occurred at lateral force level of 27 kips (120 kN) followed by flexural cracking at the top and bottom of the column. Early shear cracks formed at a lateral force level of about 65 kips (290 kN). Yielding of the transverse reinforcement first occurred at a lateral force level of 88 kips (390 kN) followed by the opening of large shear cracks near the end of the test. The final failure mode for the column was a shear failure. Figure 5.2.3 shows the large shear cracks present near the end of testing.



. Figure 5.2.1 – Column 1 Lateral Load vs. Displacement Hysteresis Curves (1 kip = 4.45 kN, 1 in. = 25.4 mm)



Figure 5.2.2 – Column 1 Test Setup

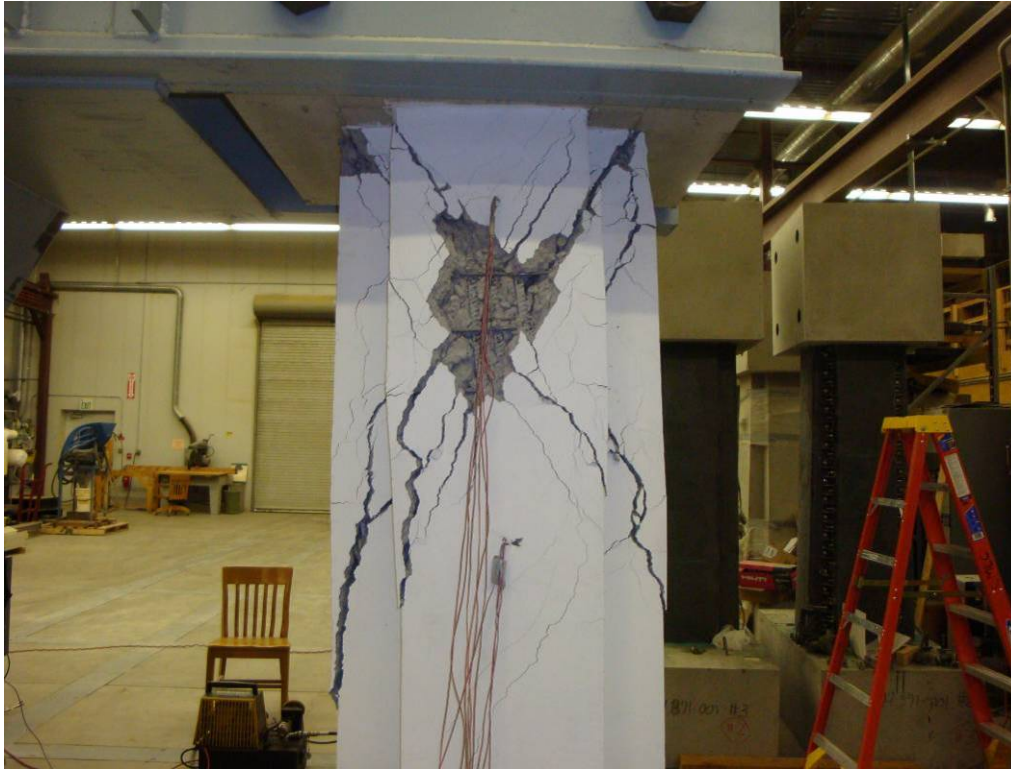


Figure 5.2.3 – Column 1 Shear Cracking Near the End of Testing.

5.2.2 – Reinforcement Strain Plots

(a) Transverse Hoop Strains

Figure 5.2.4 shows transverse hoop strains with time alongside a plot of the column load with time. Very small hoop strains were observed up to a displacement level of 1.6 in. (41 mm). During the first cycle at a displacement level of 1.6 in. (41 mm), the peak lateral force achieved was 65 kips (290 kN) and the first shear cracks appeared in the column. Strain gage 2, located slightly above the column mid-height, recorded strain values near yielding, while small strains were observed in all other strain gages. Hoop strains increased linearly in strain gages 1 and 4, located near the top and bottom of the column, respectively, up to the yield point at a displacement level of 2.4 in. (61 mm). Very large hoop strains were observed beyond the third cycle at a displacement of 2.4 in. (61 mm), corresponding to the opening of large shear cracks in the column.

(b) Longitudinal Bar Strains

Figures 5.2.5 and 5.2.6 show the strains in the longitudinal bars at the top and bottom of the column, respectively. Approximately a linear strain profile was observed in the top strain gages up to the first yield at a displacement level of 1.6 in. (41 mm). After yielding, strains stayed nearly constant until the first cycle at a displacement level of 2.4 in. (61 mm), after which very large strains in excess of 15,000 $\mu\epsilon$ were observed. Strains in the bottom strain gages reached first yield at a displacement level of about 0.8 in. (20 mm), much earlier than the top strain gages. Strains stayed nearly constant up to a displacement level of 1.6 in. (41 mm) and then increased rapidly to strains in excess of 5,000 $\mu\epsilon$ for the remainder of the test.

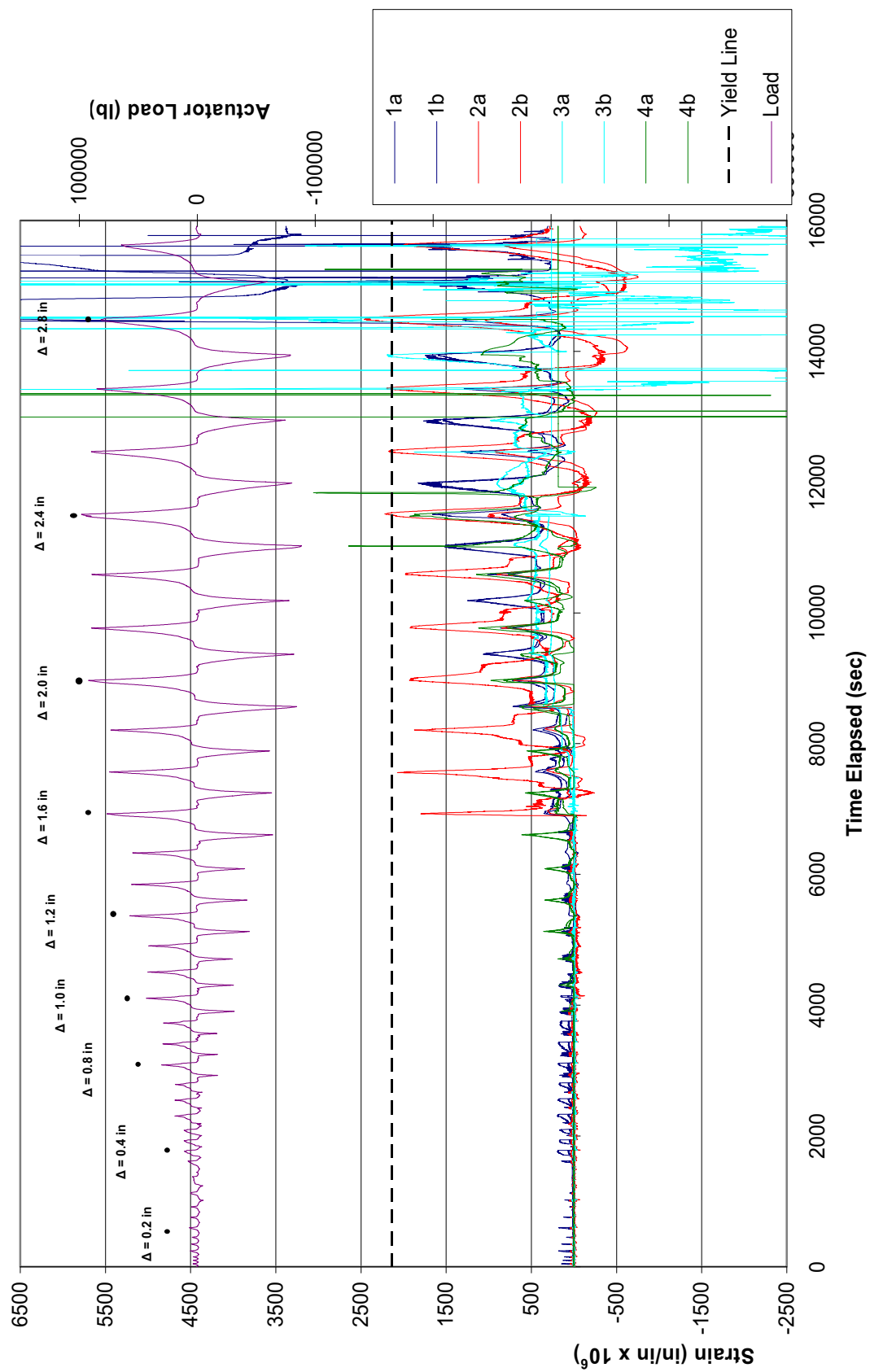


Figure 5.2.4 – Column 1 Transverse Strain Gage Data (1 kip = 4.45 kN, 1 in. = 25.4 mm)

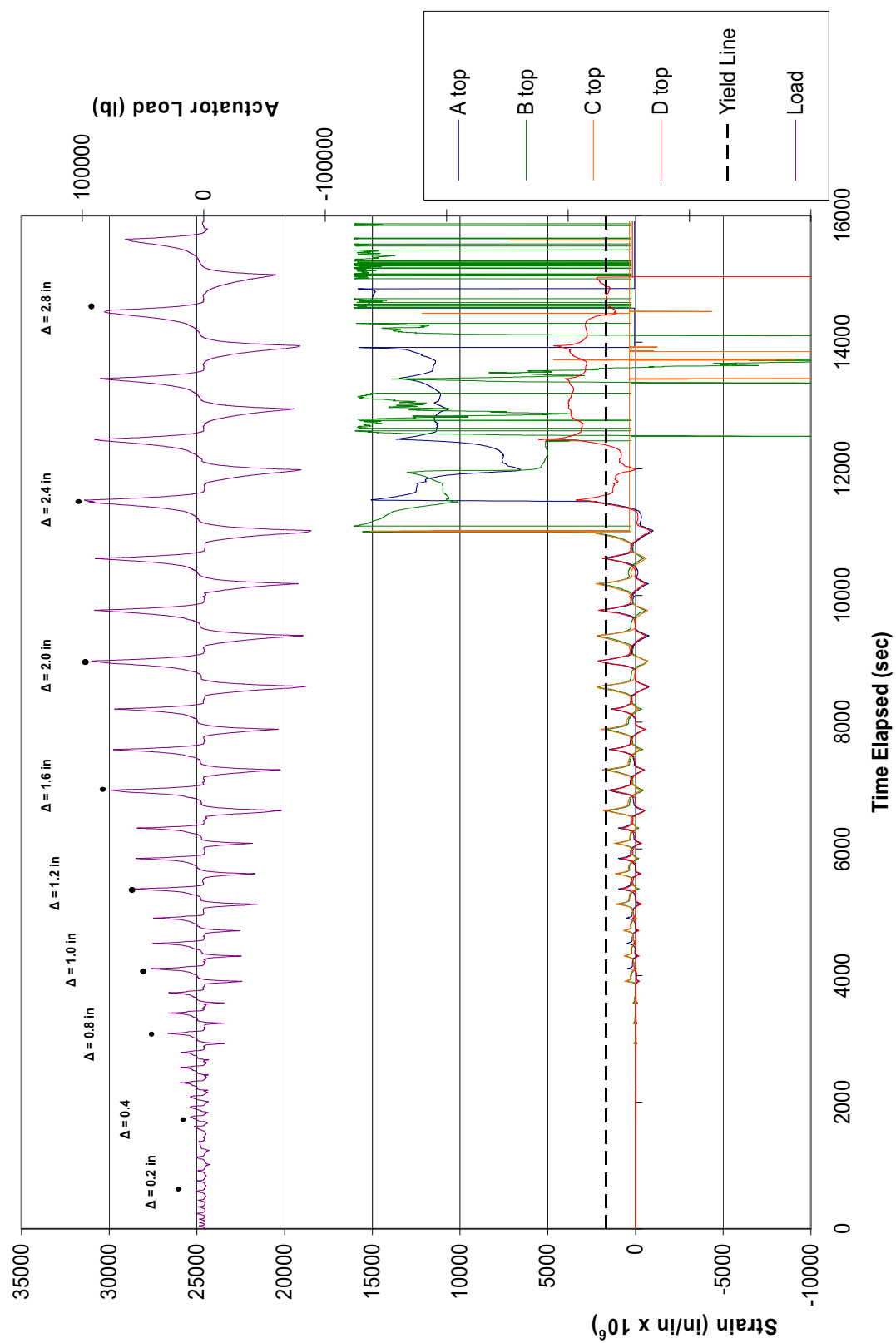


Figure 5.2.5 – Column 1 Longitudinal Bar Strain Gage Data at the Top of the Column (1 kip = 4.45 kN, 1 in. = 25.4 mm)

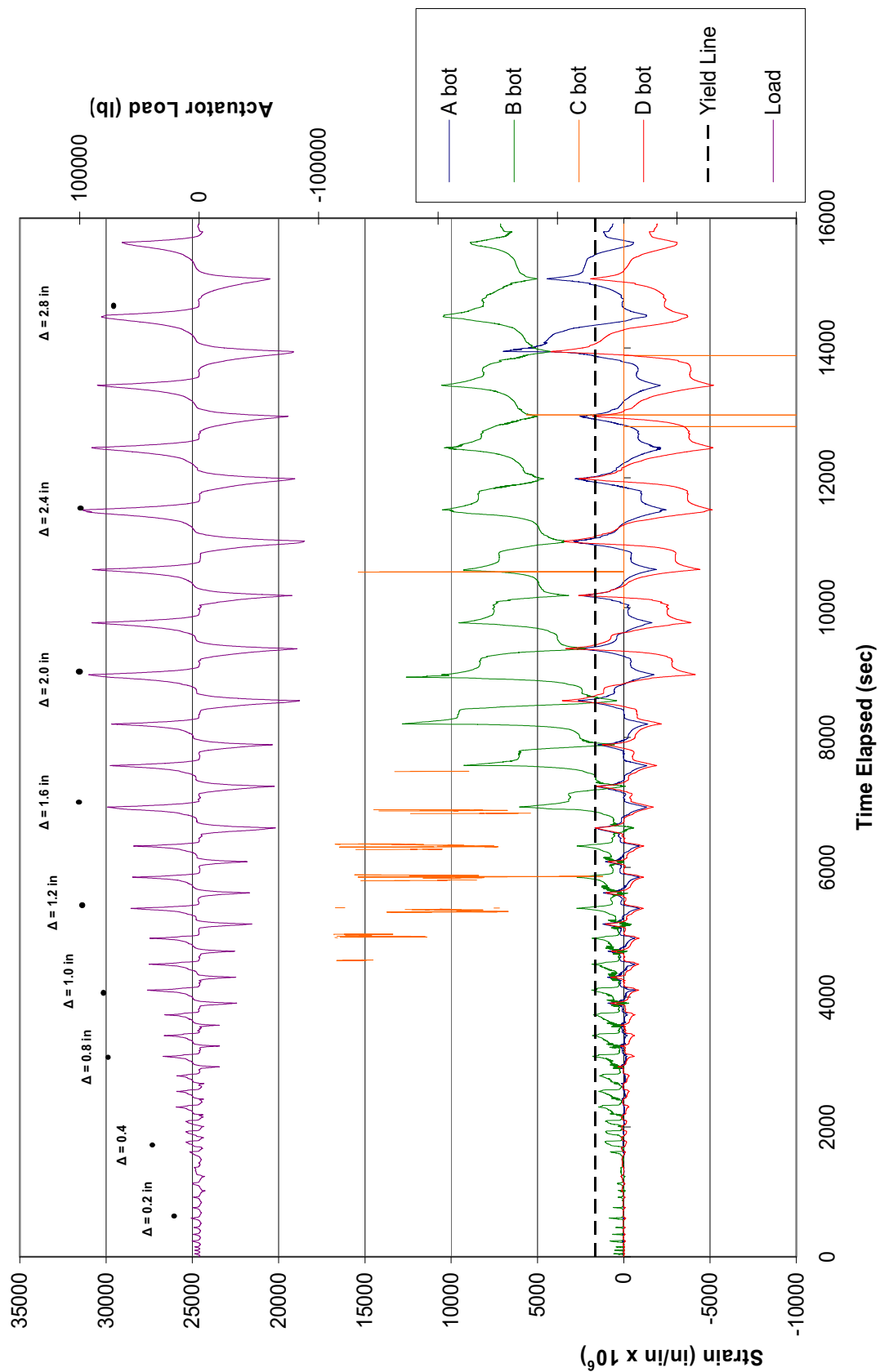


Figure 5.2.6 – Column 1 Longitudinal Bar Strain Gage Data at the Bottom of the Column (1 kip = 4.45 kN, 1 in. = 25.4 mm)

5.3 – BEHAVIOR OF AS-BUILT COLUMN 5

Column 5 was the last column to be tested in this project and was identical to Column 1. The only difference was the installation of shims between the column top block and the loading frame to remove unintentional actuator deflection and rotation. The purpose of this test was to determine if the presence of shims would impact the flexural response of the column as well as to provide a measure of the consistency in results from two nominally identical test columns.

5.3.1 – Overall Response

Figure 5.3.1 shows the overall hysteretic performance of Column 5 in terms of the lateral force vs. actuator displacement. The column exhibited moderate energy dissipation capacity but little ductility. The stiffness of the column showed minor degradation up to a displacement level of 1.2 in. (30 mm), followed by a loss in stiffness at later displacement levels up to the peak load. The peak lateral load achieved was 102 kips (453 kN) and occurred at a lateral displacement of 2.0 in. (51 mm). The column exhibited a significant decrease in lateral stiffness and strength at a displacement level of 2.0 in. (51 mm), and the applied load dropped below 80% of the peak load during the third cycle at this displacement. The test was stopped after the third cycle at a displacement level of 2.4 in. (61 mm).

Figure 5.3.2 shows Column 5 in the test setup at the beginning of the test. Yielding of the longitudinal bars first occurred at a lateral force level of 49 kips (218 kN) followed by flexural cracking at the top and bottom of the column. Early shear cracks formed at a lateral force level of about 73 kips (325 kN). Yielding of the transverse reinforcement first occurred at a lateral force level of 93 kips (414 kN) followed by the opening of large shear cracks near the end of the test. The final failure mode for the column was a shear failure. Figure 5.3.3 shows the large shear cracks present near the end of testing.

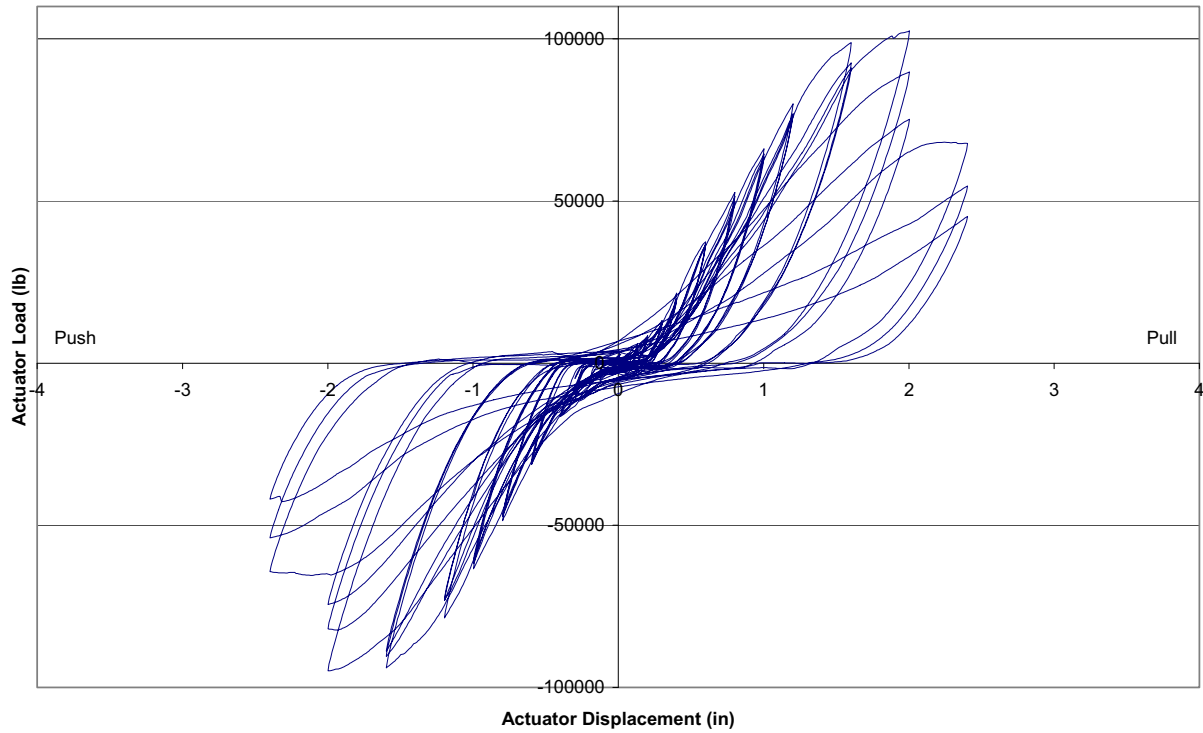


Figure 5.3.1 – Column 5 Lateral Load vs. Displacement Hysteresis Curves

(1 kip = 4.45 kN, 1 in. = 25.4 mm)



Figure 5.3.2 – Column 5 Test Setup



Figure 5.3.3 – Column 5 Shear Cracking Near the End of Testing.

5.3.2 – Reinforcement Strain Plots

(a) Transverse Hoop Strains

Figure 5.3.4 shows transverse hoop strains with time alongside a plot of the column load with time. Almost negligible hoop strains were observed up to a displacement level of 1.2 in. (30 mm). Hoop strains increased linearly up to the yield point at a displacement level of 2.0 in. (51 mm) and then decreased linearly until the end of the test.

(b) Longitudinal Bar Strains

Figures 5.3.5 and 5.3.6 show the strains in the longitudinal bars at the top and bottom of the column, respectively. A linear strain profile was observed in the top strain gages up to the first yield at a displacement level of 1.0 in. (25 mm). After yielding, strains stayed nearly constant until the first cycle at a displacement level of 1.6 in. (41 mm), after which very large strains in excess of 15,000 $\mu\epsilon$ were observed. Strains in the bottom strain gages reached first

yield at a displacement level of about 0.8 in. (20 mm). Strains stayed nearly constant up to a displacement level of 1.2 in. (30 mm) and then increased rapidly to strains in excess of 10,000 $\mu\epsilon$ for the remainder of the test.

5.3.3 – Summary of As-Built Performance

Tests on as-built Columns 1 and 5 resulted in shear failures at a displacement level of approximately 2.0 in. (61 mm), accompanied with severe strength, stiffness and physical degradation. The as-built columns achieved an average peak shear load of approximately 100 kips, about 16% higher than the shear force corresponding to the theoretical ideal flexural strength of the columns. The overall response of the two columns was similar with early shear cracks forming at a lateral force level of approximately 70 kips (311 kN) followed by flexural cracks forming at the top and bottom of the column. Yielding of the transverse reinforcement occurred at a lateral force level of approximately 90 kips (400 kN) followed by the opening of large shear cracks. The cracking pattern for both columns was similar with large shear cracks forming at the top of the column inclined at approximately 45° from the vertical axis of the column. The final failure mode for both columns was a shear failure with little ductility.

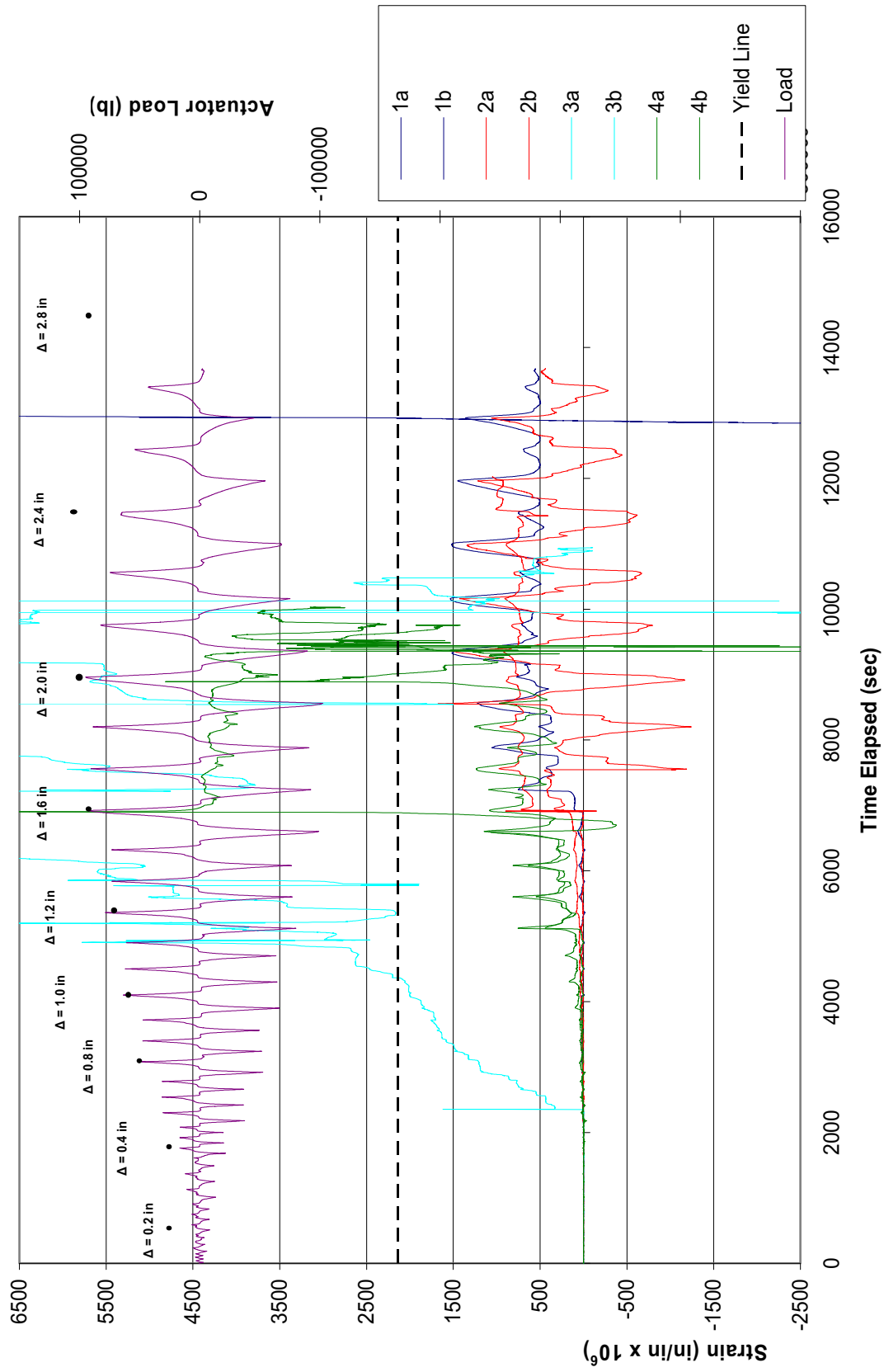


(Figure 5.3.4 – Column 5 Transverse Strain Gage Data (1 kip = 4.45 kN, 1 in. = 25.4 mm))

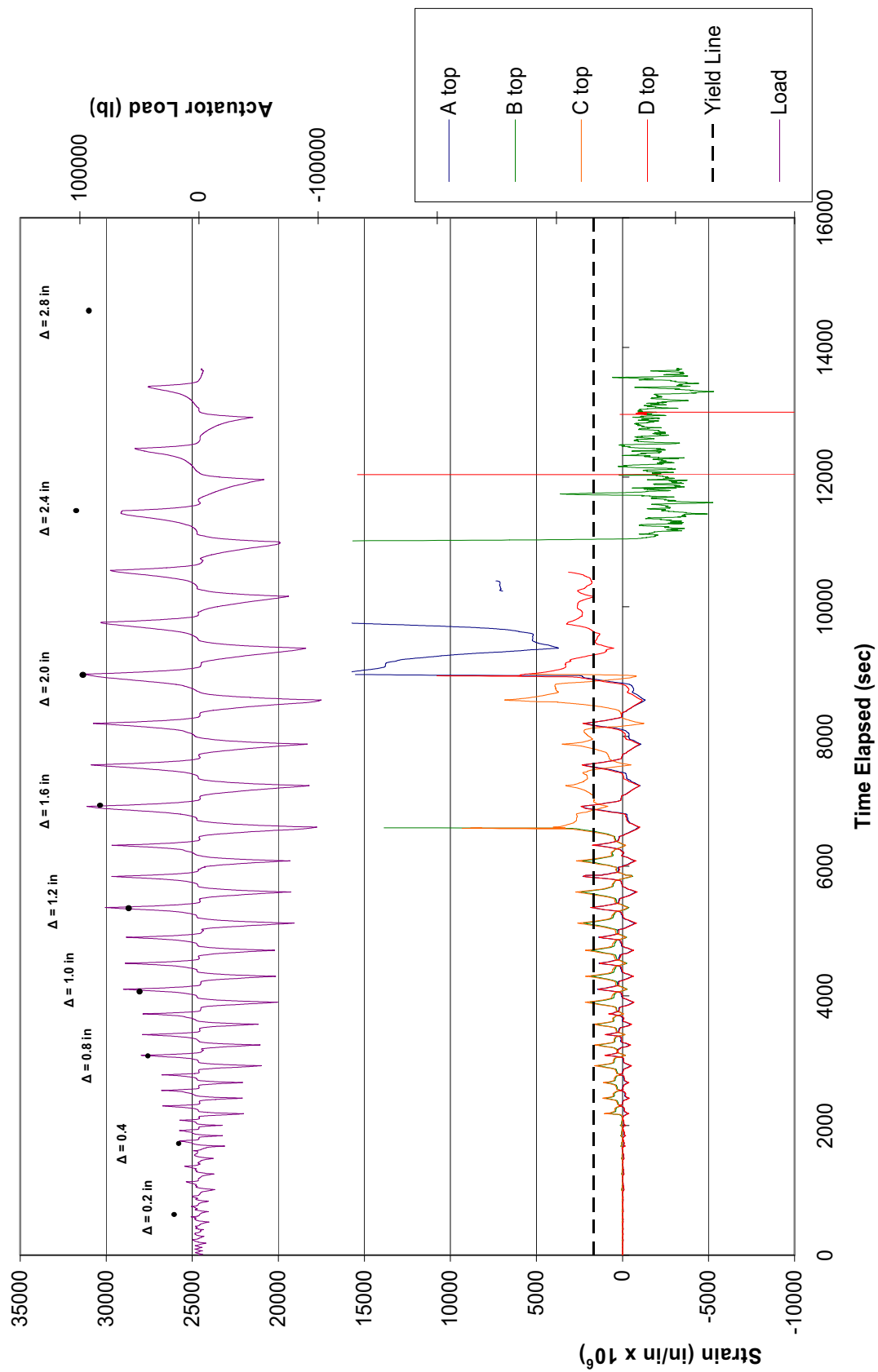


Figure 5.3.5 – Column 5 Longitudinal Bar Strain Gage Data at the Top of the Column (1 kip = 4.45 kN, 1 in. = 25.4 mm)

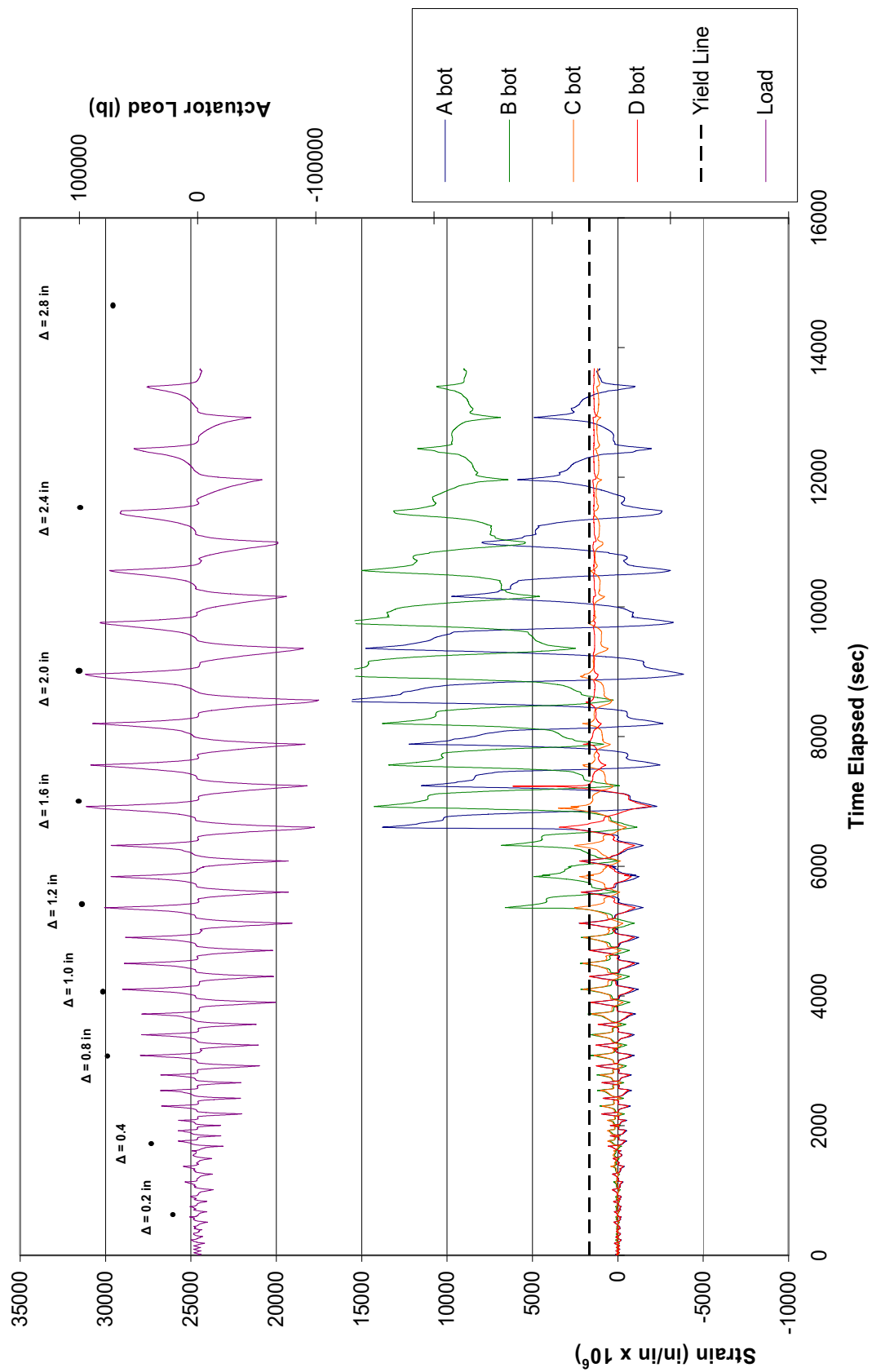


Figure 5.3.6 – Column 5 Longitudinal Bar Strain Gage Data at the Bottom of the Column (1 kip = 4.45 kN, 1 in. = 25.4 mm)

5.4 – BEHAVIOR OF RETROFITTED COLUMN 2

Column 2 was identical to the as-built Columns 1 and 5 except that it was retrofitted with an FRP wrap. No reentrant corner anchorage was provided for the FRP wrap as this test was designed to determine if such anchorage was required to engage the shear capacity of the FRP wrap.

5.4.1 – Overall Response

Figure 5.4.1 shows the overall hysteretic performance of Column 2 in terms of the lateral force vs. actuator displacement. As expected, the column exhibited a slightly improved energy dissipation capacity and ductility as compared with those for the as-built columns. The peak lateral load achieved was 101 kips (450 kN) and occurred at a lateral displacement of 2.0 in. (51 mm). The flexural response of the column remained stable through three cycles at a displacement level of 2.0 in. (51 mm), with only a minor degradation in stiffness. However, the column underwent a significant decrease in lateral stiffness and strength while cycling at a displacement level of 2.4 in. (61 mm), and the applied load dropped below 80% of the peak load during the second cycle at this displacement. The test was stopped after completing the first cycle at a displacement level of 2.8 in. (71 mm).

Figure 5.4.2 shows Column 2 at the beginning of the test. Yielding of the longitudinal bars first occurred at a lateral force level of 48 kips (214 kN) followed by flexural cracking at the top and bottom of the column. No shear distress was observed in the column up to the peak lateral load of 101 kips (450 kN). After cycling several times near 100 kips (450 kN) the FRP jacket began to pull away from the reentrant corners at the top and bottom of the column, most noticeably at the top of the column. With continued cycling, the pullout of the FRP began to extend down the column, resulting in a significant decrease in the peak lateral loads achieved.

Figure 5.4.3 shows the pullout of the FRP jacket from the reentrant corners. Yielding of the transverse reinforcement first occurred at a lateral force level of 88 kips (390 kN) during the second cycle at a displacement level of 2.0 in. (51 mm), followed by a shear crack forming under the FRP wrap. After removing the FRP jacket at the end of testing, it is evident that the final failure mode for the column was a shear failure. Figure 5.4.4 shows the large shear cracks present at the end of testing. Further inspection also showed that the pullout of FRP from the reentrant corners was likely due to spalling of the cover concrete from flexural hinging rather than debonding of the FRP jacket from the concrete.

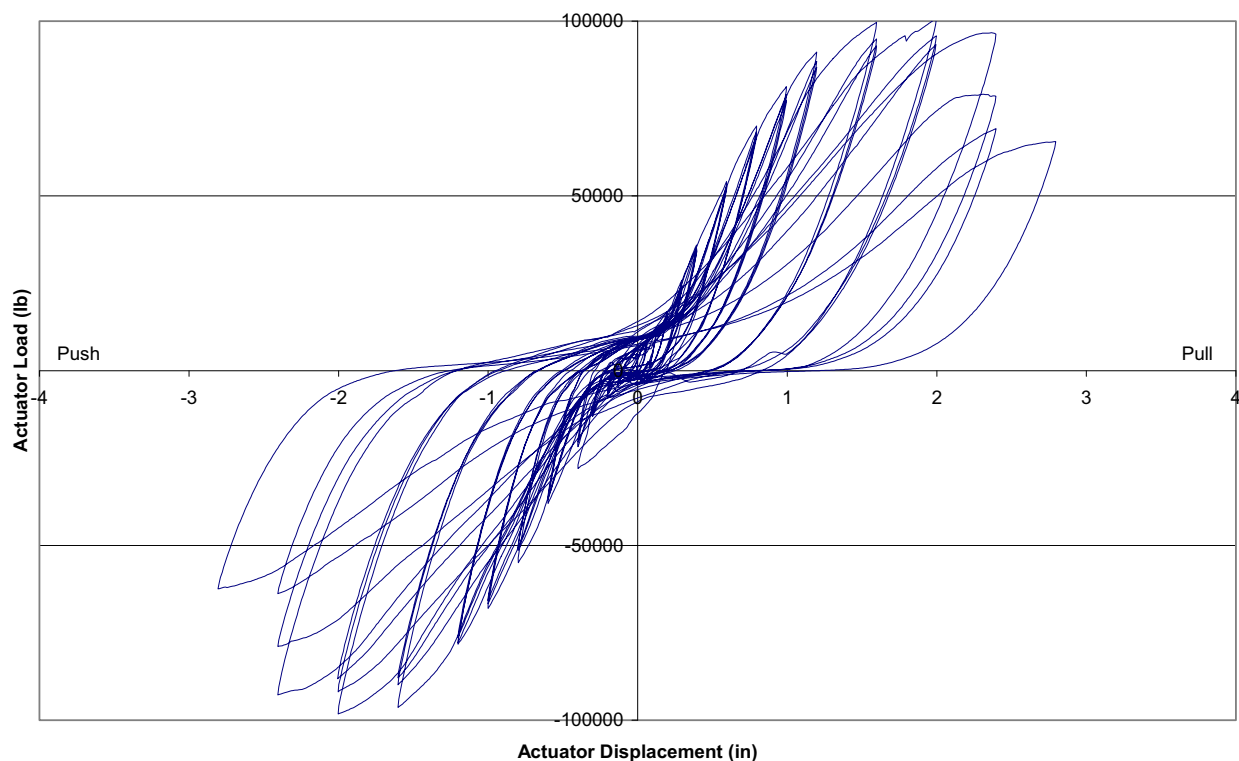


Figure 5.4.1 – Column 2 Lateral Load vs. Displacement Hysteresis Curves

(1 kip = 4.45 kN, 1 in. = 25.4 mm)



Figure 5.4.2 – Column 2 Test Setup



Figure 5.4.3 – Column 2 Pullout of FRP Jacket from Reentrant Corners



Figure 5.4.4 – Column 2 Large Shear Cracks under FRP Jacket at the End of Testing

5.4.2 – Reinforcement Strain Plots

(a) Transverse Hoop Strains

Figure 5.4.5 shows a plot of the transverse hoop strains with time. Almost negligible hoop strains were observed up to a displacement level of 0.8 in. (20 mm). A linear strain profile was then observed up to the first yield of the transverse reinforcement during the second cycle at a displacement level of 2.0 in. (51 mm). Very large hoop strains were observed during further testing as the FRP jacket pulled away from the reentrant corner and large shear cracks formed in the column.

(b) Longitudinal Bar Strains

Figures 5.4.6 and 5.4.7 show the strains in the longitudinal bars at the top and bottom of the column, respectively. A linear strain profile was observed in the top strain gages up to the first yield at a displacement level of 1.0 in. (25 mm). After yielding, strains stayed nearly constant until the first cycle at a displacement level of 1.6 in. (41 mm), after which very large strains in excess of 15,000 $\mu\epsilon$ were observed. Strains in the bottom strain gages reached first yield at a displacement level of about 0.6 in. (15 mm), much earlier than the top strain gages. Strains stayed nearly constant up to a displacement level of 1.2 in. (30 mm) and then increased rapidly to strains in excess of 10,000 $\mu\epsilon$ until a displacement level of 2.0 in. (51 mm). At a displacement level of 2.0 in. (51 mm), strains dropped significantly as the FRP jacket began to pull away from the reentrant corners.

(c) FRP Jacket Strains

Figures 5.4.8 and 5.4.9 show the strains with time for the FRP jacket strain gages parallel and perpendicular to the applied load, respectively. Almost negligible strains were observed in the parallel FRP strain gages up to a displacement level of 0.8 in. (20 mm). A linear strain profile was then observed up to the peak strain value of 2300 $\mu\epsilon$ during the first cycle at a displacement level of 2.4 in. (61 mm). Afterwards, strains decreased rapidly as the FRP jacket pulled away from the reentrant corners. All measured strains were well below the FRP jacket ultimate strain capacity of around 19,000 $\mu\epsilon$.

Negligible strains were observed in the perpendicular FRP gages near the top and bottom of the column up to a displacement level of 2.0 in. (51 mm). Strain readings spiked sharply during the first cycle at a displacement level of 2.0 in. (51 mm) at a peak strain of 2600 $\mu\epsilon$ corresponding with the beginning of pullout of the FRP jacket from the reentrant corners. Strains decreased with further testing.

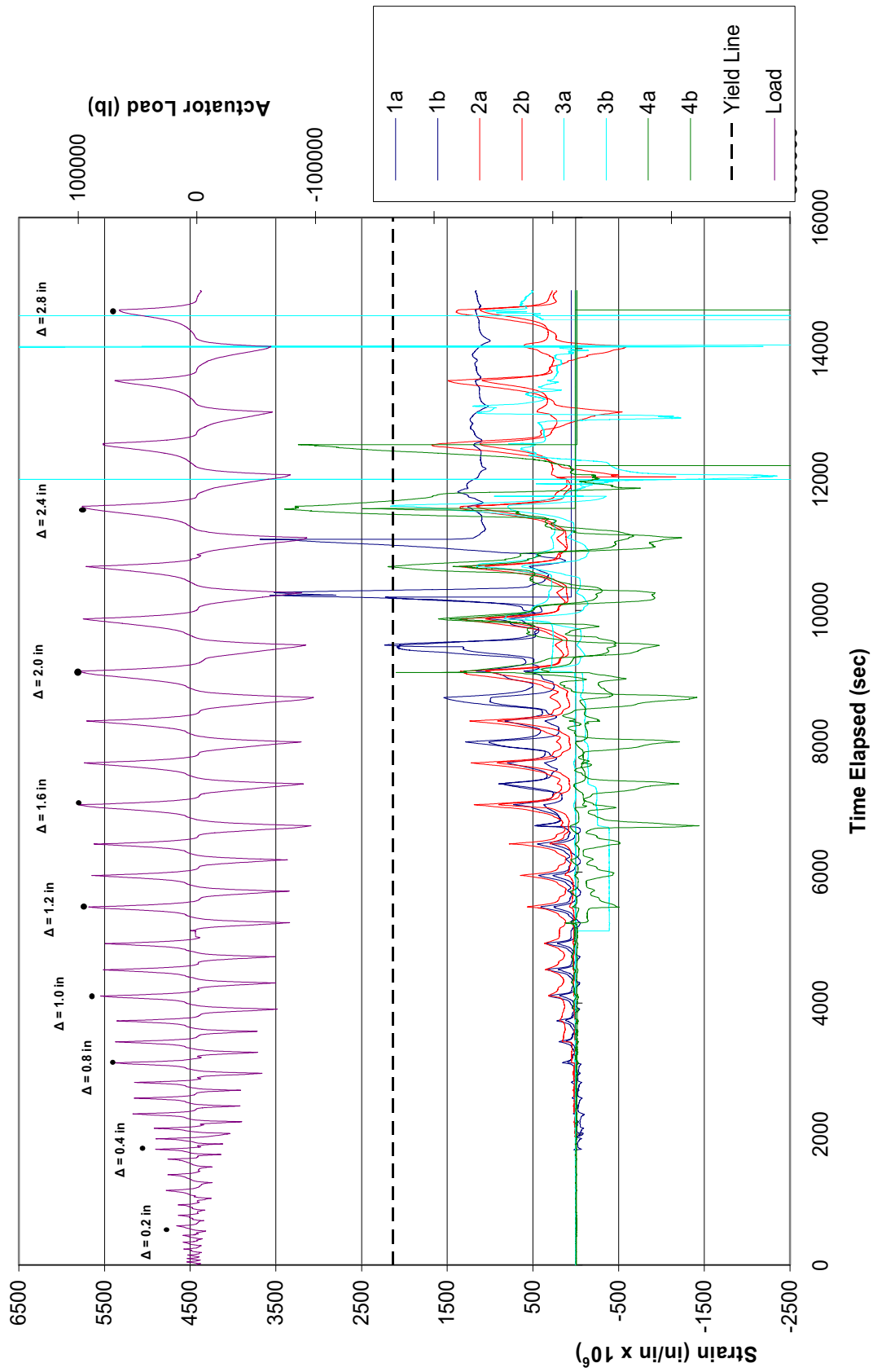


Figure 5.4.5 – Column 2 Transverse Strain Gage Data (1 kip = 4.45 kN, 1 in. = 25.4 mm)

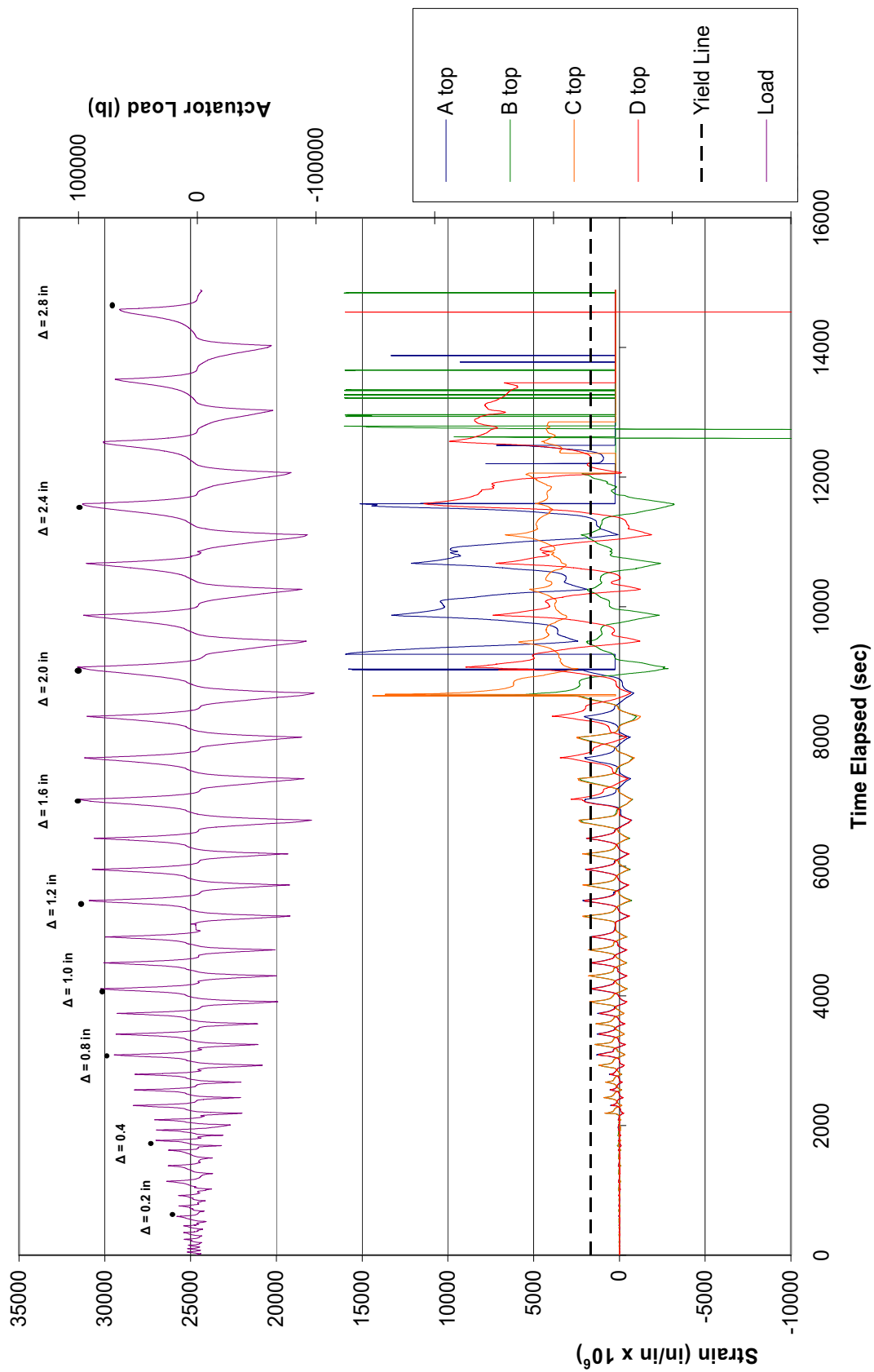


Figure 5.4.6 – Column 2 Longitudinal Bar Strain Gage Data at the Top of the Column (1 kip = 4.45 kN, 1 in. = 25.4 mm)

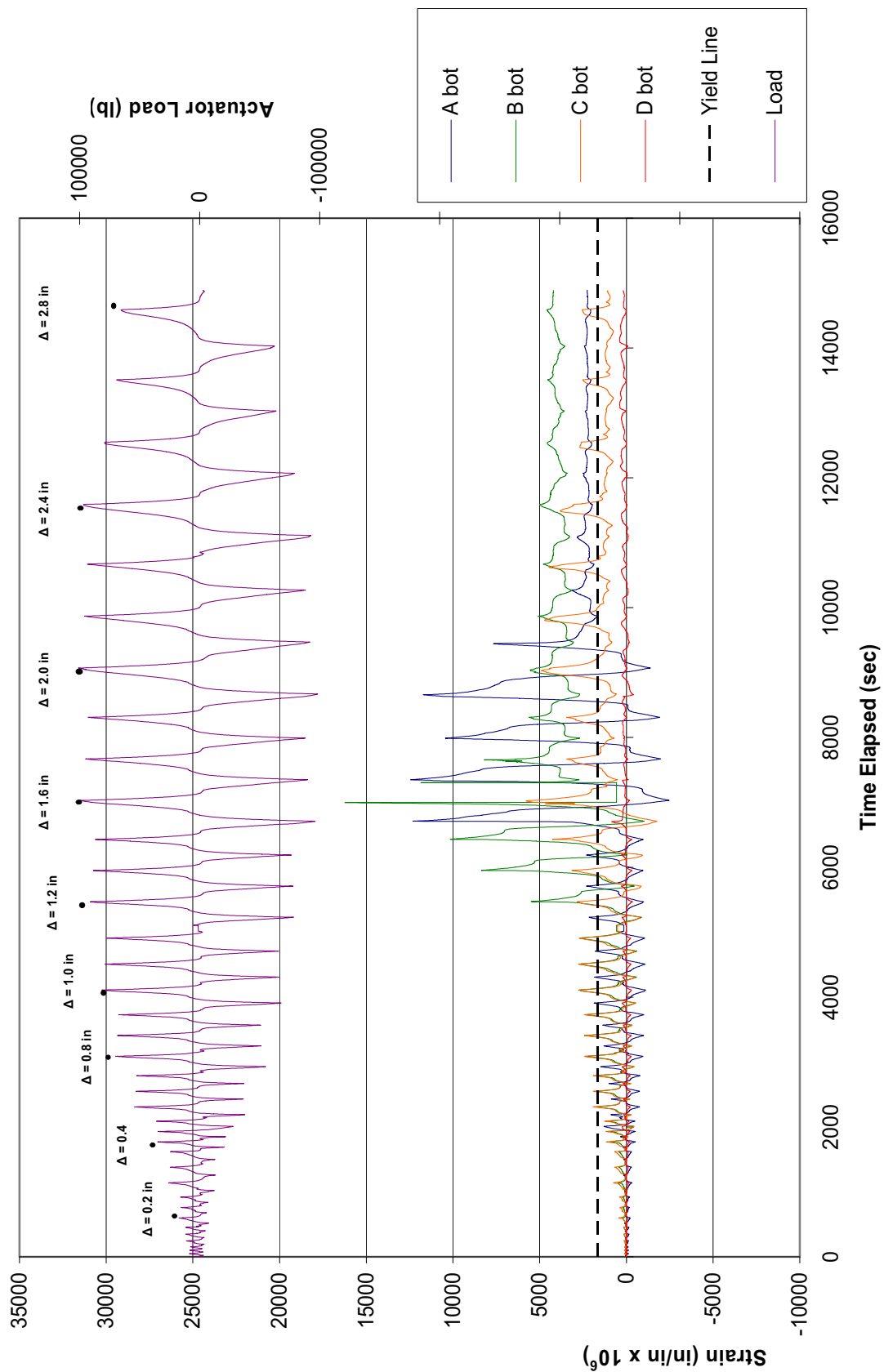


Figure 5.4.7 – Column 2 Longitudinal Bar Strain Cage Data at the Bottom of the Column (1 kip = 4.45 kN, 1 in. = 25.4 mm)

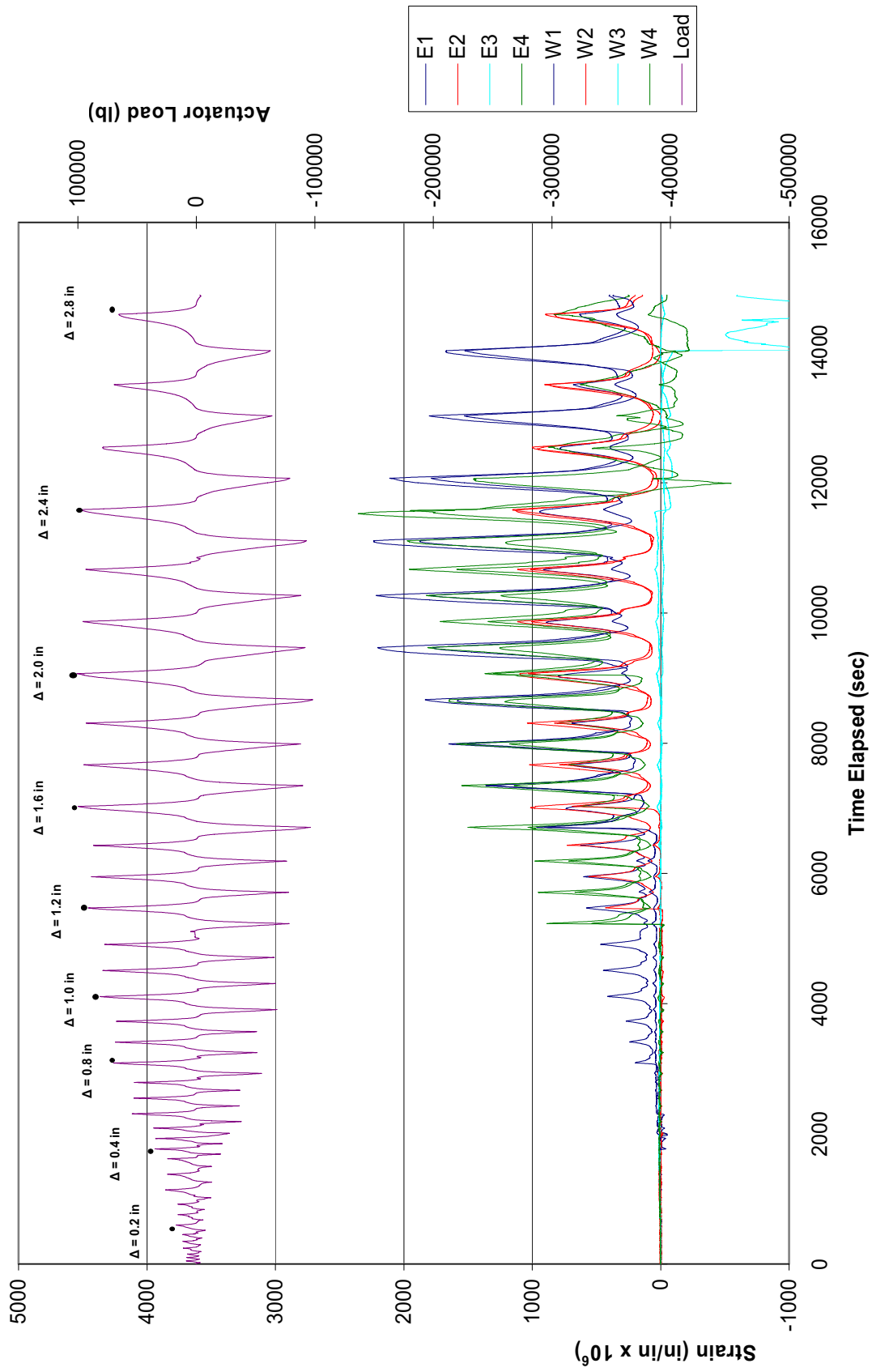


Figure 5.4.8 – Column 2 Parallel FRP Jacket Strain Gage Data (1 kip = 4.45 kN, 1 in. = 25.4 mm)

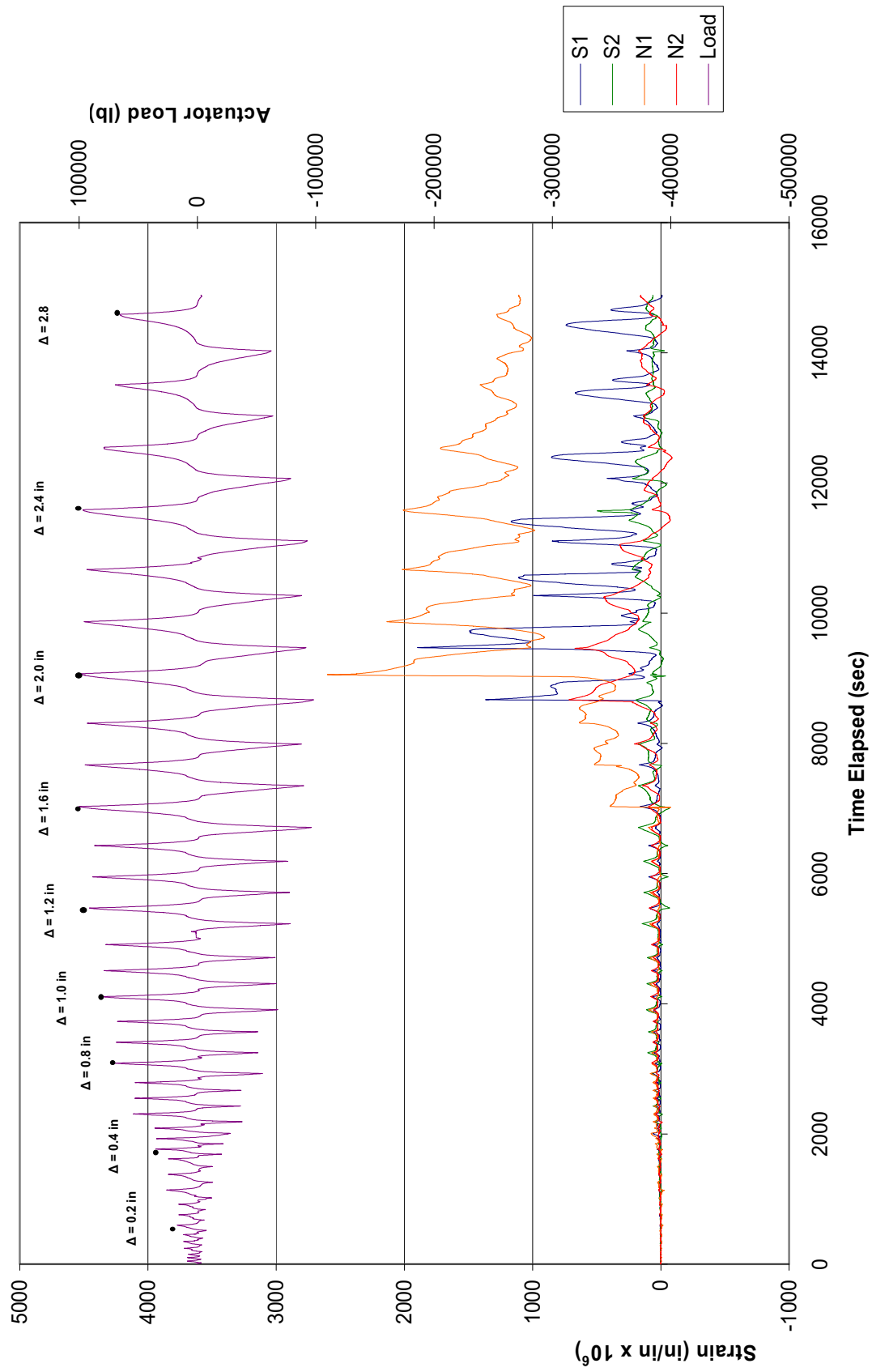


Figure 5.4.9 – Column 2 Perpendicular FRP Jacket Strain Gage Data (1 kip = 4.45 kN, 1 in. = 25.4 mm)

5.5 – BEHAVIOR OF RETROFITTED COLUMN 3

Column 3 was identical to Column 2 except that the FRP jacket was anchored in the reentrant corners of the column with steel bent plates and epoxy anchors installed over the full-height of the column. The reentrant corner anchorage was designed to develop the full strength of the FRP jacket and thus prevent the column from failing in shear.

5.5.1 – Overall Response

Figure 5.5.1 shows the overall hysteretic performance of Column 3 in terms of the lateral force vs. actuator displacement. The FRP jacket with reentrant corner anchorage exhibited a significant improvement in the overall seismic performance from the as-built columns. The peak lateral load achieved was 105 kips (470 kN) and occurred at a lateral displacement of 2.4 in. (61 mm). The flexural response of the column remained stable through three cycles at a displacement level of 2.4 in. (61 mm), with only minor degradation in stiffness. The column underwent a decrease in lateral stiffness and strength while cycling at a displacement level of 2.8 in. (71 mm), and the applied load dropped below 80% of the peak load during the third cycle at this displacement. The test was stopped after completing the first cycle at a displacement level of 3.2 in. (81 mm).

Figure 5.5.2 shows Column 3 at the beginning of the test. The response of the column was nearly identical to that of Column 2 through the early part of testing, with yielding of the longitudinal bars first occurring at a lateral force level of 50 kips (220 kN) followed by flexural cracking at the top and bottom of the column. Yielding of the transverse reinforcement first occurred at a lateral force level of 100 kips (445 kN) during the first cycle at a displacement level of 2.0 in. (51 mm). While cycling at a displacement level of 2.8 in. (71 mm) bulging began in the plastic hinge regions at the top and bottom of the column, although more pronounced at the top.

With continued cycling, the bulging increased, resulting in a decrease in the peak lateral loads.

Figure 5.5.3 shows the bulging of the FRP jacket at the top of the column. During the first cycle at a displacement level of 3.2 in. (81 mm) the epoxy anchors at the top of the column failed and the load displacement curve peaked before reaching a lateral displacement of 3.2 in. (81 mm), indicating the failure of the column. No shear distress was observed in the column throughout the test, and the final failure mechanism was development of plastic hinges at the top and bottom of the column. The failure of the epoxy anchors at the top of the column near the end of testing was likely due to crushing and degradation of the concrete under the FRP jacket in the plastic hinge region. Figure 5.5.4 shows the failure of the reentrant corner anchorage near the end of testing.

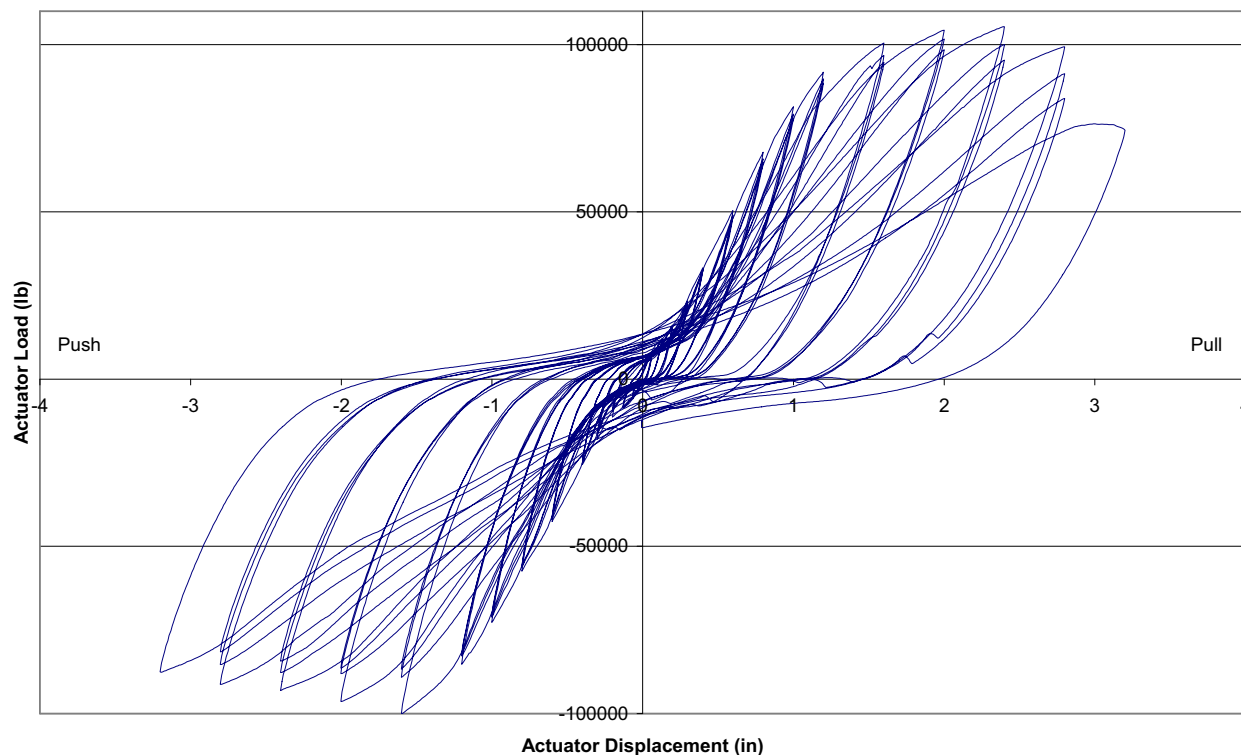


Figure 5.5.1 – Column 3 Lateral Load vs. Displacement Hysteresis Curves

(1 kip = 4.45 kN, 1 in. = 25.4 mm)



Figure 5.5.2 – Column 3 Test Setup



Figure 5.5.3 – Column 3 Bulging of FRP Jacket at the Top of the Column



5.5.4 – Column 3 Reentrant Corner Anchorage Failure

5.5.2 – Reinforcement Strain Plots

(a) Transverse Hoop Strains

Figure 5.45.5 shows a plot of the transverse hoop strains with time. Almost negligible hoop strains were observed up to a displacement level of 1.0 in. (25 mm). A linear strain profile was then observed up to the first yield of the transverse reinforcement during the first cycle at a displacement level of 2.0 in. (51 mm). The observed hoop strains were nearly constant for the remainder of the test.

(b) Longitudinal Bar Strains

Figures 5.5.6 and 5.5.7 show the strains in the longitudinal bars at the top and bottom of the column, respectively. A linear strain profile was observed in the top strain gages up to the

first yield at a displacement level of 1.0 in. (25 mm). After yielding, strains stayed nearly constant until the first cycle at a displacement level of 1.6 in. (41 mm), after which very large strains in excess of 10,000 $\mu\epsilon$ were observed for the remainder of the test. Strains in the bottom strain gages reached first yield at a displacement level of about 0.8 in. (20 mm), much earlier than the top strain gages. Strains increased linearly up to a displacement level of 1.2 in. (30 mm) and then increased rapidly to strains in excess of 10,000 $\mu\epsilon$ for the remainder of the test.

(c) FRP Jacket Strains

Figures 5.5.8 and 5.5.9 show the strains in the FRP jacket for strain gages parallel and perpendicular to the applied load, respectively. Almost negligible strains were observed in the parallel FRP strain gages up to a displacement level of 0.8 in. (20 mm). A linear strain profile was then observed up to the peak strain value of 2200 $\mu\epsilon$ during the second cycle at a displacement level of 2.8 in. (71 mm). Afterwards, strains remained nearly constant for the remainder of the test. All measured strains were well below the FRP jacket ultimate strain capacity of around 19,000 $\mu\epsilon$.

Almost negligible strains were observed in the perpendicular FRP gages near the top and bottom of the column up to a displacement level of 1.6 in. (41 mm). A linear strain profile was then observed for the remainder of the test, with a peak strain of 3900 $\mu\epsilon$ being observed at a lateral displacement of 3.2 in. (81 mm). There is a noticeable difference between the perpendicular strain gages at the top and bottom of the column, with the top strain gages reading significantly higher strains than the bottom strain gages.

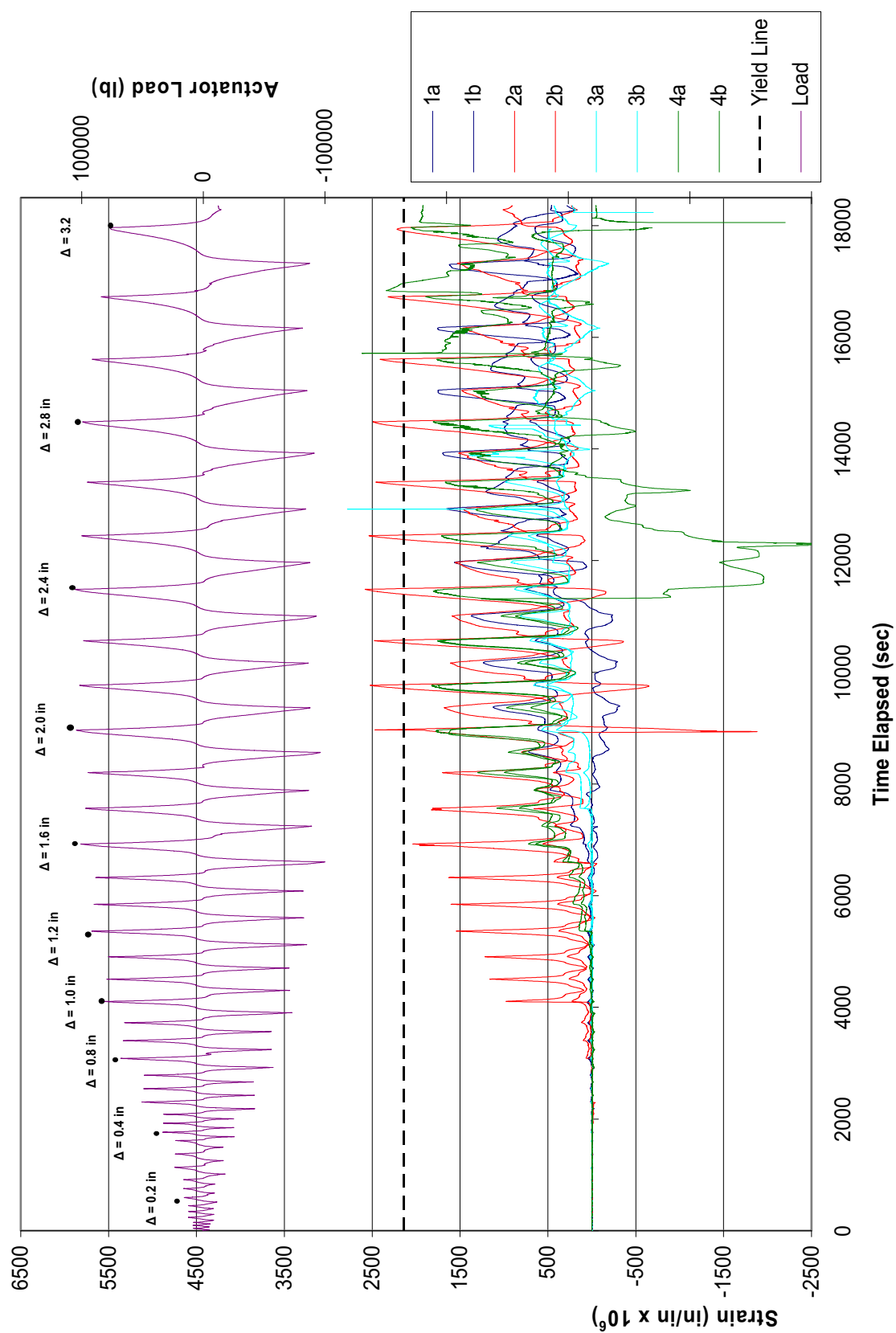


Figure 5.5.5 – Column 3 Transverse Strain Gage Data (1 kip = 4.45 kN, 1 in. = 25.4 mm) (1 kip = 4.45 kN, 1 in. = 25.4 mm)

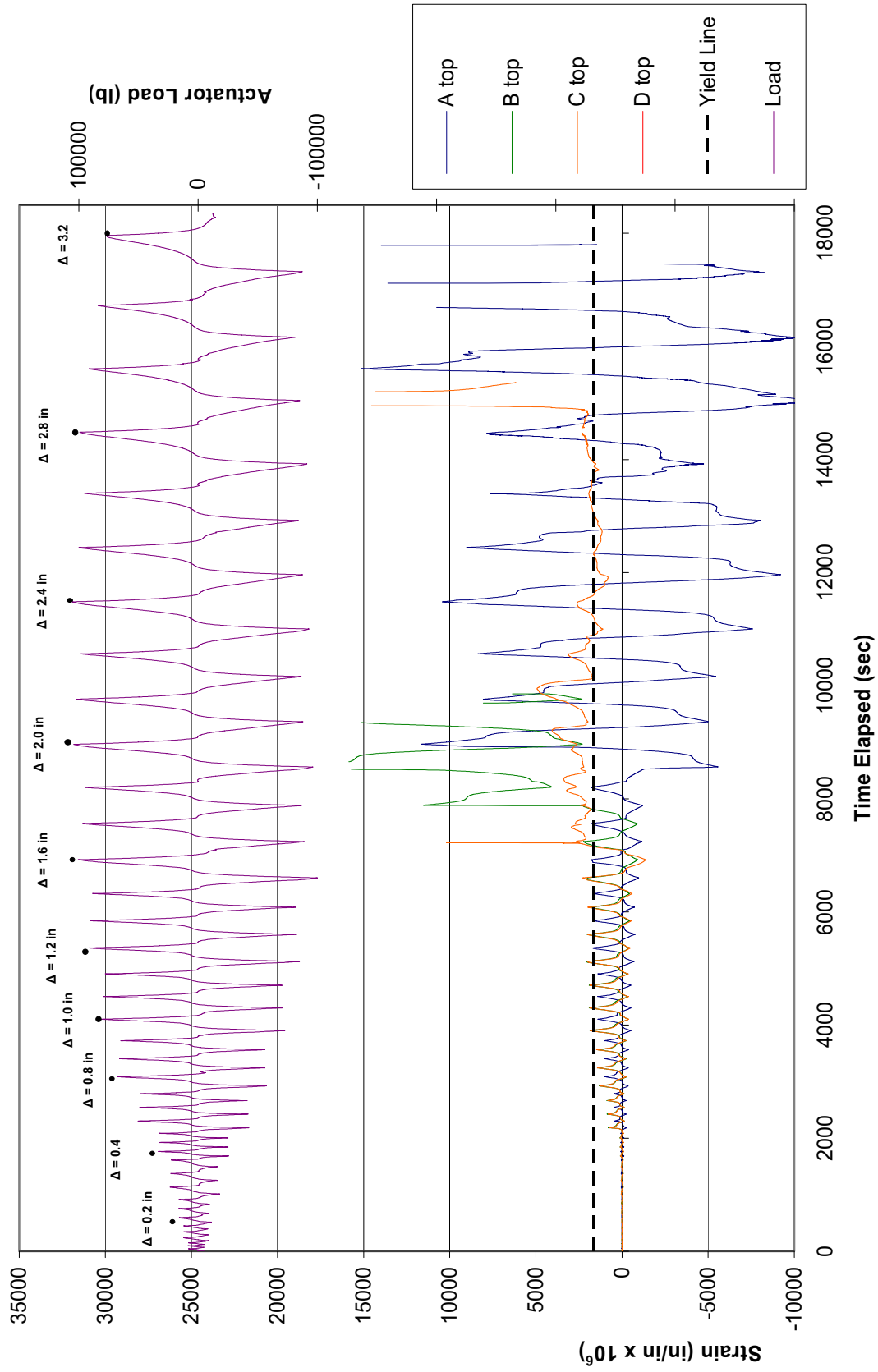


Figure 5.5.6 – Column 3 Longitudinal Bar Strain Gage Data at the Top of the Column (1 kip = 4.45 kN, 1 in. = 25.4 mm)

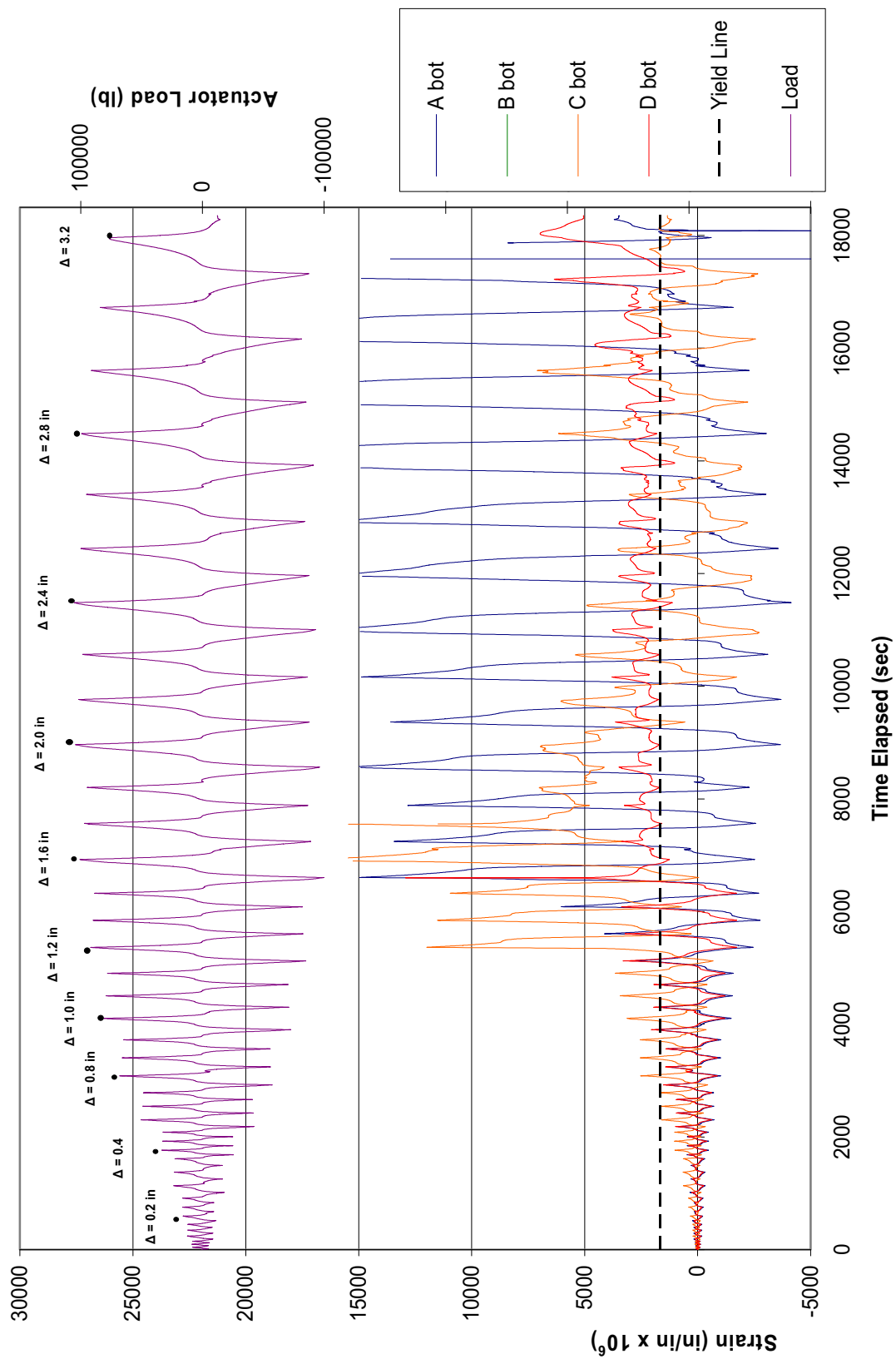


Figure 5.5.7 – Column 3 Longitudinal Bar Strain Gage Data at the Bottom of the Column (1 kip = 4.45 kN, 1 in. = 25.4 mm)

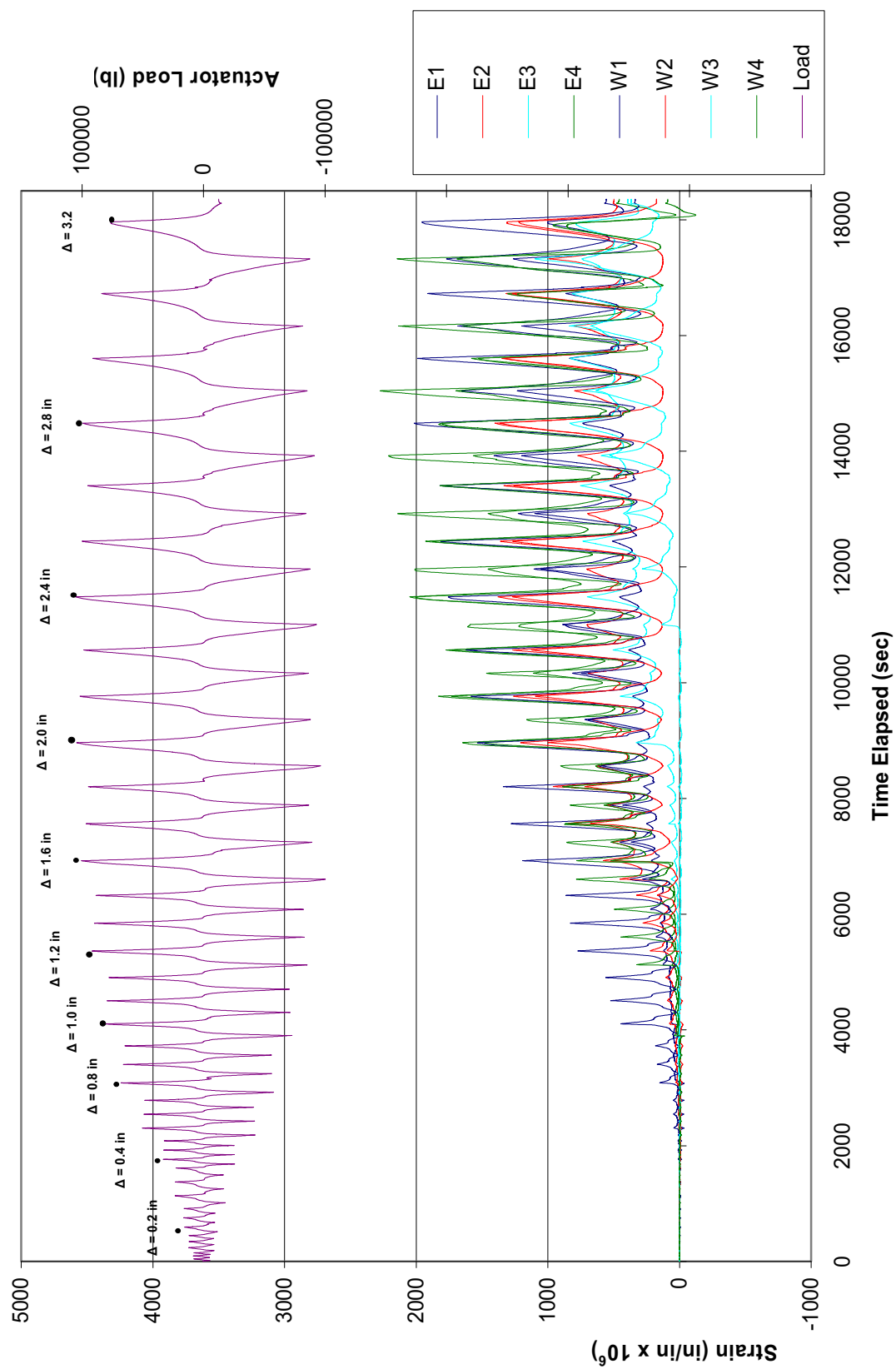


Figure 5.5.8 – Column 3 Parallel FRP Jacket Strain Gage Data (1 kip = 4.45 kN, 1 in. = 25.4 mm)

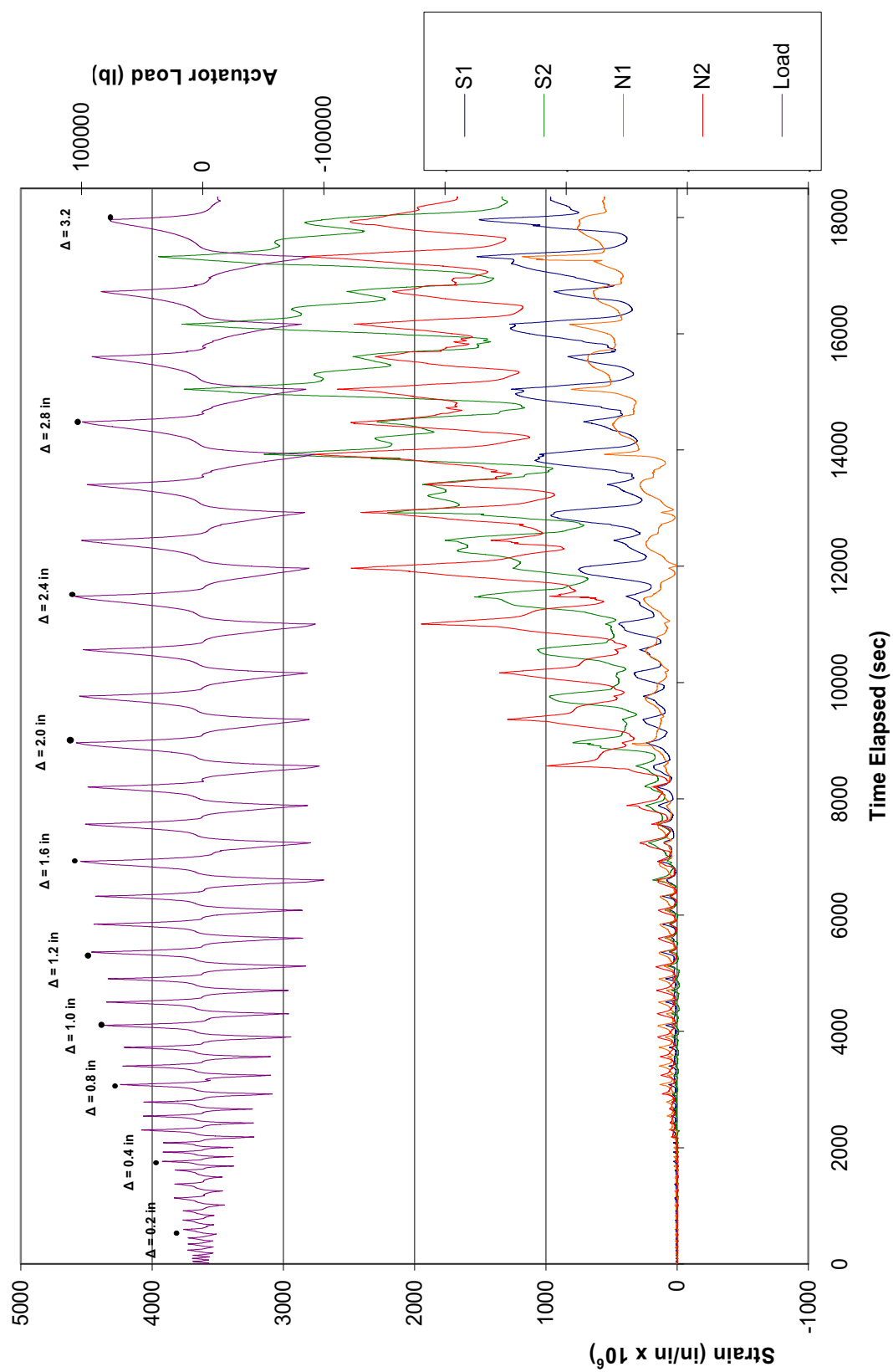


Figure 5.5.9 – Column 3 Perpendicular FRP Jacket Strain Gage Data (1 kip = 4.45 kN, 1 in. = 25.4 mm)

5.6 – BEHAVIOR OF RETROFITTED COLUMN 4

Column 4 was identical to Column 2 except that the FRP jacket was anchored in the reentrant corners of the column with FRP anchors for the full-height of the column and steel collars for confinement were located in the plastic hinge zones at the top and bottom of the column. The reentrant corner anchorage was designed to develop the full strength of the FRP jacket and thus prevent the column from failing in shear. The steel collars were designed to prevent bulging of the FRP jacket in the plastic hinge zones that occurred during testing of Column 3 and thereby improve the flexural response of the column at large displacements.

5.6.1 – Overall Response

Figure 5.6.1 shows the overall hysteretic performance of Column 4 in terms of the lateral force vs. actuator displacement. The FRP jacket with reentrant corner anchorage and plastic hinge zone confinement exhibited a significant improvement in the overall seismic performance from the as-built columns and the retrofitted columns without confinement. The peak lateral load achieved was 113 kips (503 kN) and occurred at a lateral displacement of 2.8 in. (71 mm). The flexural response of the column remained stable through three cycles at a displacement level of 3.2 in. (81 mm), with only a minor degradation in stiffness. The column underwent a decrease in lateral stiffness and strength while cycling at a displacement level of 3.6 in. (91 mm); however, the applied load remained slightly above 80% of the peak load through the third cycle at this displacement. The peak load dropped rapidly during the first cycle at a displacement level of 4.0 in. (0.1 m), and the test was stopped after completing the second cycle at this displacement level.

Figure 5.6.2 shows Column 4 at the beginning of the test. The flexural response of the column was nearly identical to that of Column 2 through the early part of testing with yielding of the longitudinal bars first occurring at a lateral force level of 55 kips (245 kN) followed by

flexural cracking at the top and bottom of the column. Strains in the transverse reinforcement were small throughout the test and did not come close to the yield strain. FRP jacket strains were slightly lower than those for Column 3 parallel to the applied load, and strains on the steel collar were almost negligible throughout the test. The applied lateral load remained nearly constant even after development of plastic hinges at the top and bottom of the column up to a displacement level of 3.6 in. (91 mm). While cycling at a displacement level of 3.6 in. (91 mm), several of the vertical rebar fractured, resulting in significant decrease in the lateral stiffness and strength. Figure 5.6.3 shows the fractured longitudinal steel which was caused by low-cycle fatigue due to the stress reversals in the plastic hinge region. The final failure mode for the column was flexural hinging leading to fracture of the longitudinal rebar with no distress observed in the FRP jacket and steel collar at the end of testing. Figure 5.6.4 shows the column at the end of testing and illustrates the significant rotation of the plastic hinge regions.

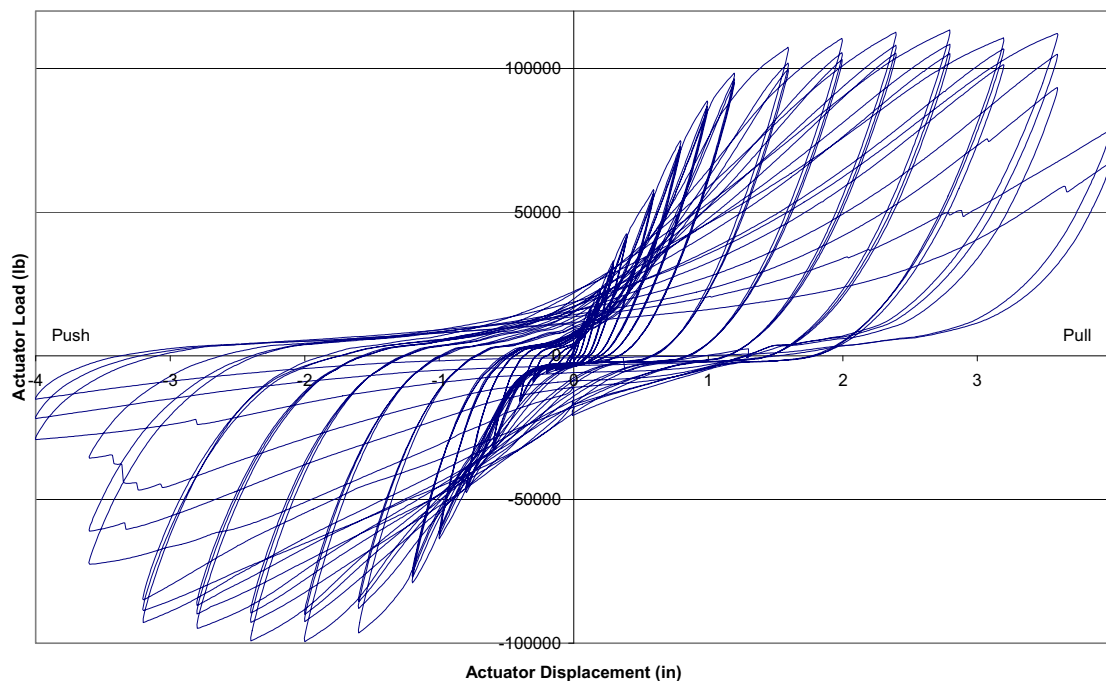


Figure 5.6.1 – Column 4 Lateral Load vs. Displacement Hysteresis Curves

(1 kip = 4.45 kN, 1 in. = 25.4 mm)



Figure 5.6.2 – Column 4 Test Setup



5.6.3 – Column 4 Longitudinal Rebar Fracture



Figure 5.6.4 – Column 4 Near the End of Testing

5.6.2 – Reinforcement Strain Plots

(a) Transverse Hoop Strains

Figure 5.6.5 shows a plot of the transverse hoop strains with time. Almost negligible hoop strains were observed up to a displacement level of 1.2 in. (30 mm). A linear strain profile was then observed up to peak strain of about $700 \mu\epsilon$ at a displacement level of 1.6 in. (41 mm). The observed hoop strains were nearly constant for the remainder of the test. The peak strain observed for the transverse hoops was far below the yield strain.

(b) Longitudinal Bar Strains

Figures 5.6.6 and 5.6.7 show the strains in the longitudinal bars at the top and bottom of the column, respectively. A linear strain profile was observed in the top strain gages up to the first yield at a displacement level of 1.0 in. (25 mm). After yielding, strains stayed nearly constant until the first cycle at a displacement level of 2.0 in. (51 mm). Very large strains in excess of 10,000 $\mu\epsilon$ were observed until a displacement level of 2.8 in. (71 mm), after which strains near the yield strain were observed for the remainder of the test.

Strains in the bottom strain gages reached first yield at a displacement level of about 0.8 in. Strains increased linearly up to a displacement level of 1.2 in. (30 mm) and then increased rapidly to strains in excess of 10,000 $\mu\epsilon$. Very large strains were observed up to a displacement level of 3.2 in. (81 mm), after which strains near the yield strain were observed for the remainder of the test.

(c) FRP Jacket and Steel Collar Strains

Figures 5.6.8 and 5.6.9 show the strains in the FRP jacket for strain gages parallel to the applied load and in the steel collar for strain gages perpendicular to the applied load. Almost negligible strains were observed in the parallel FRP strain gages up to a displacement level of 0.6 in. (15 mm). A linear strain profile was then observed up to the peak strain value of 2200 $\mu\epsilon$ at a displacement level of 2.4 in. (61 mm). Afterwards, strains remained nearly constant up to a displacement level of 3.6 in. (91 mm) and then decreased linearly for the remainder of the test. All measured strains were well below the FRP jacket ultimate strain capacity of around 19,000 $\mu\epsilon$.

Very small strains were observed in the steel collar strain gages placed perpendicular to the loading direction throughout the test and were well below the steel collar yield strain of 1300 $\mu\epsilon$.

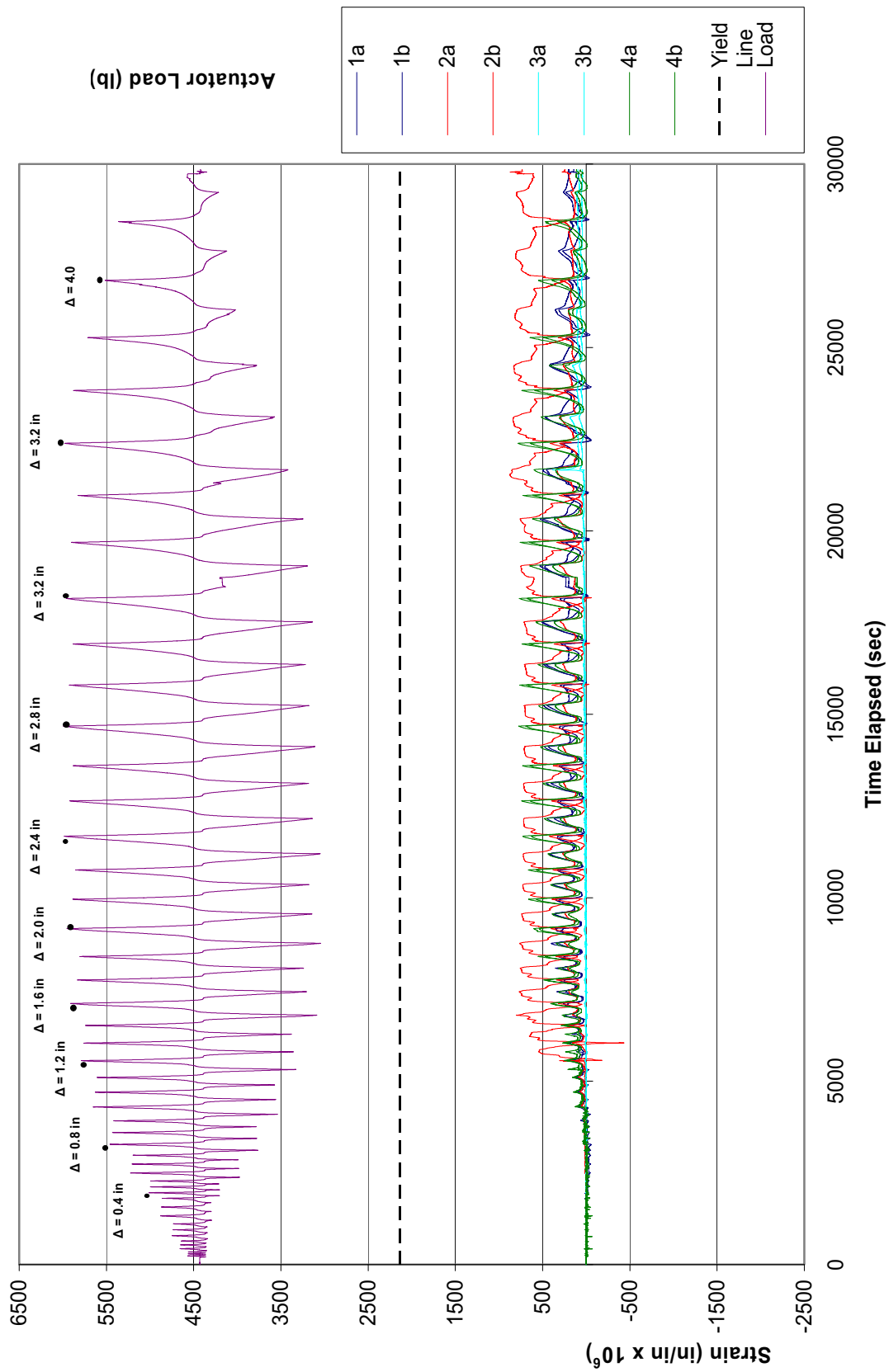


Figure 5.6.5 – Column 4 Transverse Strain Gage Data (1 kip = 4.45 kN, 1 in. = 25.4 mm)

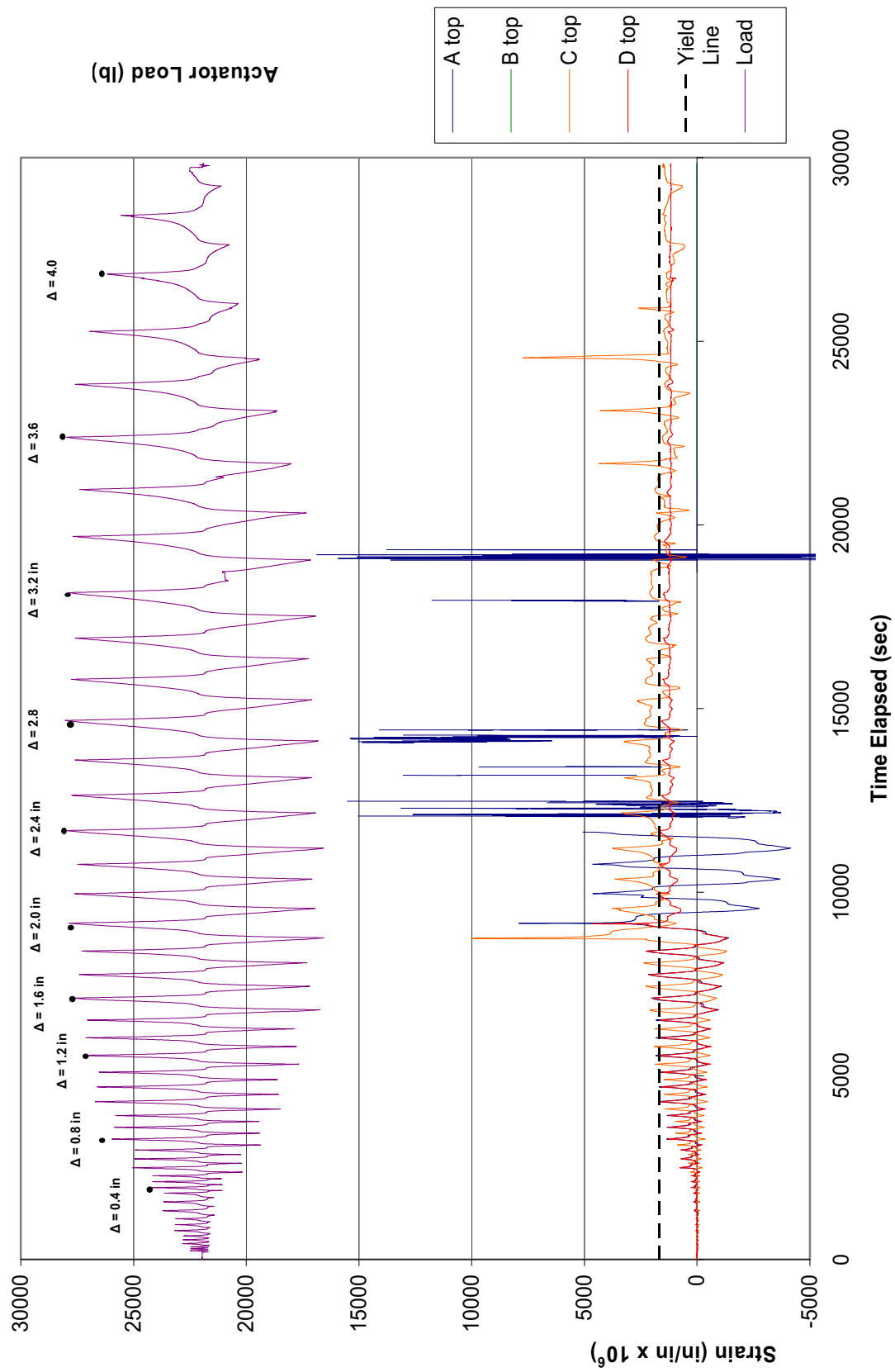


Figure 5.6.6 – Column 4 Longitudinal Bar Strain Gage Data at the Top of the Column (1 kip = 4.45 kN, 1 in. = 25.4 mm)

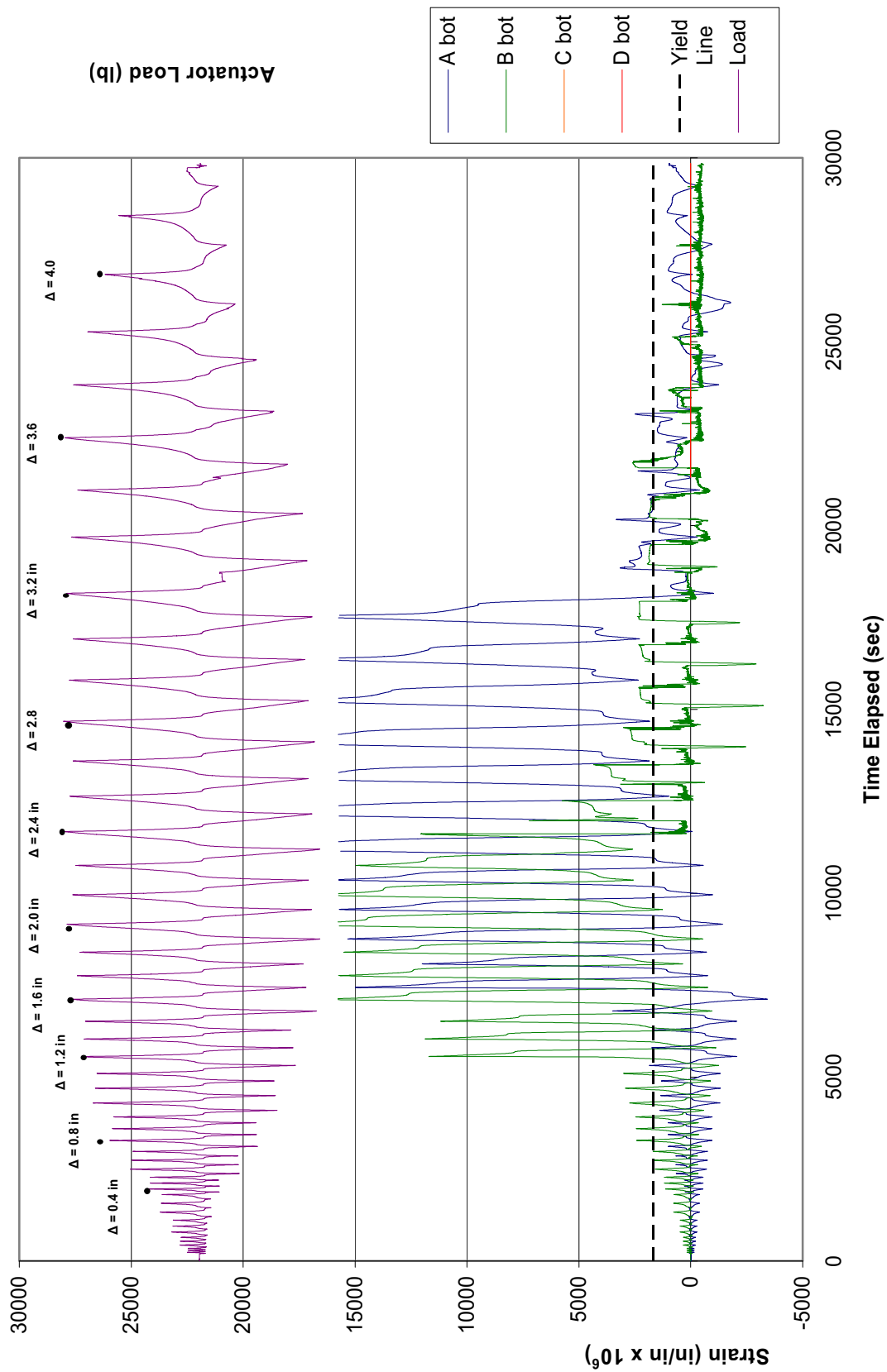


Figure 5.6.7 – Column 4 Longitudinal Bar Strain Gage Data at the Bottom of the Column (1 kip = 4.45 kN, 1 in. = 25.4 mm)

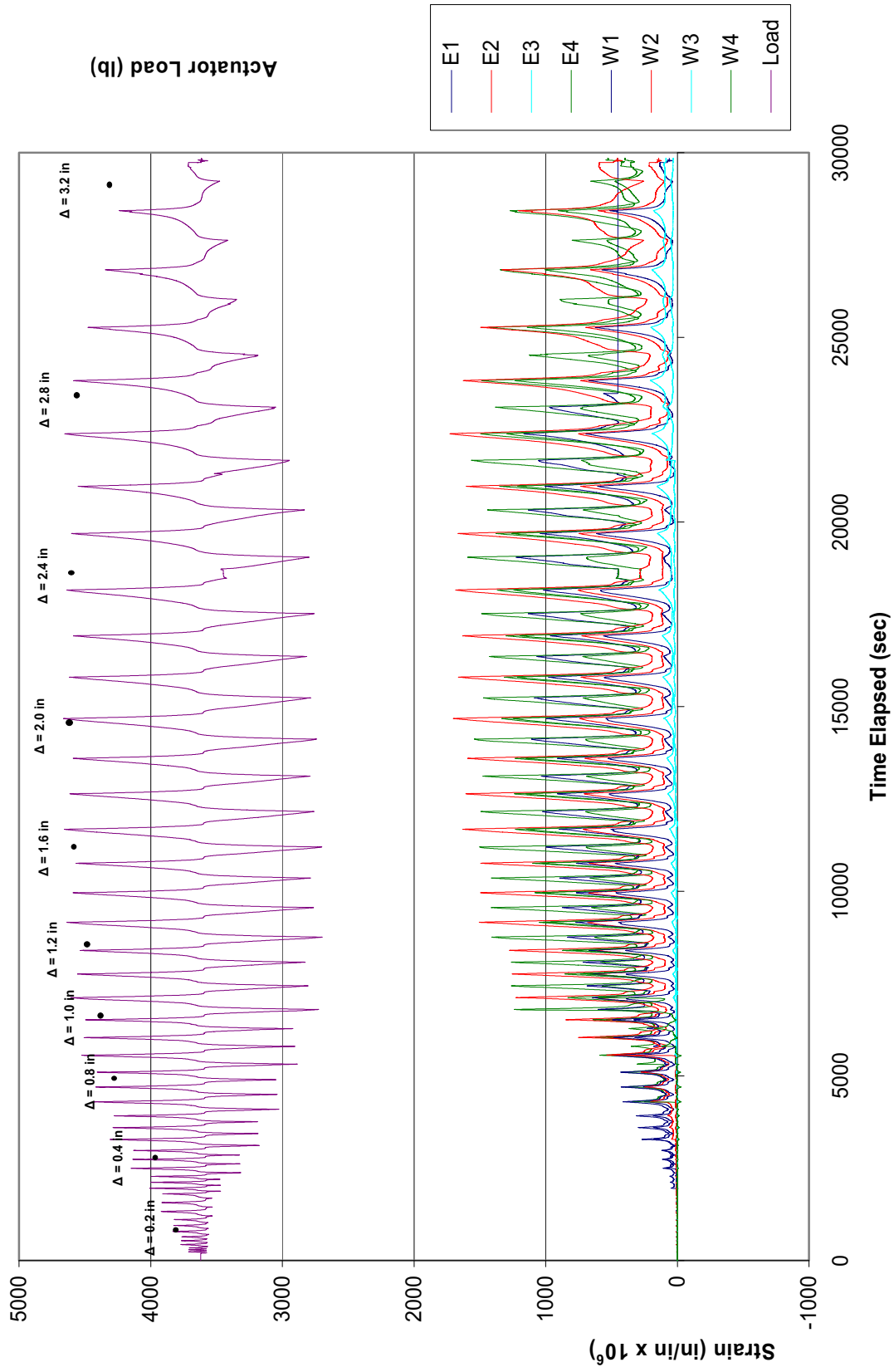


Figure 5.6.8 – Column 4 Parallel FRP Jacket Strain Gage Data (1 kip = 4.45 kN, 1 in. = 25.4 mm)

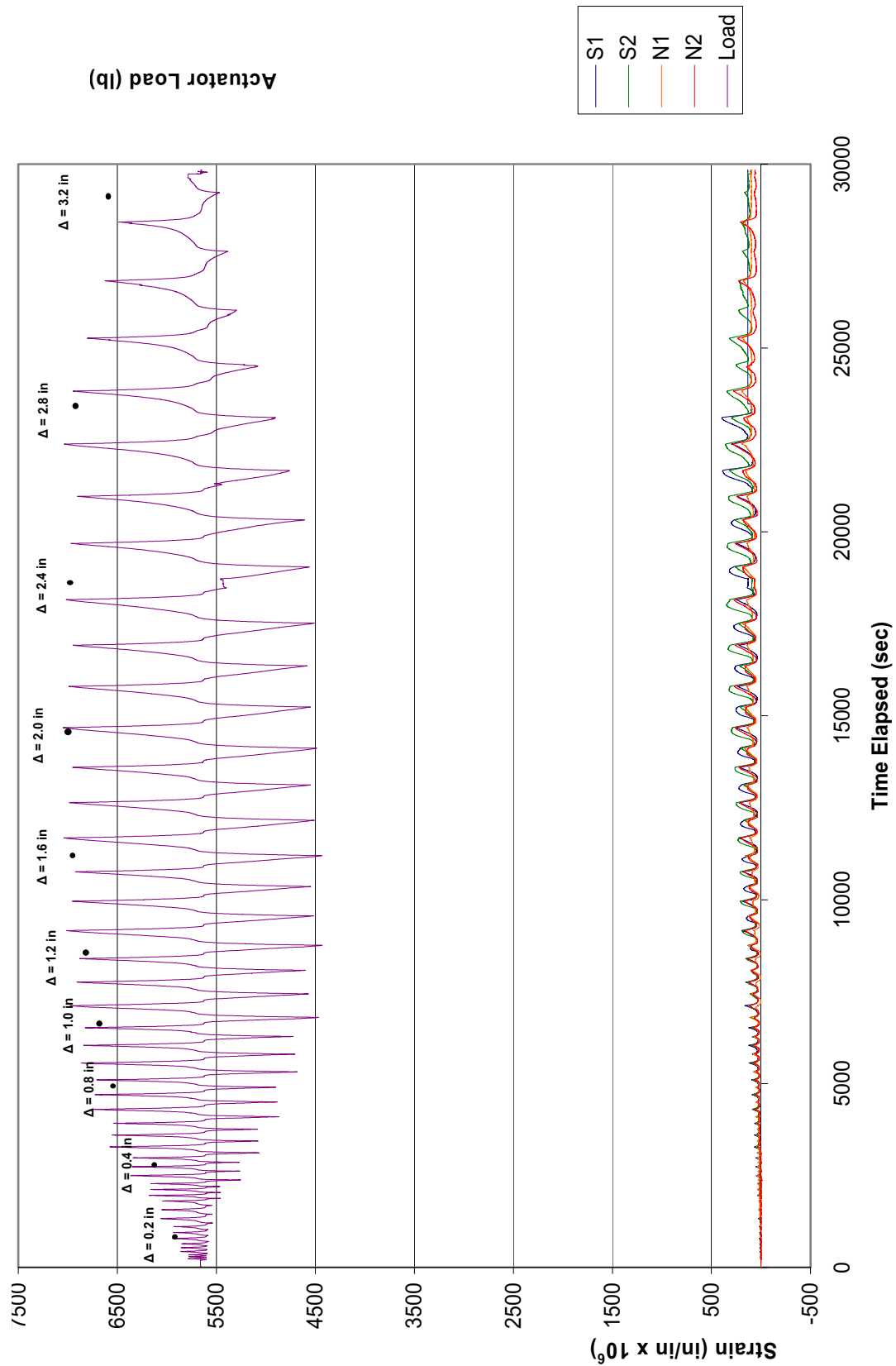


Figure 5.6.9 – Column 4 Perpendicular Steel Collar Strain Gage Data (1 kip = 4.45 kN, 1 in. = 25.4 mm)

5.7 – COMPARISON OF AS-BUILT AND RETROFITTED COLUMNS

Tests on as-built Columns 1 and 5 resulted in shear failures at a displacement level of about 2.0 in. (61 mm), accompanied with severe strength, stiffness and physical degradation. Column 2 retrofitted with an FRP jacket but no reentrant corner anchorage showed a moderate improvement in the energy dissipation capacity of the column but still failed in shear with limited ductility. Column 3 retrofitted with an FRP jacket as well as reentrant corner anchorages consisting of bent plates and epoxied anchors showed improvement in the overall seismic response with significant enhancement of seismic energy dissipation capacity and displacement levels sustained prior to failure. Failure in Column 3 was caused by bulging in the hinge regions, leading to crushing of the concrete and anchorage failure. Column 4 retrofitted with an FRP jacket with reentrant corner anchorages consisting of FRP anchors along with steel collars in the hinging regions provided the best seismic response. Good seismic energy dissipation along with a ductile response was achieved. Failure in Column 4 occurred due to extensive flexural hinging leading to low-cycle fatigue fracture of the longitudinal reinforcing bars.

A summary of relevant characteristics of the test specimens is presented in Table 5.7.1. Listed characteristics include the effective secant stiffness and shear force corresponding to the first yield of the longitudinal reinforcement, the maximum observed column shear strength, the maximum displacement ductility and drift ratio attained at the maximum response, and the total amount of energy dissipated throughout the test. Figure 5.7.1 shows the envelope lateral load vs. actuator displacement curves for Columns 1-5.

Table 5.7.1: Column Test Results

Column	V_y (1)	Δ_y (2)	K_y (3)	V_{exp} (4)	V_{exp}/V_{if} (5)	Δ_{max} (6)	μ_{Δ} (7)	Drift (8)	E_{total} (9)
1	26.8	0.444	60.5	98.1	1.16	2.51	5.65	3.80	292.7
2	48.5	0.534	90.8	100.8	1.19	2.81	5.25	4.25	398.0
3	50.4	0.62	81.3	105.4	1.25	3.20	5.16	4.85	493.4
4	55.6	0.592	93.9	113.4	1.34	4.00	6.76	6.07	648.2
5	48.7	0.543	89.6	102.5	1.21	2.21	4.06	3.34	303.9

Note: 1 kip = 4.45 kN, 1 in. = 25.4 mm

(1): Shear at first yield of longitudinal reinforcement (kips)

(2): Measured actuator displacement at first yield of longitudinal reinforcement (in.)

(3): Effective Secant Stiffness $\{(1) / (2)\}$ (kips/in.)

(4): Maximum measured shear force (kips)

(5): Ratio of maximum measured shear force to shear force corresponding to the theoretically computed ideal flexural capacity of the column.

(6): Maximum measured actuator displacement (in.)

(7): Displacement ductility at maximum shear force $\{(6) / (2)\}$

(8): Drift ratio at maximum shear force (%)

(9): Total energy dissipated during testing (k-in.)

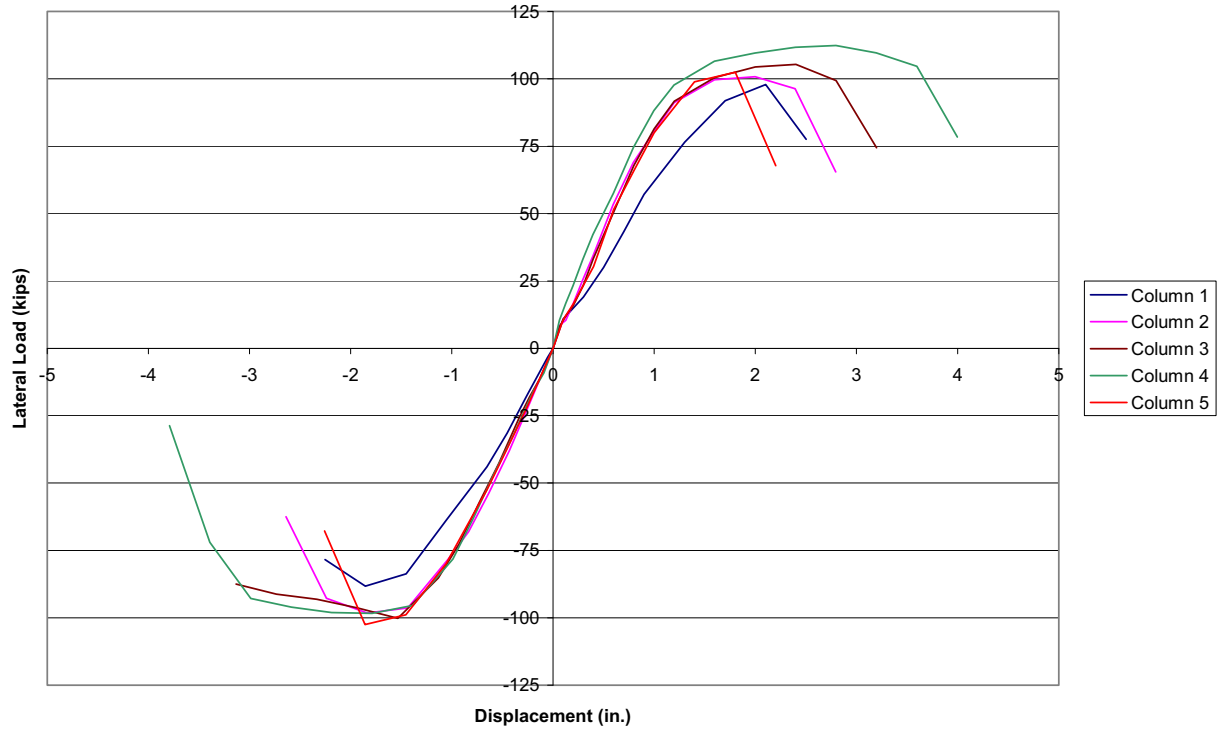


Figure 5.7.1 – Envelope Lateral Load vs. Displacement Hysteresis Curves

(1 kip = 4.45 kN, 1 in. = 25.4 mm)

The performance of the specimens is evaluated through the following discussion.

(a) Effective Secant Stiffness

The ratio of the lateral force corresponding to the first yield of the longitudinal reinforcement to the first yield column tip displacement is termed the effective secant stiffness of the columns, K_y . The values of this parameter are given in column 3 of Table 5.7.1, and it can be seen that the implementation of FRP jackets and reentrant corner anchorage on the test specimens did not result in a significant increase in stiffness over the as-built columns. For the retrofitted specimens, FRP jacket fibers were oriented in the horizontal direction only, and for the specimen with steel plate reentrant corner anchorages, the steel plates were installed in segments of 2 ft (0.6 m) or less for ease of construction and to prevent increases in column stiffness or flexural capacity. The lower stiffness value obtained for Column 1 is likely due to the

fact that there was some unintentional displacement between the loading pins in the column top block and the loading frame. This unintentional displacement was significantly reduced for later tests by installing metal shims prior to testing.

(b) Ratio of the Experimental Shear Strength to the Ideal Flexural Strength

Table 5.7.1 also illustrates the value of the ratio of the experimentally observed maximum shear strength of the test columns, V_{exp} , to the shear force corresponding to the theoretically computed ideal flexural capacity, $V_{if} = 86.4$ kips (384 kN), based on a moment-curvature analysis using assumed material properties and a maximum concrete compression strain of $\epsilon_{cu} = 0.005$. A brittle shear failure or limited ductile shear dominated behavior was expected with such low ratios for the as-built columns, as a capacity design approach would require the shear strength to be at least 25% greater than the ideal flexural strength.

For the as-built Columns 1 and 5, the ratio V_{exp}/V_{if} averaged about 1.18, with a limited ductile response followed by a brittle shear failure. Column 2 with a full-height FRP jacket and no reentrant corner anchorage achieved a similar V_{exp}/V_{if} ratio of 1.19 and also failed in a relatively brittle manner. Columns 3 and 4 with a full-height FRP jacket wrap and reentrant corner anchorages achieved stable and ductile hysteretic responses. The V_{exp}/V_{if} ratios for Columns 3 and 4 were 1.25 and 1.34 respectively, consistent with acceptable column shear strengths from a capacity design approach.

(c) Maximum Displacement Level Attained

The as-built Columns 1 and 5 attained their theoretical ideal flexural capacity at a displacement level of about 1.3 in. (33 mm), and then failed in a brittle manner at a displacement level of about 2.0 in. (61 mm). Column 2, with a full-height FRP jacket and no reentrant corner anchorage, also failed in a brittle manner but at a slightly higher displacement level of 2.4 in. (71

mm). Stable and ductile hysteretic responses were obtained for both Columns 3 and 4. Column 3 developed plastic hinges at the top and bottom of the column at a displacement level of 3.2 in. (81 mm), while Column 4 achieved a displacement level of 3.6 in. (91 mm) without any signs of physical, strength or stiffness degradation. Column 4 failed at a displacement level of 4.0 in. (0.1 m) due to fracture of the longitudinal reinforcement in the plastic hinge zones.

(d) Energy Dissipation Capacity

Columns 3 and 4, which were retrofitted with reentrant corner anchorages, displayed large and stable hysteresis loops even at large displacement levels. These loops demonstrate a significant improvement over the seismic energy dissipation capacity of the original as-built columns with thin and pinched hysteresis loops. The ratio of the values of the total energy absorbed by the retrofitted columns up to the peak response to the average energy absorbed by the as-built columns at peak response, E_{ret}/E_{ab} , is equal to 1.33, 1.65, and 2.17 for Columns 2, 3, and 4 respectively.

CHAPTER SIX

CONCLUSIONS AND RECOMMENDATIONS

6.1 – CONCLUSIONS

The experimental results of this study indicate that the cruciform-shaped columns located in the Aurora Avenue Bridge have inadequate shear strength from a capacity design approach. Failure in the specimens representing the as-built condition was caused by the opening of large shear cracks near the top of the column. Modest energy dissipation was achieved in the as-built specimens; they failed in a brittle manner at a displacement level of approximately 2.0 in. (51 mm).

The column specimen retrofitted with an FRP jacket and no reentrant corner anchorage showed a slight improvement in energy dissipation capacity and ductility compared to the as-built specimen; however, the specimen still underwent a brittle shear failure at a displacement level of 2.4 in. (61 mm) following pullout of the FRP jacket from the reentrant corners of the column. This pullout was not due to debonding of the FRP jacket from the concrete, but rather it was due to spalling of the concrete in the hinging region. Thus, reentrant corner anchorage is required to prevent pullout and develop the full shear capacity of the FRP jacket.

Both specimens retrofitted with an FRP jacket and reentrant corner anchorages developed flexural hinging and failed in a ductile manner with no evidence of shear distress. The specimen retrofitted with bent steel plate anchored in the reentrant corners with epoxy anchors showed a significant improvement in the energy-dissipation capacity over the as-built specimen and achieved a displacement level of 2.8 in. (71 mm) before failure. Failure of this specimen was caused by bulging of the FRP jacket in the plastic hinge region resulting in severe concrete degradation and failure of the epoxy anchors. The FRP jacket was not adequate at providing the required confinement in the plastic hinge region. To provide additional confinement in the plastic

hinge region, Column 4 was retrofitted with a grout-filled steel collar at the top and bottom of the column in addition to FRP anchors for reentrant corner anchorage. This retrofit showed a dramatic improvement in energy dissipation capacity and developed the full flexural capacity of the specimen without any bulging in the plastic hinge region. The specimen achieved a displacement level of 3.6 in. (91 mm) before failure due to low-cycle fatigue fracture of the longitudinal reinforcement in the plastic hinging regions.

The results of this study show that the FRP wrap was effective at providing the required shear strength enhancement to prevent a brittle shear failure. Evaluation of the FRP jacket stresses indicated that the FRP jacket remained elastic even under large cyclic shear forces well in excess of the shear force corresponding to the ideal flexural capacity of the column; however, this jacket needs to be anchored into the reentrant corners of the column in order to be effective. In addition, the FRP jacket does not provide adequate confinement in the plastic hinge region. A steel collar filled with high-strength grout was effective at providing the required confinement. The final retrofit design incorporating both reentrant corner anchorage and steel collar confinement developed the full flexural capacity of the column and resulted in fracture of the column longitudinal steel. Both the steel bent plates with epoxy anchors and the FRP anchors were effective at anchoring the FRP jacket into the reentrant corners of the column; however, the FRP anchors did not significantly alter the appearance of the bridge columns.

6.2 - RECOMMENDATIONS

FHWA procedures were used for the design of the FRP jacket, as given in Equation 3-2 and repeated here for convenience. From this equation, a FRP composite jacket thickness of 0.03 in. (0.76 mm) was calculated as the required thickness to develop the ultimate moment capacity of the column.

$$V_{FRP} = 2 * f_{jd} * t_j * D * \cot(\theta) \quad (\text{Equation 3-2})$$

Each retrofitted specimen in this study was wrapped with two layers of 0.014 in. (0.36 mm) FRP fabric resulting in a final composite FRP jacket thickness of 0.046 in. (1.17 mm). This FRP jacket design provided the required shear strength enhancement, and it is recommended that a similar FRP jacket design be used in the final retrofit design.

The results of this study show that both steel bent plates with epoxy anchors and FRP anchors were effective at anchoring the FRP jacket to the reentrant corners of the column. The steel bent plate significantly altered the appearance of the column due to the heads of the epoxy anchors protruding from the face of the column, and the plates imposed many construction difficulties due to anchors being placed on perpendicular surfaces at very tight clearances. Anchor hole locations had to be held to very tight tolerances to avoid damaging column longitudinal reinforcement and to allow proper fit up of the steel bent plate in the reentrant corner. The FRP anchors; however, did not significantly alter the shape of the column and were significantly easier to construct due to the flexibility of the location of the anchor holes. Thus, it is recommended that FRP anchors be utilized in the actual retrofit.

Design of the FRP anchors used in this study was based on a required anchor force of 12.8 k/ft (187 kN/m) of column height. Each ½-in. (13-mm) diameter FRP anchor was assumed to provide an effective tensile force of 6.3 kip (28 kN). Anchors were assumed to be effective in tension only, thus a spacing of 4 in. (0.1 m) on center was required on each face of the reentrant corner. This design provided the required anchorage of the FRP jacket to the column, and it is recommended that similar anchor spacing, after accounting for scaling effects, be used in the final retrofit design.

REFERENCES

- ACI 318-05 (2005). *Building Code Requirements for Structural (ACI 318-05)*. American Concrete Institute, Farmington Hills, Michigan.
- ACI 440-02 (2002). *Guide for the design and construction of externally bonded FRP systems for strengthening concrete structures (ACI 440.2R-02)*. American Concrete Institute, Farmington Hills, Michigan.
- American Association of State Highway Officials (1931). "Standard Specification for Highway Bridges and Incidental Structures"
- California Department of Transportation (1996). "Memo to Designers, 20-4"
- Chai, Y. H.; Priestley, M. J. N.; Seible, F. (1991). "Retrofit of Bridge Columns for Enhanced Seismic Performance," *Seismic Assessment and Retrofit of Bridges*, SSRP 91/03, PP. 177-196.
- Endeshaw, Mesay A. (2008). "Retrofit of Rectangular Bridge Columns Using CFRP Wrapping," M.S. Thesis, Department of Civil and Environmental Engineering, Washington State University.
- Federal Emergency Management Agency (2000). "Prestandard and Commentary for the Seismic Rehabilitation of Buildings"
- Haroun, M. A. and Elsanadedy, H. M. (2005). "Fiber-Reinforced Plastic Jackets for Ductility Enhancement of Reinforced Concrete Bridge Columns with Poor Lap Splice Detailing," *ASCE Journal of Bridge Engineering*, Vol. 1, No. 6, 749-757
- Iacobucci, R. D.; Sheikh, S. A.; Bayrak, O. (2003). "Retrofit of Square Concrete Columns with Carbon Fiber-Reinforced Polymer for Seismic Resistance," *ACI Structural Journal*, Vol. 100, No. 6, 785-794.
- Memon, M. S. and Sheikh, S. A. (2005). "Seismic Resistance of Square Concrete Columns Retrofitted with Glass Fiber-Reinforced Polymer," *ACI Structural Journal*, Vol. 102, No. 5, 774-783.
- Ozbakkaloglu, T. and Saatcioglu, M. (2009). "Tensile Behavior of FRP Anchors in Concrete," *Journal of Composites for Construction*, March/April, 2009, 82-92.

Priestley, M. J. N. and Seible, F. (1991). "Design of Seismic Retrofit Measures for Concrete Bridges," *Seismic Assessment and Retrofit of Bridges*, SSRP 91/03, University of California, San Diego, pp. 197-234.

Priestley, M. J. N.; Seible, F.; Verma, R. and Xiao, Y. (1993). "Seismic Shear Strength of Reinforced Concrete Columns," SSRP 93/06, University of California, San Diego, 112 pp.

Priestley, M. J. N.; Seible, F. and Calvi, G. M. (1996). *Seismic Design and Retrofit of Bridges*, John Wiley & Sons, Inc., New York.

Seible, F.; Priestley, M. J. N. and Chai, Y. H. (1995). *Earthquake Retrofit of Bridge Columns with Continuous Carbon Fiber Jackets*, Advanced Composites Technology Transfer Consortium, Report No. ACTT-95/08, La Jolla, California.

Seismic Retrofitting Manual for Highway Structures: Part 1 – Bridges (2006). Federal Highway Administration, Report NO. FHWA-HRT-06-032.

SEQAD Consulting Engineers (1993), *Seismic Retrofit of Bridge Columns Using High Strength Fiberglass/Epoxy Jackets*, Solana Beach, California.

Verma, R.; Priestley, M. J. N. and Seible, F. (1993). "Assessment of Seismic Response and Steel Jacket Retrofit of Squat Circular Reinforced Concrete Bridge Columns," SSRP 92/07, University of California, San Diego, 375 pp.

Washington State Department of Transportation (1930). "Bridge 99-560 Approach Span As-Built Plans"

Washington State Department of Transportation (2006). "Bridge Design Manual M 23-50"

Xiao, Y. and Wu, H. (2003). "Compressive Behavior of Concrete Confined by Various Types of FRP Composite Jackets," *SAGE Journal of Reinforced Plastics and Composites*, Vol. 22, No. 13, 1187-1202.

APPENDIX

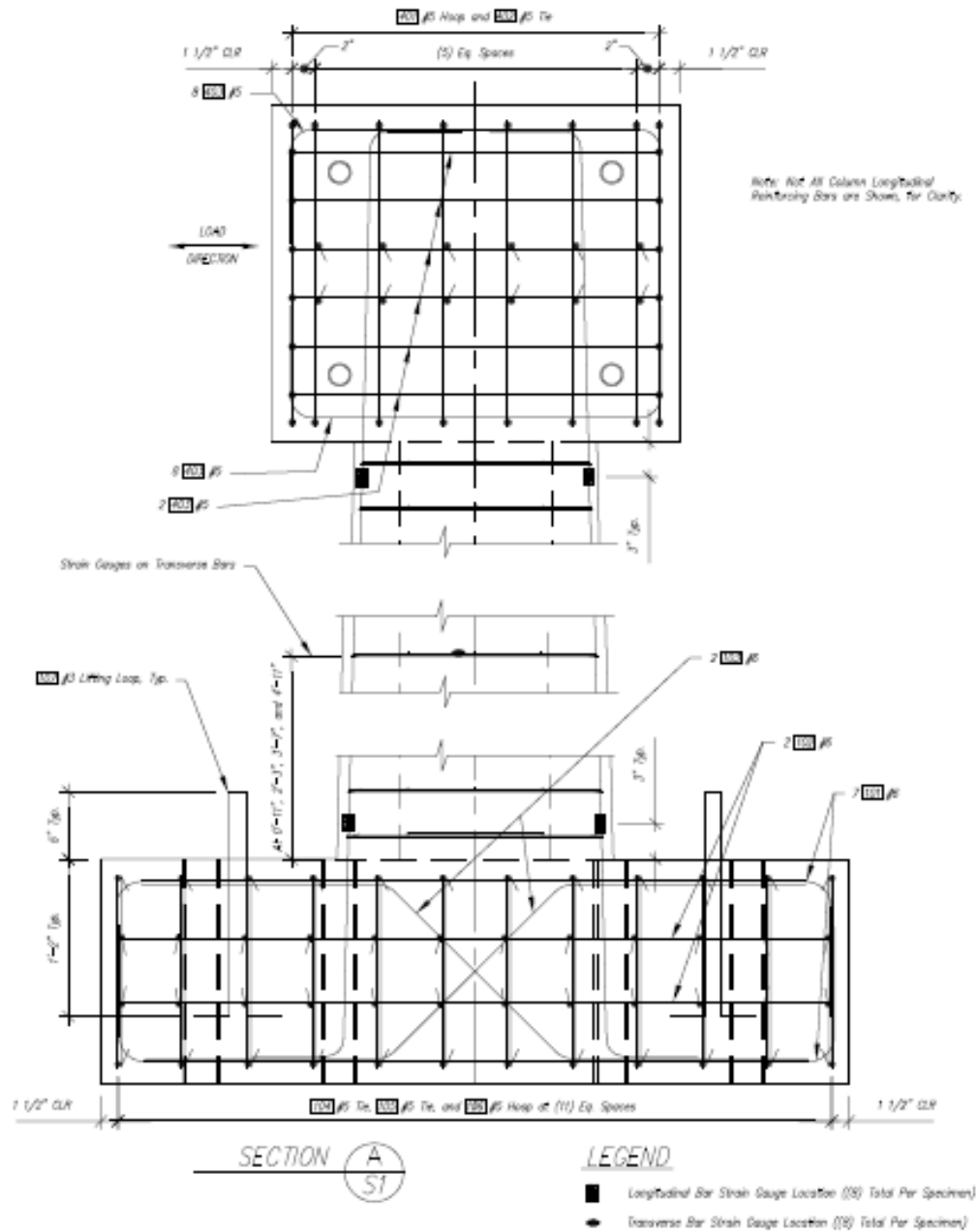
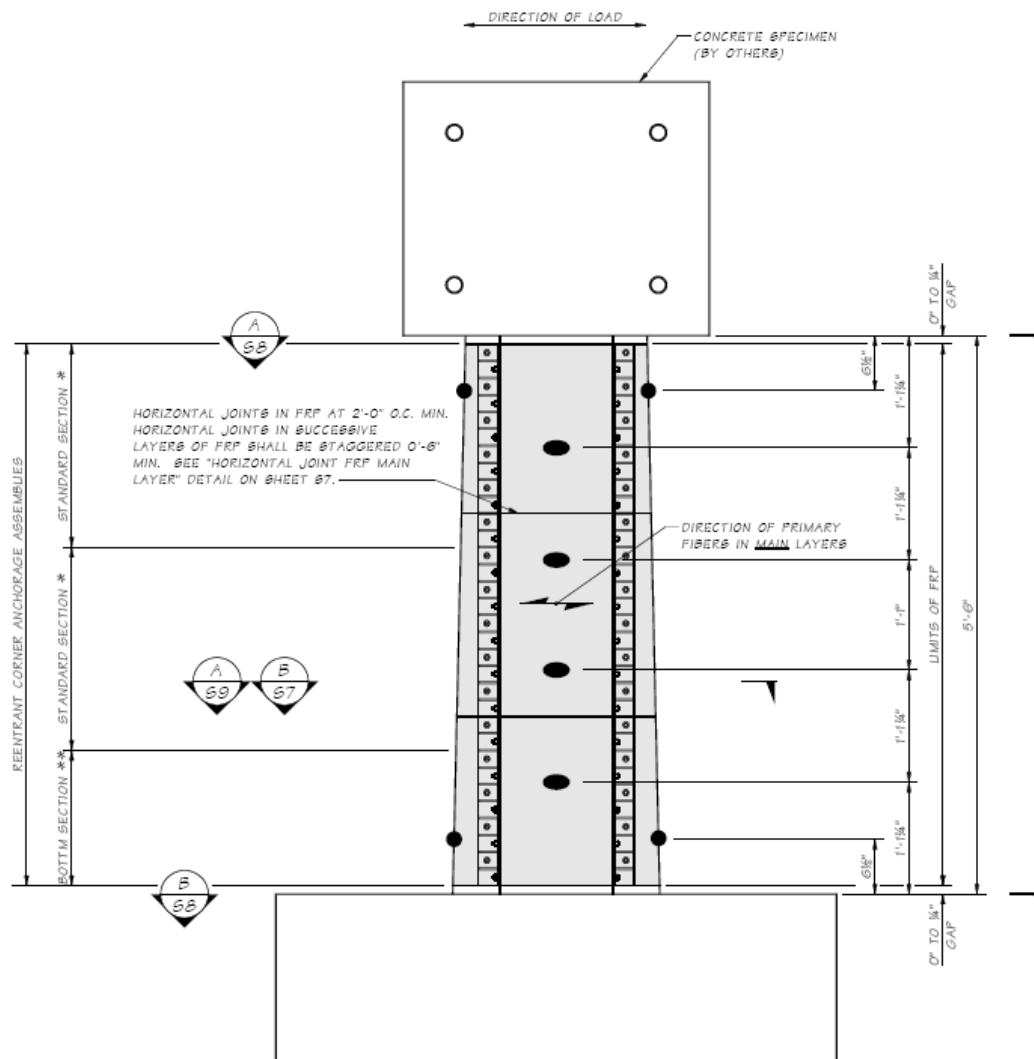


Figure A-1 – Strain Gage Locations Inside All Specimens (1 in. = 25.4 mm)



LEGEND

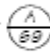

- - STRAIN GAUGE ON FRP, ON SPECIMAN FACES PERPENDICULAR TO DIRECTION OF LOAD (4 TOTAL). SEE DETAIL  FOR LOCATION
- - STRAIN GAUGE ON FRP, ON SPECIMAN FACES PARALLEL TO DIRECTION OF LOAD (8 TOTAL) SEE DETAIL  FOR LOCATION

Figure A-2 – Strain Gage Locations on Retrofitted Specimens (1 in. = 25.4 mm)

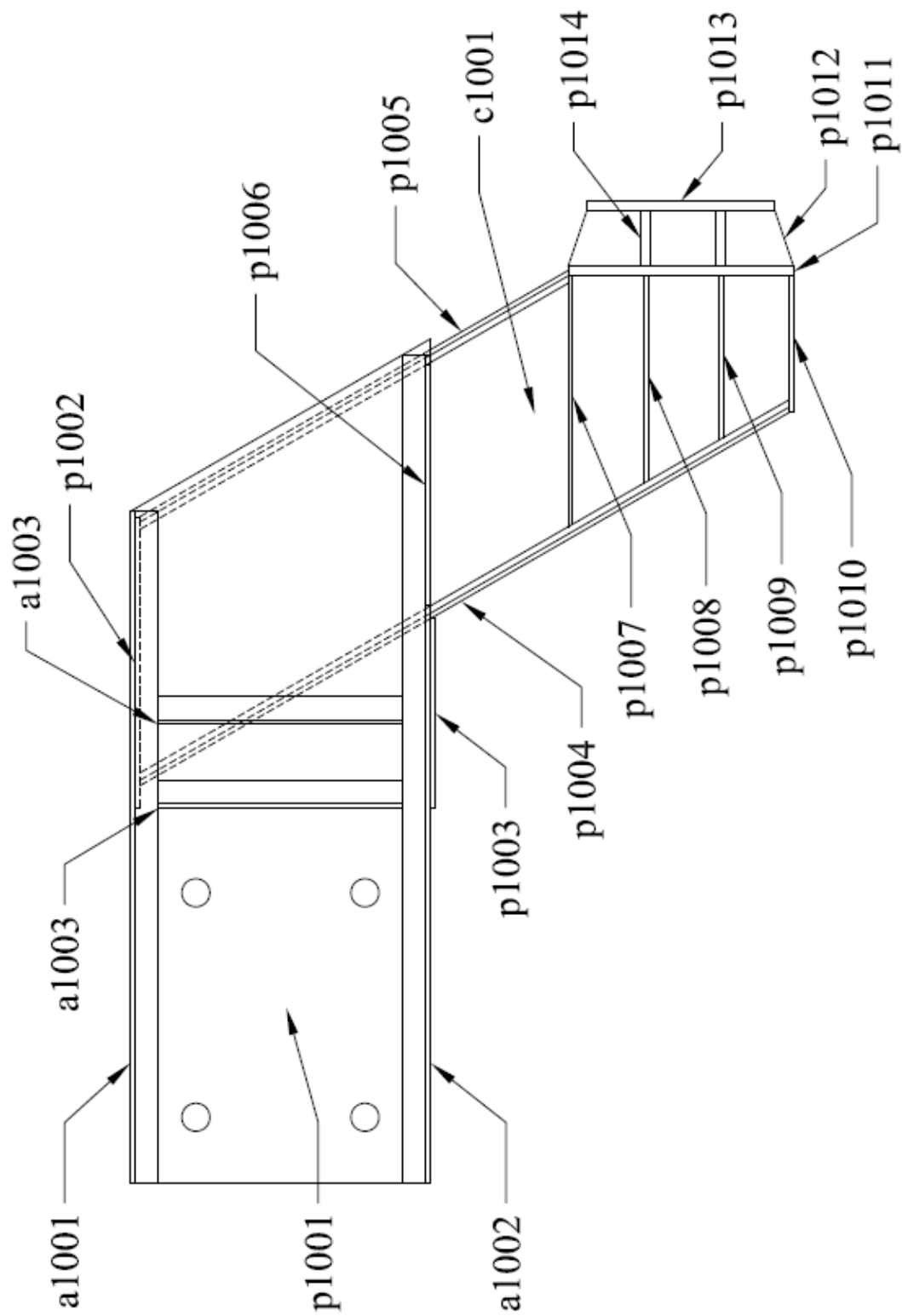


Figure A-3 Loading Frame Assembly Diagram

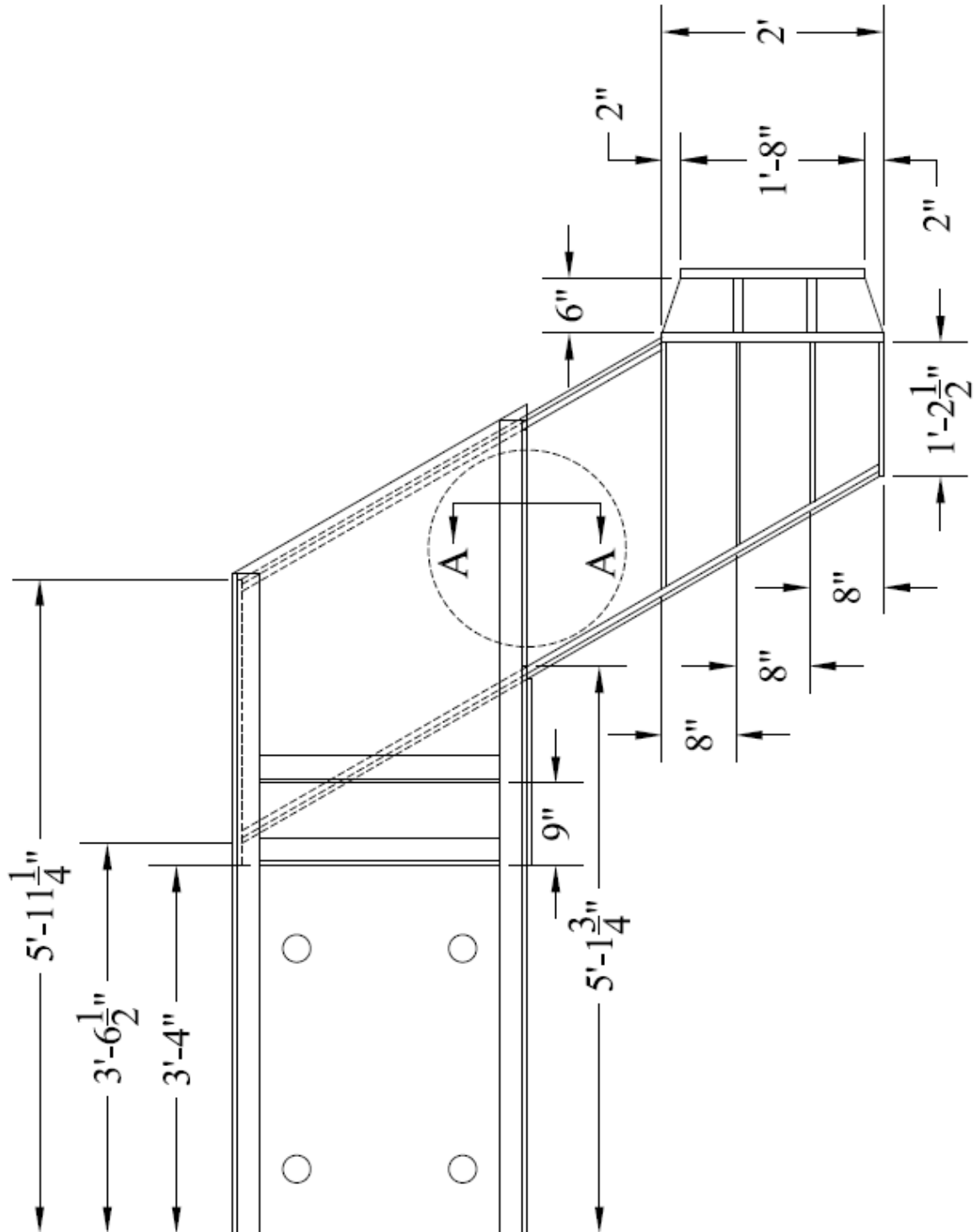


Figure A-4 – Loading Frame Front View (1 in. = 25.4 mm)

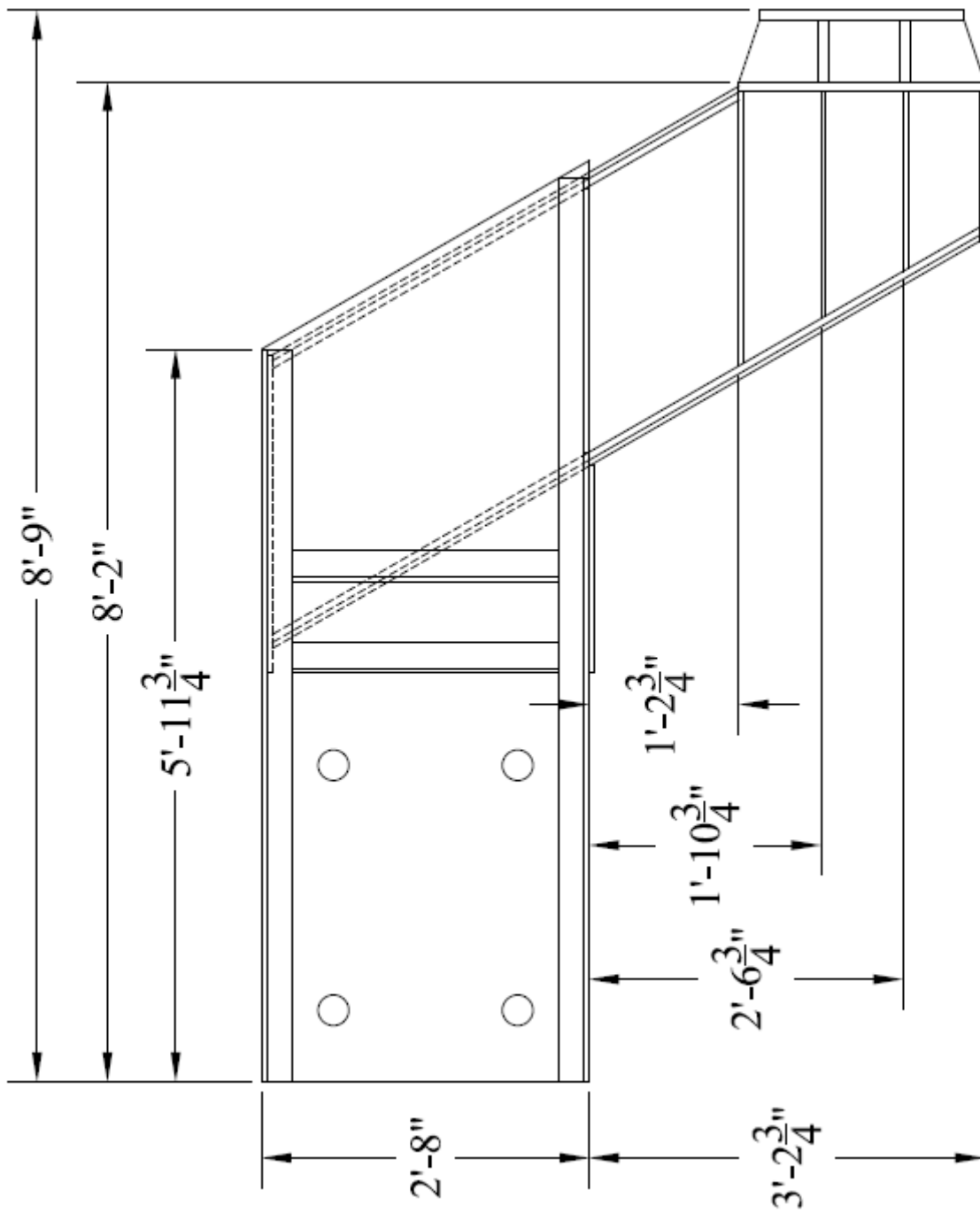


Figure A-5 - Loading Frame Front View (2) (1 in. = 25.4 mm)

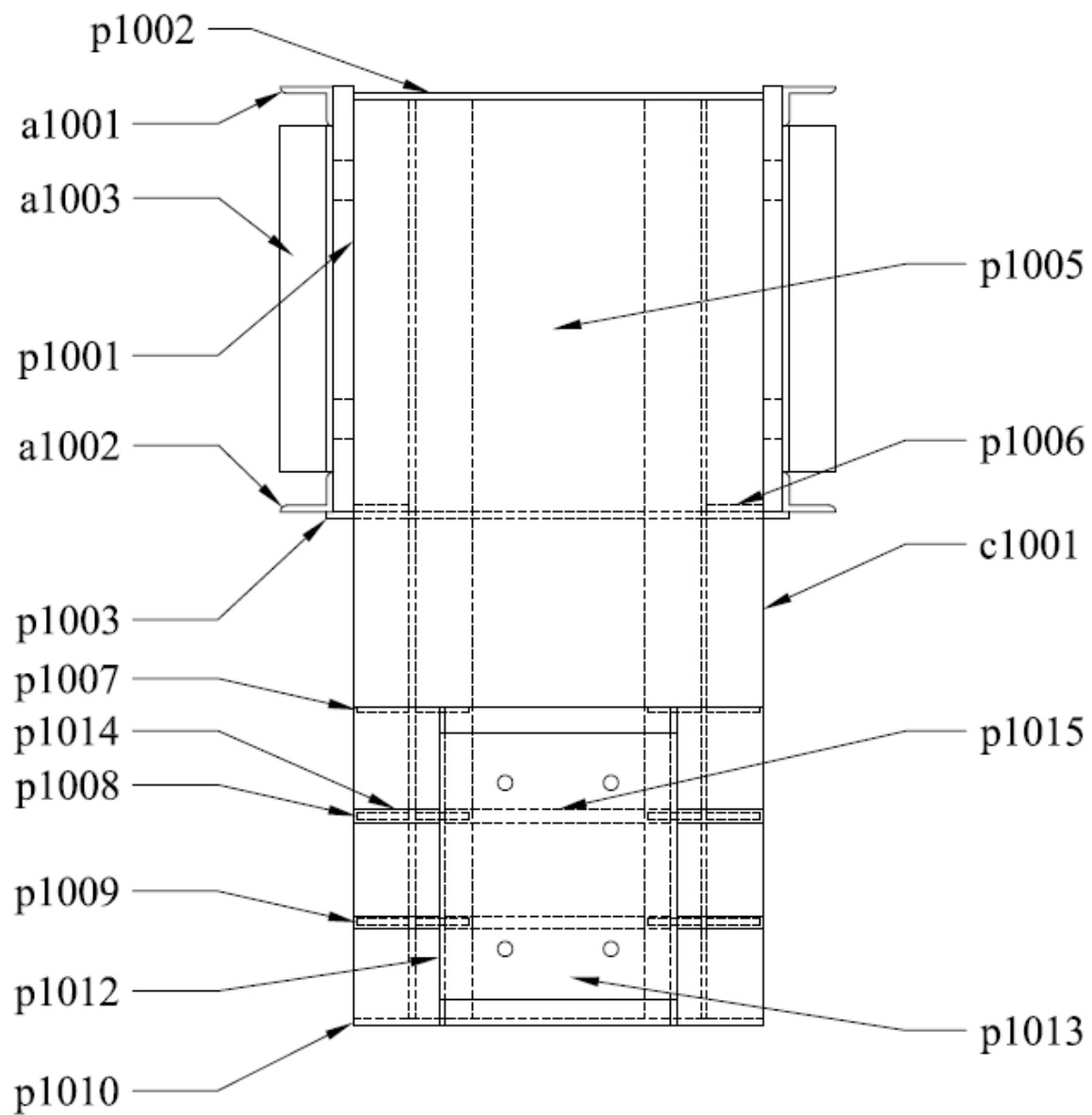


Figure A-6 – Loading Frame Side View

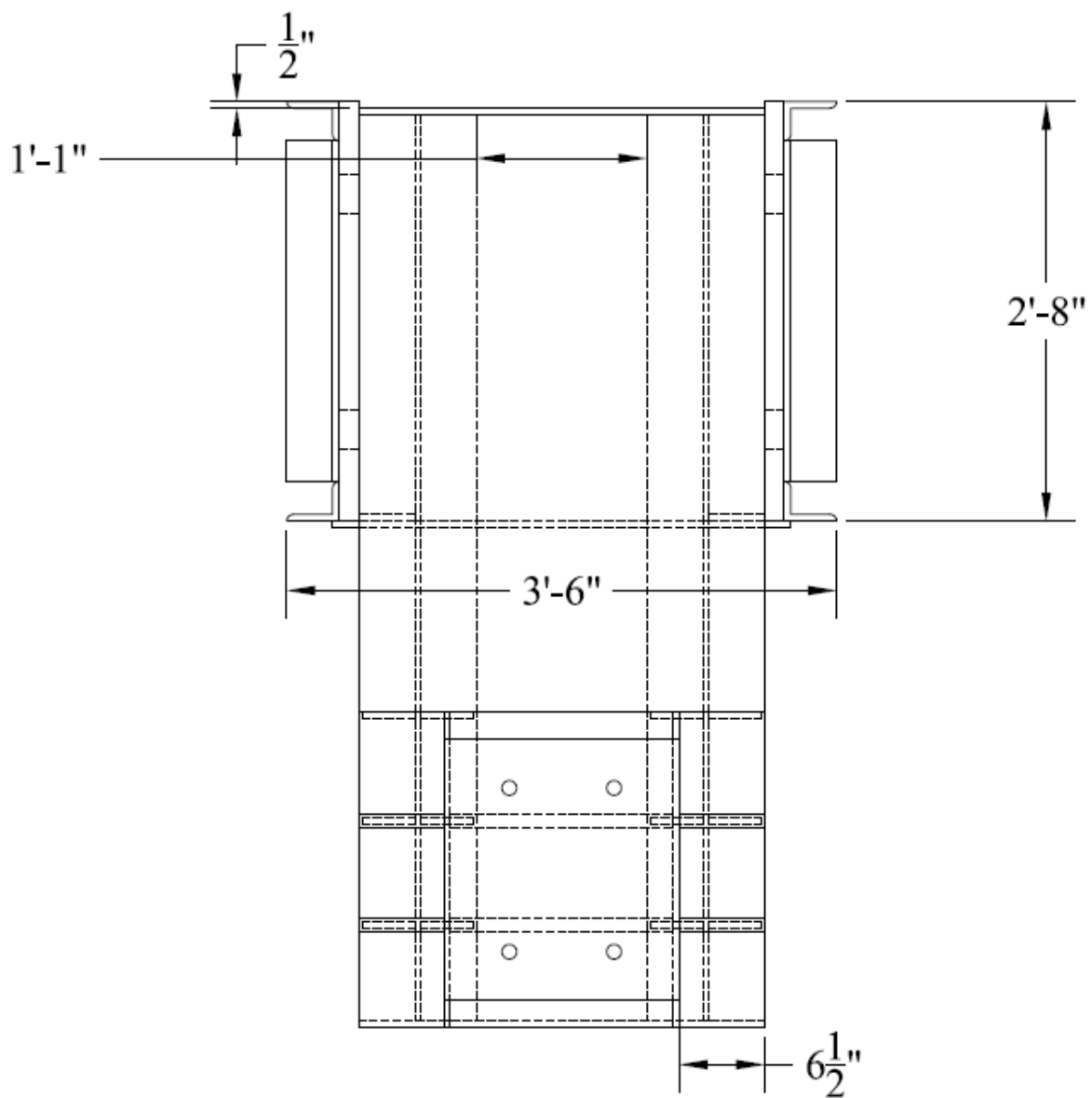


Figure A-7 – Loading Frame Side View (2) (1 in. = 25.4 mm)

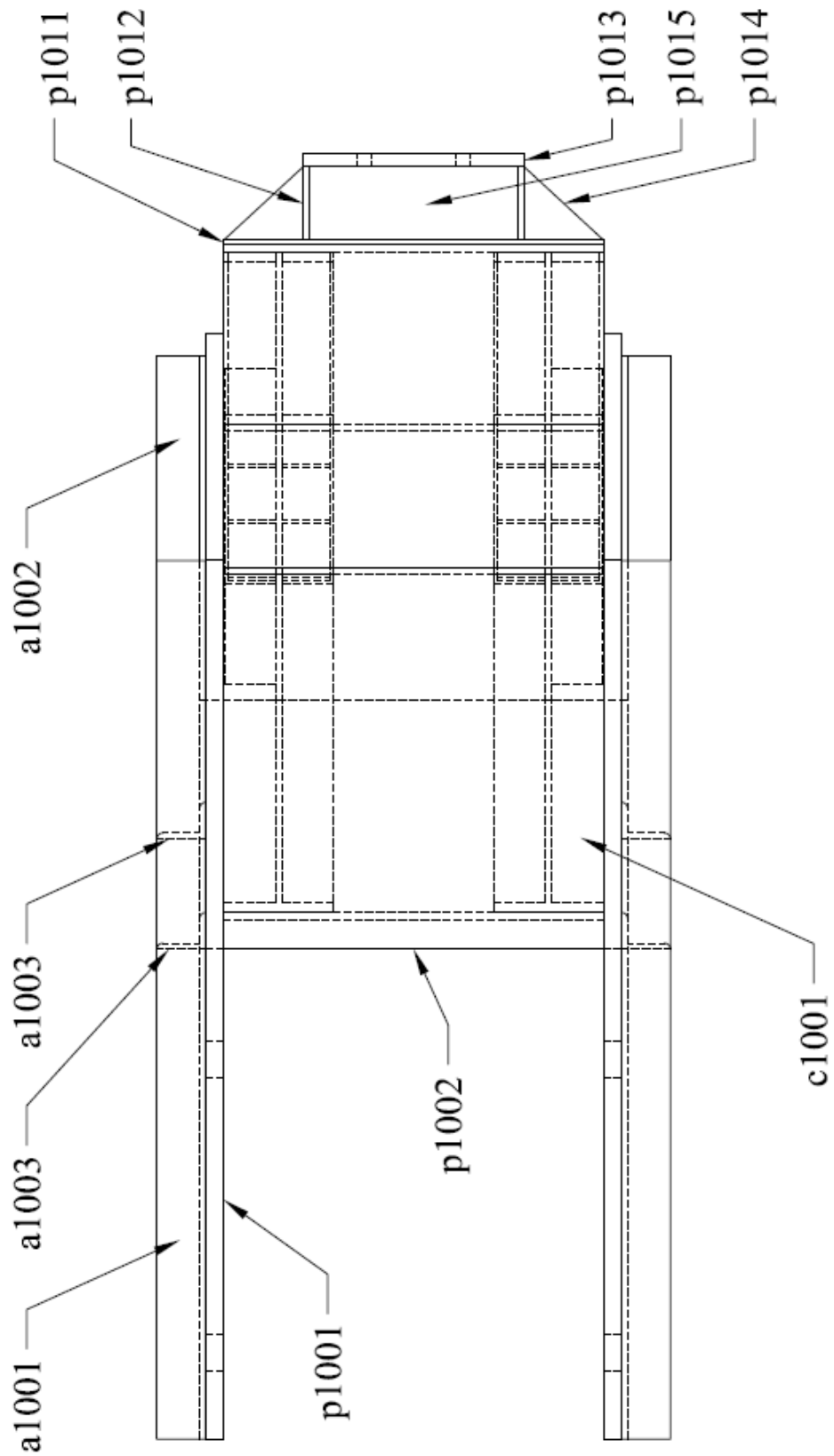


Figure A-8 – Loading Frame Top View

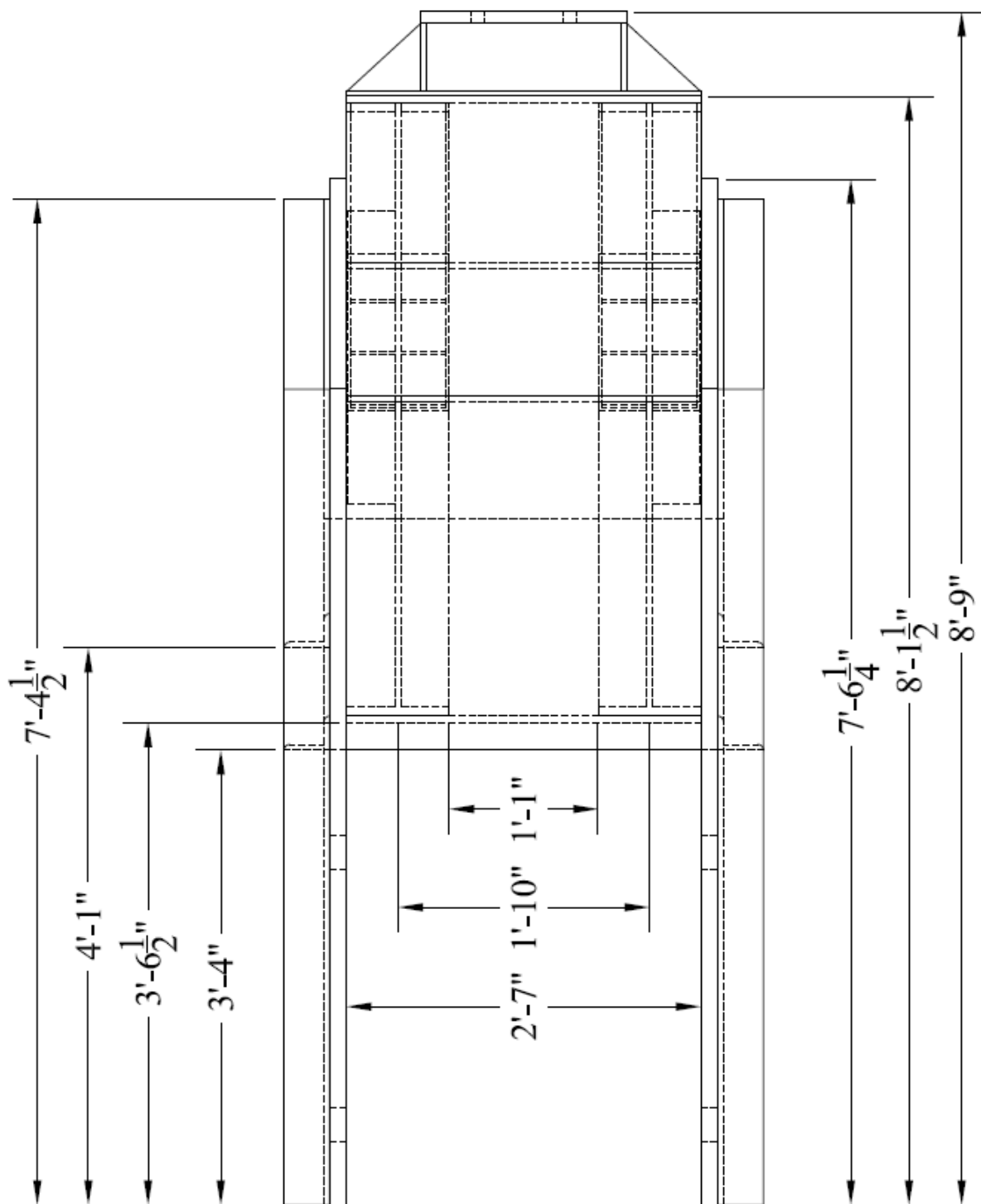


Figure A-9 – Loading Frame Top View (2) (1 in. = 25.4 mm)

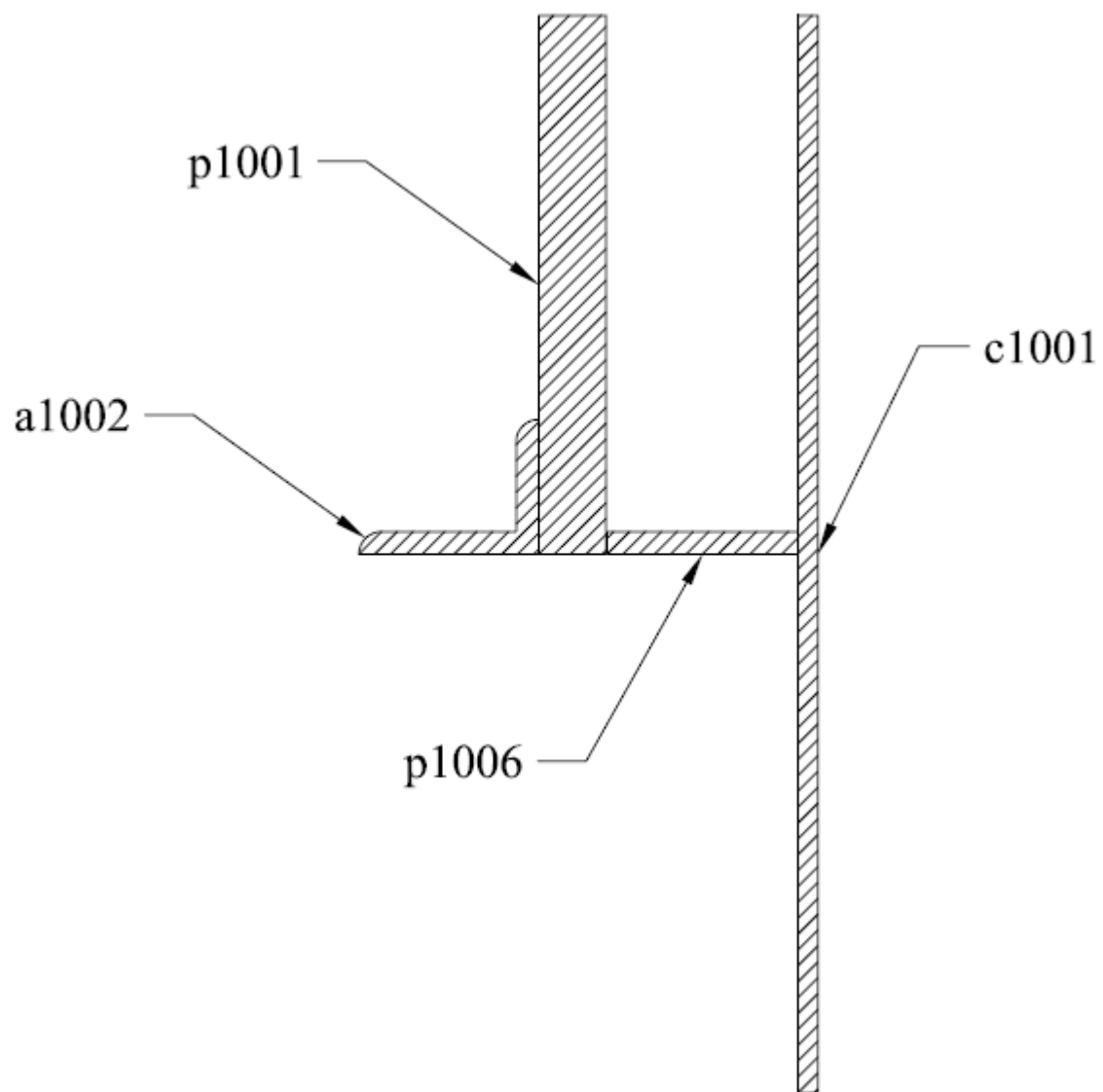


Figure A-10 – Loading Frame Section A-A

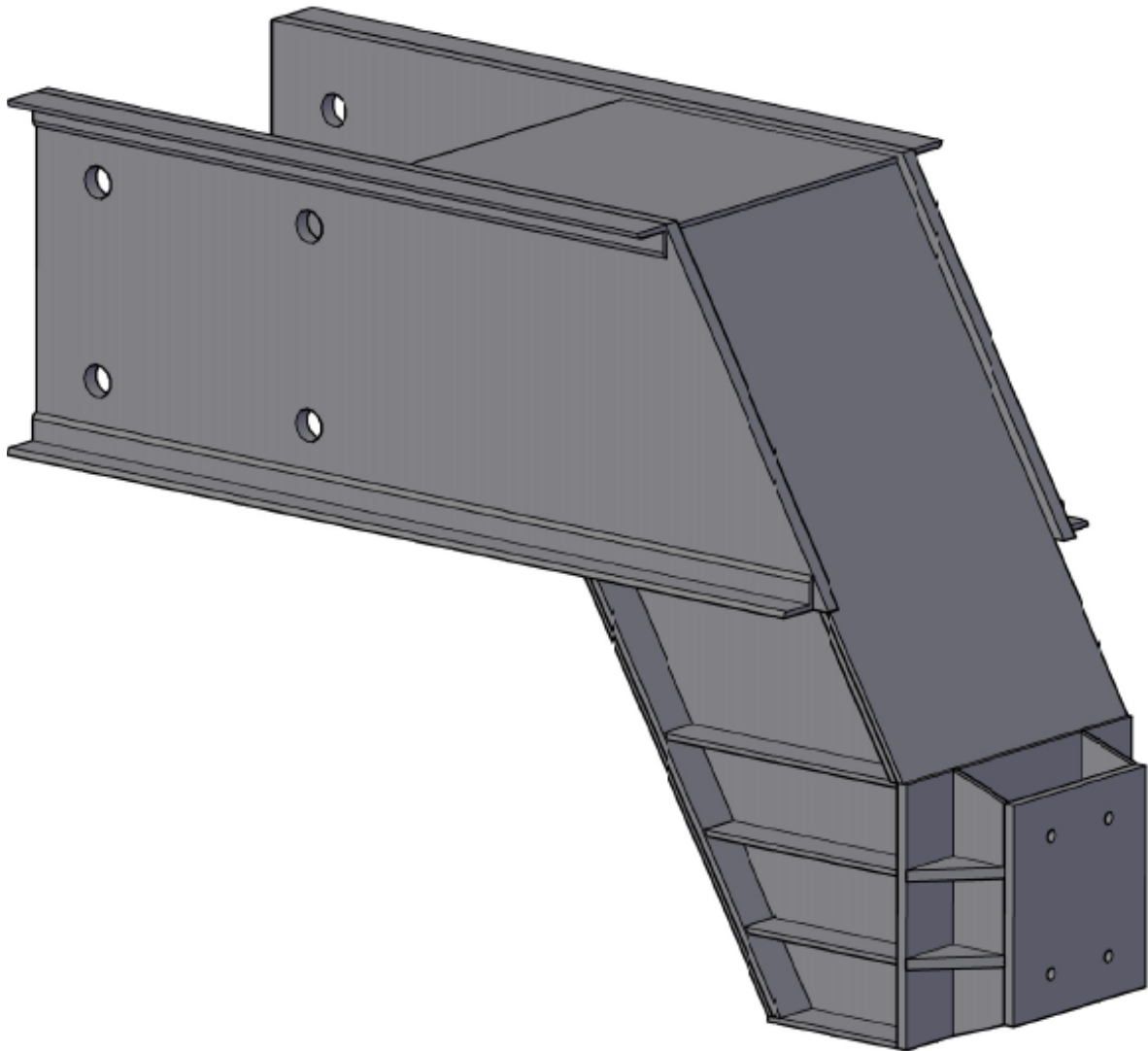


Figure A-11 – Loading Frame Isometric View

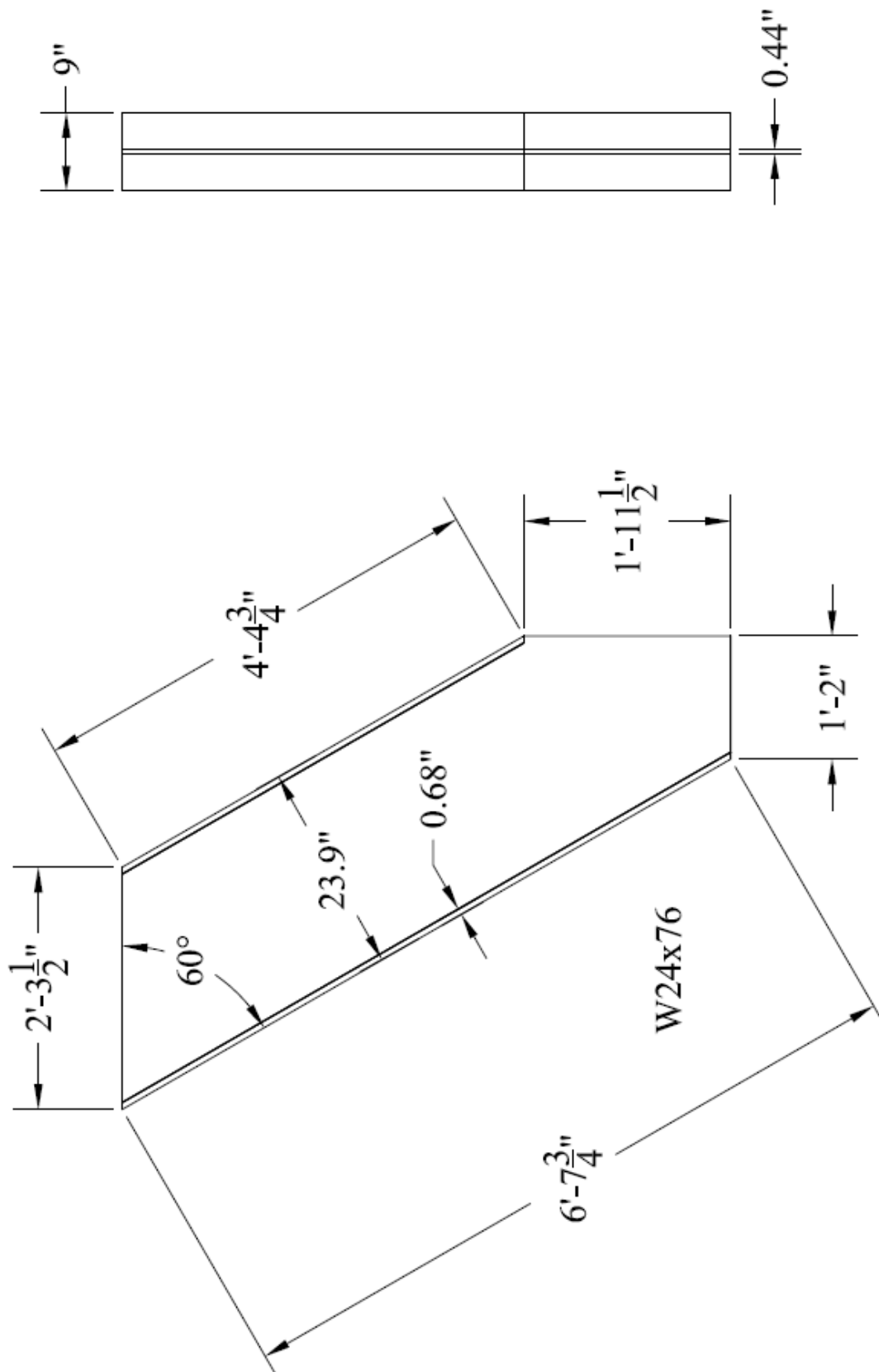


Figure A-12 – Loading Frame c1001 (1 in. = 25.4 mm)

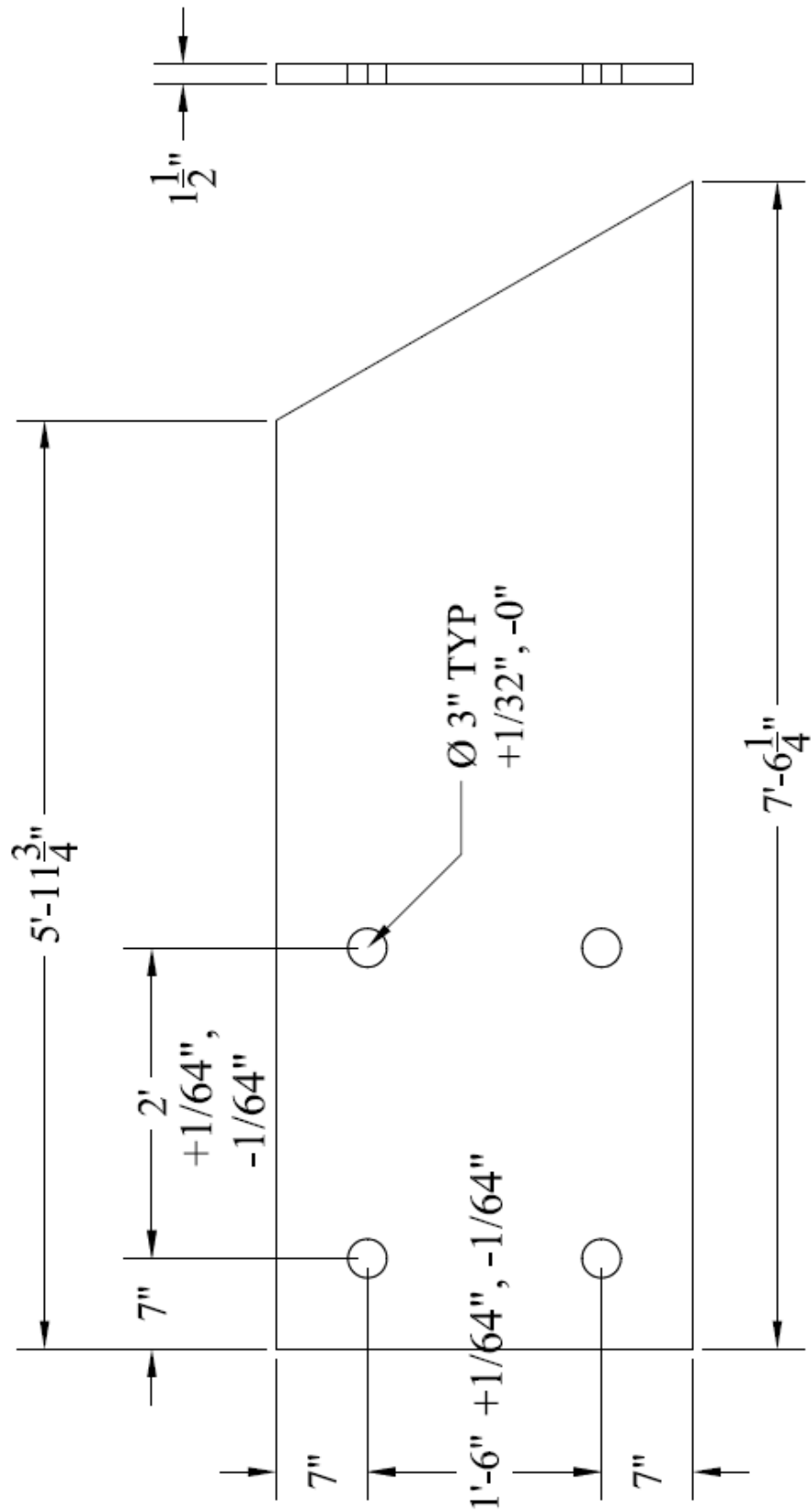


Figure A-13 – Loading Frame p1001 (1 in. = 25.4 mm)

Table A-1 Loading Frame Bill of Materials

(1 kip = 4.45 kN, 1 in. = 25.4 mm)

Piece Number	Description	Quantity	Length (in.)	Width (in.)	Thickness (in.)	Area (in ²)	Weight (lb)
a1001	L4x3x1/2	2	71.75			3.25	132.2
a1002	L4x3x1/2	2	88.5			3.25	163.1
a1003	L4x3x1/2	4	26			3.25	95.8
c1001	W24x76	2	80			22.4	1016.3
p1001	1½" plate	2	81	32	1.5		2205.0
p1002	½" plate	1	31	31.25	0.5		137.4
p1003	½" plate	1	35	20.25	0.5		100.5
p1004	½" plate	1	31	80	0.5		351.6
p1005	½" plate	1	31	53	0.5		232.9
p1006	½" plate	2	4.25	25.75	0.5		31.0
p1007	½" plate	4	4	26.75	0.5		60.7
p1008	½" plate	4	4	22.25	0.5		50.5
p1009	½" plate	4	4	17.5	0.5		39.7
p1010	½" plate	4	14.5	31	0.5		254.9
p1011	1" plate	1	24	31	1		211.0
p1012	½" plate	2	22	6	0.5		37.4
p1013	1" plate	1	18	20	1		102.1
p1014	1" plate	4	6	3	1		20.4
p1015	1" plate	2	17	6	1		57.8

Total = 5300 lb